Zentrum für Molekulare Neurobiologie Hamburg
Institut für Biosynthese Neuraler Strukturen

The interaction between the neural cell adhesion molecule L1 and β-amyloid peptide: potential relevance in Alzheimer's disease

Dissertation
Zur Erlangung der Würde des Doktors der Naturwissenschaften des Fachbereichs Biologie, der Fakultät für Mathematik, Informatik und Naturwissenschaften,
der Universität Hamburg

vorgelegt von

Nevena Djogo
aus Sarajevo

Hamburg, 2013

Genehmigt vom Fachbereich Biologie
der Fakultät für Mathematik, Informatik und Naturwissenschaften
an der Universität Hamburg
auf Antrag von Frau Professor Dr. M. SCHACHNER
Weiterer Gutachter der Dissertation:
Professor Dr. C. LOHR
Tag der Disputation: 18. Oktober 2013

Hamburg, den 07. Oktober 2013

Professor Dr. C. Lohr
Vorsitzender des
Fach-Promotionsausschusses Biologie

Universitätsklinikum Hamburg-Eppendorf

Zentrum für Molekulare Neurobiologie

Research Group:
Neuronal Translational Control

Falkenried 94
20251 Hamburg

Dr. Kent Duncan
Telefon: +49(0)40 7410-56274
Telefax: +49(0)40 7410-53436

Kent.Duncan@zmnh.uni-hamburg.de
www.zmnh.uni-hamburg.de

Universitätsklinikum Hamburg-Eppendorf Martinistraße 52 20246 Hamburg
Zentrum für Molekulare Neurobiologie - Forschergruppen

To whom it may concern:

Nevena Djogo is submitting her doctoral dissertation in English. The title of her thesis is: 'The interaction between the neural cell adhesion molecule L1 and β-amyloid peptide: potential relevance in Alzheimer's disease'.

I hereby certify as a native speaker and molecular biologist that the English language used in this thesis is sufficiently correct for submission.

Universität Hamburg
Universitätsklinikum Hamburg-Eppendorf
Zentrum für Molekulare Neurobiologie
AG Duncan
Falkenried 94 · D-20251 Hamburg

Kent Duncan, Ph.D.

Hamburg, 20.08.2013

Eidesstattliche Versicherung

Hiermit erkläre ich an Eides statt, dass ich die vorliegende Dissertationsschrift selbst verfasst und keine anderen als die angegebenen Quellen und Hilfsmittel benutzt habe.

Nevena Djogo

Table of Contents

1. INTRODUCTION

1.1 Pathology and etiology of Alzheimer's disease

Alzheimer's disease (AD) is a neurodegenerative disorder affecting mostly, but not only, elderly individuals causing progressive dementia and loss of cognitive functions. The disease is characterized by massive neurodegeneration in brain regions involved in learning, memory and emotions including neocortex, hippocampus and amygdala, basal forebrain cholinergic system and brainstem monoaminergic system, which are reduced in size due to neuronal death, astrogliosis, microgliosis and synaptic degeneration (Albert, 2011; Hardy, 2006; Jucker and Walker, 2011; Mattson, 2004). All these changes are thought to be caused by accumulations of insoluble protein depositions: intracellular neurofibrillary tangles, composed of microtubule-associated tau protein and extracellular amyloid plaques, composed of β-amyloid peptide (Aβ), derived from amyloid precursor protein (APP).

Most of the cases of AD are sporadic, with late onset of the disease. Increasing age is the greatest known risk factor; almost half of individuals older than age 85 develop AD (Bermejo-Pareja et al., 2008, Hebert et al., 2003). The most important genetic risk factor is *APOE4* allele of apolipoprotein E; the risk of the disease is increased by 3 times in heterozygotes and by 15 times in homozygotes for *APOE4* allele (Blennow et al., 2006). Among other important risk factors are gender (women have slightly higher risk), head trauma and cardiovascular risk factors, such as hypercholesterolaemia, hypertension, diabetes, obesity and smoking (Andersen 1999; Rossendorff et al., 2007).

A small percentage of AD cases have an autosomal dominant inheritance (familial AD, FAD) which is usually coupled with an early onset of disease. Most of them are due to mutations in one of the three genes: APP and presenilins 1 and 2 (PS1 and PS2).

The disease was first described by Alois Alzheimer in 1906. Initially the term AD was used to describe rare cases of the early age onset presenile dementia, while the late onset, senile dementia, was considered to be a consequence of arteriosclerosis. After the finding that the majority of cases with senile dementia show the same "plaque and tangle" pathology seen in presenile dementia (Blessed et al., 1968; Tomlinson et al., 1968, 1970), AD has become a field of major research interest.

Neurofibrillary tangles are found in many brain diseases (Buée et al., 2000; Arai et al., 2001; Goedert et al., 2004), suggesting that they could be a secondary response to brain damage. They are also normally present in all aging non-demented individuals (Bouras et al., 1994), but only in the hippocampus, unlike in demented subjects who have widespread and dense

neurofibrillary changes in the neocortex (Tomlinson et al., 1970). Neurofibrilar pathology is well correlated with cognitive decline (Braak and Braak, 1991).

Amyloid plaques are often found in elderly persons but are not universal (Davies et al., 1998; Braak et al., 2011; Jicha et al., 2012). They can be divided in two subtypes, “diffuse plaques” and “neuritic plaques”, which are surrounded by degenerating axons and dendrites that often contain hyperphosphorylated tau aggregates (Wisniewski et al., 1982; Terry et al., 1994). The presence of neuritic plaques is more likely to be associated with cognitive impairment and is currently considered an important diagnostic criterion for AD.

Two hypotheses were proposed to explain the etiology of AD, based on these two main pathological features of the disease. The “amyloid cascade hypothesis” states that aggregation of Aβ is the initial event which triggers pathological cascade leading to development of AD (Hardy and Higgins, 1992). On the other side, the “neuronal cytoskeletal degeneration hypothesis” proposes cytoskeletal changes related to tau aggregation as the basis of neurodegeneration in AD (Braak and Braak, 1991).

Although the neurofibrilar pathology shows the best correlation with cognitive changes in AD, amyloid cascade hypothesis has dominated the research in AD field for the past twenty years, based on the evidence described in the following chapter.

1.1.1 The amyloid cascade hypothesis

According to the amyloid cascade hypothesis (Hardy and Higgins, 1992; Hardy et al., 1998; Hardy and Selkoe, 2002), deposition of Aβ peptide triggers a sequence of events that finally results in AD. This hypothesis was based on two seminal discoveries. The first was isolation of Aβ from brains of AD and Down syndrome patients (Glenner and Wong, 1984a,b), the latter based on the universal occurrence of AD in trisomy 21 (Olson and Shaw, 1969). Subsequently, the gene encoding the Aβ sequence was cloned and localized to chromosome 21 (Goldgaber et al., 1987; Kang et al., 1987; Robakis et al., 1987), revealing that the Aβ peptide was a part of a much larger precursor protein, β-amyloid precursor protein (βAPP or APP). The finding that a mutation in the APP gene can cause AD (Goate et al., 1991) was the second discovery leading to the emergence of amyloid cascade hypothesis. Further support for the hypothesis came from the finding that autosomal dominant mutations in proteins involved in Aβ generation, presenilin 1 (Sherrington et al., 1995) and presenilin 2 (Levy-Lahad et al., 1995; Rogaev et al., 1995), could also be the cause of AD.

The most common risk factor for late onset AD is the *APOE4* allele of apolipoprotein E (APOE) gene; *APOE3* allele can be considered neutral, while *APOE2* is protective (Corder et al., 1993, 1994; Farrer et al., 1997). It was shown that APOE is involved in Aβ clearance, which is differentially affected by APOE isoforms (Castellano et al., 2011). Recently, genome wide association studies have discovered new risk alleles for late onset AD (Harold et al. 2009; Hollingworth et al. 2011; Naj et al. 2011), such as alleles involved in cholesterol metabolism and in the complement cascade (Jones et al. 2010), which is involved in removal of Aβ deposits. In conclusion, both late onset AD genetic risk factors and FAD mutations have influence over Aβ metabolism, suggesting central role of Aβ in AD etiology.

It is noteworthy that mutations in the tau gene alone can cause autosomal dominant neurodegenerative disorder called frontotemporal lobe dementia with Parkinsonism linked to chromosome 17 (FTDP-17) (Hutton et al., 1998). This is an extremely rare condition, but it demonstrates that tau pathology alone can cause neuronal loss and dementia without amyloid pathology. This suggests that tau pathology may be downstream to Aβ pathology in AD.

1.2 Amyloid precursor protein (APP)

1.2.1 APP family

APP is a member of an evolutionarily conserved protein family (Coulson et al., 2000), which in mammals consists of APP, APLP1 (amyloid precursor-like protein 1) (Wasco et al., 1992) and APLP2 (Wasco et al., 1993). APP-like proteins have also been identified in *Drosophila melanogaster* (APPL) (Rosen et al., 1989) and *Caenorhabditis elegans* (APL-1) (Daigle et al., 1993). In mammals, APP family of proteins is abundantly expressed in the brain. APLP1 expression is restricted to neurons (Lorent et al., 1995), while APP and APLP2, although highly enriched in the brain, especially at the synapses, can be detected in most other tissues as well. Aβ sequence is not present in the relevant region of the APLPs, indicating that only APP can directly give rise to the AD-causing amyloid plaques.

APP family members play roles in neuronal development with functions to promote neurite outgrowth, neural cell migration and copper homoeostasis (Muller et al., 1994; Zheng et al., 1995; White et al., 1999; Heber et al., 2000; Herms et al., 2004; Young-Pearse et al., 2007). Single knockouts of APP, APLP1 or APLP2 proteins are viable and show relatively mild phenotypes, mostly distinct for different family members (Dawson et al., 1999; Heber et al., 2000). This might be due to functional redundancy between APP, APLP1 and APLP2. However, APP-APLP2 and APLP1-APLP2 double knockouts show a lethal phenotype early

postnatally (Heber et al., 2000). Surprisingly, APP-APLP1 mice are viable and seem to be apparently normal (Heber et al., 2000). No detectable gross or histopathological abnormalities were observed in any of these lines, whereas triple APP-APLP1-APLP2 knockouts, which die *in utero,* show neuronal ectopias similar to type II lissencephaly (Herms et al., 2004).

1.2.2 Structure of APP

APP is a type I transmembrane glycoprotein of 110 kDa encoded by a single gene located on a chromosome 21 (Robakis et al., 1987). Three major isoforms are produced by alternative splicing and are designated according to their lengths as APP695, APP751, and APP770 (Tanaka et al., 1988). Other isoforms of APP (consisting of 752, 733, 714, 696, and 677 amino acid residues) are also produced albeit in much smaller amounts, by alternative splicing.

General domain structure of APP is shown in Figure 1.1. The ectodomain consists of E1 domain and carbohydrate domain. At the N-terminus of E1 domain is the growth factor-like domain (GFLD, Rossjohn et al., 1999), which is followed by copper-binding domain (CuBD, Kong et al., 2007). The GFLD binds to heparin and is involved in neurite outgrowth (Small et al, 1994) and MAP kinase activation (Greenberg et al, 1995).

The E1 region is linked via the acidic region to the carbohydrate domain. The Kunitz-type protease inhibitor domain (KPI) is present between the acidic and carbohydrate domain in APP751 and APP770 (Ponte et al., 1988), and APP770 additionally contains domain similar to the OX-2 antigen (Clark et al., 1985).

The carbohydrate domain contains the two N-glycosylation sites of the ectodomain. It can be subdivided into the E2 domain (Wang and Ha, 2004), also called central APP domain (CAPPD), and a linker or juxtamembrane domain. E2 domain contains RERMS sequence and another heparin-binding site.

The carbohydrate domain is followed by the transmembrane and the APP intracellular domain (AICD). Amino acids 1–27 of Aβ sequence lie outside the cell membrane and the rest of it lies within the membrane. AICD is the most conserved region. It contains conserved YENPTY motif (residues 682–687) which is important for clathrin-mediated endocytosis and binding to numerous proteins (King and Turner, 2004).

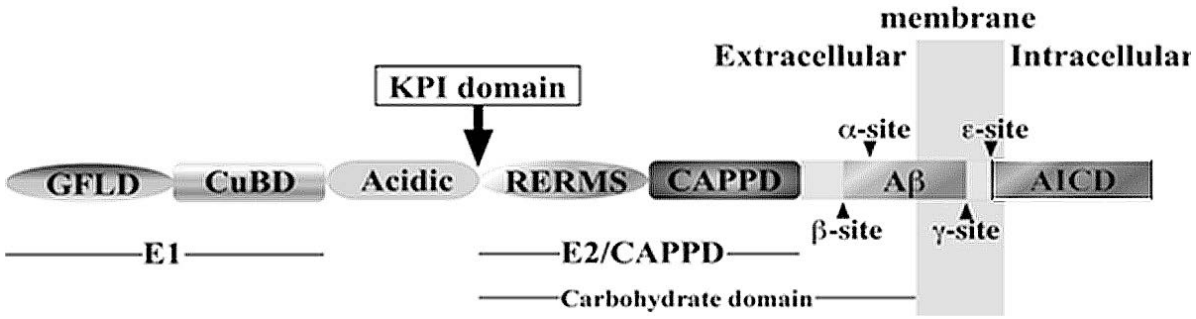

Figure 1.1 Schematic representation of APP695 domain structure of APP including the relative position of the α-, β- and γ-secretase cleavage sites. The E1 domain contains N-terminal growth factor-like domain (GFLD) and copper-binding domain (CuBD). It is linked via acidic domain to the carbohydrate domain including E2 domain, which consists of RERMS sequence and central APP domain (CAPPD). E2 domain is followed by the Aβ region, and the intracellular domain (AICD). Kunitz protease inhibitor (KPI) domain is present at the indicated site in APP-751 and APP-770, while APP-695 lacks this domain. The Ox2 sequence is present in APP770.

APP is widely expressed in different tissues. APP isoforms containing the KPI domain are expressed in most non-neural tissues (e.g. spleen, thymus, muscle, kidney, liver, lung, and heart), while APP695 is predominantly expressed in the brain (Neve et al., 1988; Arai et al., 1991). Within the brain, APP695 mRNA is expressed at high levels and APP751/770 mRNAs at lower levels, with regional differences in levels of expression. For example, APP695 is expressed at higher levels in association cortices and APP751 and APP770 are expressed at higher levels in the hippocampus than in other brain regions (Neve et al., 1988). APP695 is expressed almost exclusively by neurons, whereas APP751/770 isoforms are expressed mainly in glial cells including astrocytes, microglia, and oligodendrocytes (Abe et al., 1991; Forloni et al., 1992; Konig et al., 1992; Monning et al., 1992; Sandbrink et al., 1994). During development, peak of the expression of APP isoforms coincides with the period of synaptogenesis (Loffler and Huber, 1992).

1.2.3 Proteolytic processing of APP

APP is processed via two different proteolytic pathways (Figure 1.2). Non-amyloidogenic pathway, which accounts for approximately 90% of APP processing, includes shedding of soluble sAPP-α ectodomain by a protease called α-secretase. Alpha-secretases are metalloproteases that belong to the ADAM family (a disintegrin and metalloproteinase). α-secretases involved in APP processing are ADAM9 (Koike et al., 1999), ADAM10 (Lammich et al., 1999) and ADAM17 (also called TACE, tumor necrosis factor-α

converting enzyme; Buxbaum et al., 1998), but only ADAM10 is a constitutive α-secretase in neurons (Jorissen et al., 2010; Kuhn et al., 2010). α-secretase cleaves the APP molecule near the cell surface within the Aβ sequence, and therefore precludes Aβ generation. In amyloidogenic pathway, alternative shedding by β-secretase produces slightly shorter soluble ectodomain sAPP-β, leaving Aβ sequence intact. β-secretase (or BACE-1, for β-site APP cleaving enzyme) is a type I transmembrane protein with aspartyl protease activity (Vassar et al., 1999). BACE belongs to the pepsin family of aspartyl proteases and it is the only enzyme with β-secretase activity, as there is no generation of Aβ in its absence (Cai et al., 2001; Luo et al., 2001). BACE-2, a close homolog of BACE-1 was identified; however, it shows an α-secretase-like activity and cleaves APP in the middle of Aβ region (Farzan et al., 2000). After the ectodomain shedding, γ-secretase cuts the remaining membrane-bound stub called C83 (or CTFα), generated by α-secretase or C99 (or CTFβ) generated by β-secretase. In the process the APP intracellular domain (AICD) is released, as well as either Aβ (via the β-secretase pathway) or the N-terminally truncated peptide p3 (via the α-secretase pathway).

Gamma-secretase is a complex composed of four membrane proteins: presenilin (PS), nicastrin, anterior pharynx defective 1 (APH1) and presenilin enhancer 2 (PEN2) (De Strooper, 2010). This protease complex cuts within the transmembrane domain of APP in a process called regulated intramembrane proteolysis (RIP). PS is a catalytically active subunit of the complex; it is an aspartyl protease (Xia and Wolfe, 2003) with two isoforms, PS1 and PS2. In humans, there are also two homologues of APH1: APH1A, occurring in two splice variants, and APH1B - so in total six different γ-secretase complexes are possible, which may have different substrate specificities and therefore different biological roles (Serneels et al., 2005).

Aβ accumulated in AD brains is heterogeneous at its C-terminus, ranging in size from 39 to 43 amino acids. Diffuse senile plaques consist predominantly of Aβ42/43, whereas classic senile plaques contain both Aβ40 and Aβ42/43, as well as shorter N-terminally truncated peptides (Iwatsubo et al., 1994; Savage et al., 1995). Aβ may exist in a soluble form as well as in a beta-sheet conformation. Residues 14-21 and 29-39/42 of Aβ possess the beta-sheet forming properties (Barrow et al., 1991). Jarrett et al. (1993) showed that Aβ42 is less soluble and forms fibrils faster than shorter isoforms *in vitro*, indicating that C-terminal sequence of Aβ is critical in determining the solubility of the peptide. It has been hypothesized that the amyloid deposition *in vivo* may be seeded by Aβ 1-42 fibrils and grow

rapidly by assembly of Aβ 1-40, which is the most abundant isoform produced by cultured cells (Suzuki et al., 1994). Therefore, even a slight increase in the amount of Aβ 1-42 might be sufficient to lead to beta-amyloidosis (Younkin, 1995; Hardy, 1997).

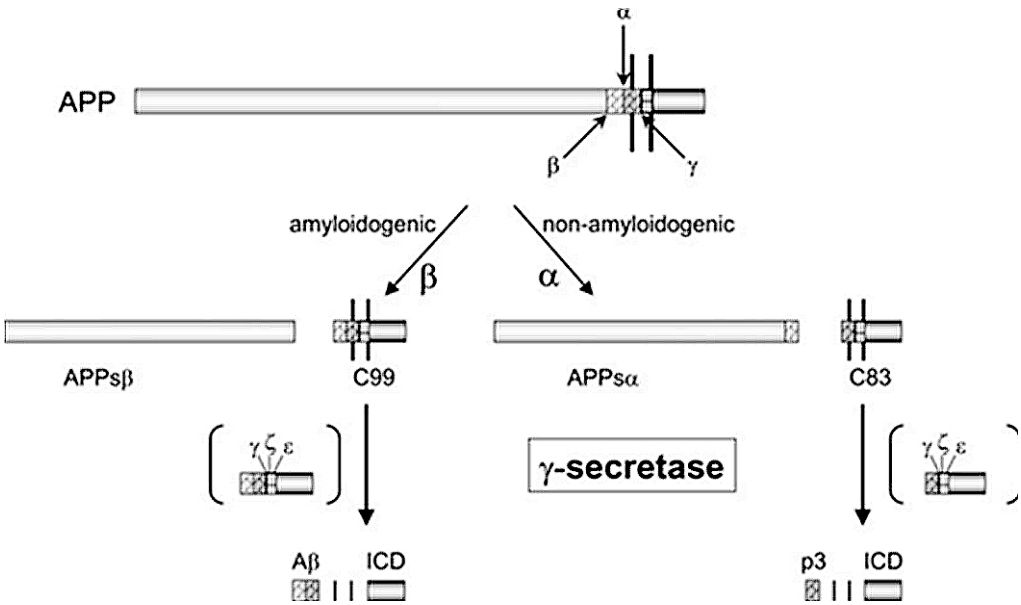

Figure 1.2. Schematic diagram of APP processing pathways. In the non-amyloidogenic pathway, α-secretase cleaves in the middle of the β-amyloid (Aβ) region to release the soluble APP-fragment APPsα. The APP C-terminal fragment 83 (C83) is then cleaved by γ-secretase to release the APP intracellular domain (ICD) and p3 fragment. In the amyloidogenic pathway, β-secretase cleaves APP to produce the soluble fragment APPsβ. APP-C99 is then cleaved by γ-secretase to produce Aβ and ICD. (Modified from Walsh et al., 2007.)

1.2.4 Functions of APP

Although of the role of APP in AD is well understood, the normal physiological functions of this protein are still not clear (De Strooper and Annaert, 2000).

The overall structure of the protein suggests that APP may function as a receptor or growth factor (Kang et al., 1987; Rossjohn et al., 1999. Also, the turnover of APP is quite fast (30–90 min, Herreman et al, 2003), suggesting that APP have a regulatory, rather than a structural function in the cell. Brain injury induces APP expression, which suggests that APP plays a repair role in this context (Mattson et al., 1997; Murakami et al., 1998). The correlation of AD with head trauma may reflect an increase in APP expression and consequently Aβ generation. Cu^{2+} and Zn^{2+} binding activities of APP are well studied. The Zn^{2+} binding is assumed to play mainly a structural role (Bush et al., 1993), whereas APP is able to catalyze a reduction of Cu^{2+} to Cu^{1+} (Multhaup et al., 1996). RERMS sequence is

implicated in the growth-promoting properties of APP (Ninomiya et al, 1993; Li et al, 1997). Soluble APP released from the cell membrane may serve as a signaling molecule; it plays a role in the growth of fibroblasts in culture (Park et al., 2006), and it was found to be neuroprotective for primary neurons in culture, preventing elevations in intracellular Ca^{2+} levels caused by glucose deprivation and raising the excitotoxic threshold of glutamate (Mattson et al., 1993), as well as mediating axonal and dendritic growth (Perez et al., 1997). Impairment in spatial learning and long-term potentiation (LTP) in APP knockout mice can be rescued by a knock-in allele of sAPP-α (Ring et al., 2007).

The idea that APP functions as a receptor came from the similarity of Notch receptor signaling with proteolytic processing of APP (Annaert and De Strooper, 1999; Selkoe and Kopan, 2003). Notch signaling is initiated by interaction with cognate ligands, which triggers shedding of the Notch ectodomain by ADAM10 and ADAM17, metalloproteases, which also shed the ectodomain of APP. Remaining membrane-associated stub of Notch is then cut by γ-secretase (De Strooper et al., 1999), releasing an intracellular domain that translocates to the nucleus and interacts with certain transcription factors to control gene expression and cell fate. However, the search for ligands or receptors that interact with the ectodomain of APP has not been very successful. Neuronally secreted glycoprotein F-sponding has been shown to prevent shedding of the APP ectodomain and reduce Aβ production (Ho and Sudhof, 2004) and reelin, an extracellular matrix molecule that shares homology with F-spondin, was shown to increase binding of the reelin signaling mediator Dab1 to APP (Hoe et al., 2006a). Nogo-66 receptor has been reported to interact with the APP ectodomain and inhibit Aβ production (Park et al., 2006). LDL receptor-related protein (LRP) binds to and internalizes APPs containing the KPI sequence (Kounnas et al., 1995; Knauer et al., 1996), whereas sorting protein-related receptor containing LDLR class A repeats (sorLA) bind to the APP ectodomain and influence Aβ production, independently of KPI sequence (Andersen et al., 2005; Bu et al., 2006). Indirect triggering of β- and γ-secretase cleavage of APP has been reported for platelet-derived growth factor and certain cytokines (Gianni et al., 2003; Liao et al., 2004), and activation of protein kinase C leads to APP proteolysis through the γ- secretase pathway (Buxbaum et al., 1993).

APP may also serve as an adhesion molecule: it binds to extracellular matrix proteins such as heparin and collagen (Beher et al., 1996; Multhaup, 1994). Homo- and heterodimerization between the APP family members in adjacent cells has also been suggested to promote intercellular adhesion (Soba et al., 2005).

Numerous proteins that interact with the intracellular tail of APP (AICD) have been identified. These include proteins that play a role in vesicular or protein trafficking: X11 (Mint1) and X11L (Mint2) involved in vesicle exocytosis; Jun N-terminal-kinase interacting protein 1 (JIP-1), a scaffold protein that binds kinesin light chain 1 and coordinates transport of phosphorylated APP into neurites; kinesin 1; Pat1a, a microtubule interacting protein that plays a role in anterograde transport of APP and APLPs; and autosomal recessive hypercholesteremia (ARH) protein, an adaptor protein involved in the internalization of LDL receptors (Kamal et al., 2000; King et al., 2004; Kuan et al., 2006; Muresan and Muresan, 2005; Zheng et al., 1998; Noviello et al., 2003). APP-binding proteins are also involved in brain development: the Fe65 proteins transmit an APP-dependent signal important for neuronal positioning in the developing cortex; mDab1 plays a key role in reelin signaling in the developing cortex; and Numb is a scaffold protein important for Notch signaling (Guénette et al., 2006; Hoe et al., 2006b; Roncarati et al., 2002). Other APP-tail-binding proteins are implicated in regulating cell cycle progression; these include Go, PAK3, APP-BP1 (Chen et al., 2007; Chen et al., 2003; Giambarella et al., 1997; McPhie et al., 2003). Interaction of the APP tail with Shc and Grb2 is thought to lead to signaling through the Ras-Raf-MAPK pathway, and APP-Shc-Grb2 complexes have been reported to be increased in AD patients (Russo et al., 2005). Phosphorylation has been shown to regulate which proteins bind to the APP tail. Phosphorylation of the intracellular tail is mediated by several kinases: Ser/Thr kinases JNK, CDK5, GSK-3β, which phosphorylate Thr668, and the non-receptor tyrosine kinases Abl and Src, and nerve growth factor tyrosinekinase receptor A (TrkA), which phosphorylate Tyr682 (Russo et al., 2005).

The APP-interacting protein that has been most studied is Fe65, because a ternary complex consisting of Fe65, APP and the histone acetyltransferase Tip60 has been shown to activate transcription (Baek et al., 2002; Cao and Sudhof, 2001; Cao and Sudhof, 2004). Nuclear translocation of Fe65 is required for transactivation, and γ-secretase-mediated cleavage of APP can facilitate this event. However, Hass and Yankner (2005) showed APP-Fe65-Tip60 signaling occurring independently of γ-secretase cleavage. Candidate AICD-target genes have been suggested (e.g. tetraspanin CD82, APP, GSK3β and neprilysin), although one report provides evidence that the expression of none of these is γ-secretase dependent and that Fe65 has a weak stimulating effect on various promoters (Hebert et al., 2006). EGFR promoter was identified as a target for AICD in mouse brain and embryonic fibroblasts (Zhang et al., 2007). Regulators of actin dynamics have been identified as AICD regulated

candidate genes, but a direct association of Fe65 or AICD with their promoters remains to be demonstrated (Muller et al., 2007). AICD has also been implicated in regulating phosphoinositide-mediated Ca^{2+} signaling (Leissring et al., 2002).

1.2.5 FAD-linked mutations

Missense mutations in APP and PS1 lead to familial forms of AD by different mechanisms. Over 30 mutations in the *APP* gene have been identified in 85 families (AD & FTD Mutation Database, http://www.molgen.vib-ua.be/ADMutations). They account for 10% to 15% of early-onset familial AD. They cluster at three secretases sites. Mutations around BACE site, such as "Swedish double mutation" at positions 670/671 (Mullan et al., 1992), increase the rate of proteolysis of APP by BACE and hence increase supply of C99 APP for γ-secretase to produce all Aβ species without affecting the ratio of Aβ42/40 (Cai et al., 1993). The mutations around the γ-secretase cleavage site alter the cleavage position of Aβ to increase the ratio of Aβ42/40. To that group belong e.g. "London mutation" at position 717 that was the first mutations described (Goate et al., 1991), "Florida mutation" at position 716 (Eckman et al., 1997) and "Australian mutation" at position 723 (Kwok et al., 1998). The mutations in the mid-domain of Aβ can have various effects that are currently not well understood; different mutations on the same codon can result in different phenotypes, such as AD, vascular dementia or mixed phenotypes (van Broeckoven and Kumar-Singh, 2006; Zhang-Nunes et al., 2006). The "Dutch mutation" at position 693 near the α-secretase site results in vascular amyloid deposition and cerebral hemorrhage (Levy et al., 1990), whereas "Flemish mutation" at position 692, produces a phenotype which combines features of Alzheimer disease with those of hereditary cerebral hemorrhage with amyloidosis (Hendriks et al., 1992).

Currently, more than 180 FAD-linked PS1 mutations are known (AD & FTD Mutation Database). PS2-containing γ-secretase complexes do not have a major role in mediating amyloid-β production and therefore there are fewer PS2 mutations that lead to FAD (Herreman et al., 1999). FAD-linked mutations in PS1 cause a partial loss of protein function (Baumeister et al., 1997; Song et al., 1999) and most them actually reduce the overall amount of Aβ (Bentahir et al., 2006). However, all of them increase the ratio of Aβ42/Aβ40, showing that Aβ peptide ratios are more important than their absolute levels in the pathogenicity of FAD-linked PS mutations (De Strooper, 2007; Wolfe, 2007). Increased Aβ42/Aβ40 ratio and the reduction in the total amount of Aβ can be explained by reduced

enzyme efficiency by following mechanism. γ-secretase first cleaves Aβ50/Aβ49 or Aβ49/Aβ48 residues (ε-cleavage) and then progresses in a stepwise fashion to produce the shorter forms of amyloid-β (Yagishita et al., 2006; Takami et al., 2009). If the enzyme efficiency is reduced as a consequence of an FAD mutation, the time taken for longer forms of the peptide to diffuse away from the active site between cleavage events increases.

1.3 Treatment of Alzheimer's disease

At the moment, there is no efficient therapy for AD that can cure or slow the progression of the disease. Five drugs are approved to treat the cognitive manifestations of AD: memory loss, confusion, and problems with thinking and reasoning. Four of them are acetylcholinesterase inhibitors (tacrine, rivastigmine, galantamine and donepezil) and one is NMDA receptor antagonist (memantine). Acetylcholinesterase inhibitors increase the concentration of acetylcholine, thus ameliorating cholinergic deficit caused by the death of cholinergic neurons in AD, while NMDA receptor antagonist memantine acts on glutamate receptors and protects from glutamate excitotoxicity. These drugs show only moderate effects on cognitive deficits in AD, and only for a limited period of time, as they cannot compensate for progressing loss of neurons and their circuits.

Several lines of research are currently directed to different facets of the disease process. Most promising are approaches targeted on the reduction of Aβ accumulation by immunotherapy and γ-secretase inhibitors. Pre-clinical studies showed that immunization against Aβ can prevent, but also reverse amyloid pathology and cognitive decline in animal models (Delrieu et al., 2012). Passive immunization in mouse models of AD has demonstrated that peripherally administered antibodies against Aβ can cross blood-brain barrier and reduce amyloid deposits and reverse memory loss (Bard et al., 2000; Kotilinek et al., 2002). Possible mechanisms of Aβ clearance by immunotherapy are phagocytosis by microglia, disaggregation of amyloid deposits after antibody binding and absorption of Aβ from the brain into the bloodstream (Lemere et al., 2006). However, clinical trials showed that although Aβ immunization can reduce plaque load, that effect alone is not enough to improve cognitive functions (Holmes et al., 2008). Monoclonal antibodies against different parts of Aβ (bapineuzumab, solanezumab, gantenerumab, ponezumab) have also been used in clinical trials with moderate success in improving cognitive functions (Delrieu et al., 2012; Robert et al., 2012). Additionally, immunotherapy is often associated with adverse

effects: cerebral amyloid angiopathy that causes micro-hemorrhaging (passive immunization) and autoimmune Th1-cell response (active immunization).

Recent clinical trials with γ-secretase inhibitor semagacestat failed, as this drug not only did not improve, but had worsening effect on cognitive decline, and also caused skin cancers and infections (Doody et al., 2013). However, γ-secretase modulators are promising candidates for drug development, as they can shift production of Aβ species without adverse effects of complete inhibition of γ-secretase (Dimitrov et al., 2013).

Several epidemiological studies suggest that long-term use of non-steroidal anti-inflammatory drugs (NSAID) may prevent the development of AD, but they are ineffective once the disease has started (Imbimbo et al., 2010).

Despite all these novel attempts, supported by recent increase in the social awareness and funding for AD related basic and clinical research, there is still a great demand for further strategies in treatment and prevention of AD.

1.4 Cell adhesion molecule L1

1.4.1 Structure of L1

L1 is a cell adhesion molecule (CAM) and a founding member of the L1 family. The L1 family belongs to the immunoglobulin (Ig) superfamily and in vertebrates it consists of four members: L1, close homologue of L1 (CHL1), neuroglia related CAM (Nr-CAM) and neurofascin (Hortsch, 2000; Maness and Schachner, 2007).

L1 is a 200-220 kDa type I membrane glycoprotein. It consists of six Ig-like domains of the C2-type and five fibronectin type III repeats in the ectodomain, followed by a transmembrane region fo by a highly conserved cytoplasmic tail (Fig 1.3) (Moos et al, 1988). Alternative splicing generates a neuronal isoform of L1 containing RSLE sequence in the cytoplasmic domain that enables clathrin-mediated endocytosis (Kamiguchi et al., 1998) and another insertion in the Ig2 domain that increases homophilic binding (Jacob et al., 2002).

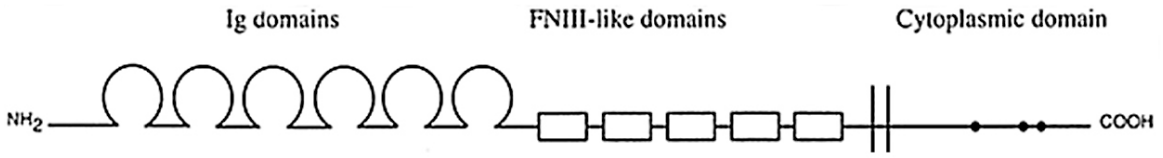

Figure 1.3. Schematic representation of the neural cell adhesion molecule L1 structure. The domain structure of L1 showing the six immunoglobulin (Ig), five fibronectin type III (FnIII), transmembrane, and cytoplasmic domains.

Ectodomain of L1 is heavily glycosylated, including both O- and N-linked glycans (Lindner et al., 1983; Rathjen and Schachner 1984).

1.4.2 Expression and functions of L1 in the nervous system

In the developing nervous system, L1 is expressed in neurons and has an important role in neuronal migration, axonal growth and synapse formation (Dahme et al., 1997; Cohen et al., 1998; Demyanenko et al., 1999; Manes and Schachner, 2007; Schmid et al. 2008). Expression starts early during development, in postmitotic neurons as they start to migrate to their final location (Lindner et al., 1983; Asou et al., 1992). After migration, L1 is predominantly found on growing and fasciculating axons (Fischer et al., 1986; Lagenaur and Lemmon, 1987; Chang et al., 1987). In adult brain the protein remains expressed on nonmyelinated axons, for example in the molecular layer of the cerebellum or the hippocampus, but disappears from myelinated axons, i.e. white matter (Bartsch et al., 1989; Martini and Schachner, 1986). In the peripheral nervous system, L1 is also expressed by nonmyelinating Schwann cells (Martin and Schachner, 1986).

L1 is involved in adhesion between neurons and between neurons and Schwann cells (Rathjen and Schachner, 1984; Faissner et al., 1984), and in myelination (Wood et al., 1990a,b). In addition, L1 has been implicated in axonal regeneration (Martini and Schachner, 1988), learning and memory formation (Rose, 1995), and establishment of inhibitory perisomatic synapses in the hippocampus (Saghatelyan et al., 2004). L1 knockout mice show several structural abnormalities: abnormal pyramidal decussation (Cohen et al., 1998), smaller hippocampus with lower number of principal neurons, reduced size of corpus callosum, enlarged ventricles (Demyanenko et al., 1999), abnormal localization of dopaminergic neurons in mesencephalon and diencephalon (Demyanenko et al., 2001).

Importance of L1 is reflected in pathological mutations in the human L1CAM gene, which underlie a variety of neurological conditions collectively referred to as CRASH (corpus callosum hypoplasia, retardation, adducted thumbs, spastic paraplegia, and hydrocephalus) syndrome or L1 syndrome (Jouet et al., 1995; Weller et al., 2001).

The various functions of L1 involve complex homo- and heterophilic interactions of its six Ig-like and five FnIII-like extracellular domains. These interactions occur in “cis” (between molecules located in the membrane of one cell) or “trans” (between molecules located in the membranes of adjacent cells) conformation. L1 can mediate cell adhesion by several mechanisms, such as homophilic binding involving L1-L1 interactions (Kadmon et al.,

1990a) and assisted homophilic binding between L1 and L1/NCAM complexes at the surface of adjacent cells (Kadmon et al., 1990b). L1 interacts with the axon-associated CAM axonin-1 (Kuhn et al., 1991) and the GPI-anchored molecule CD24 (Kadmon et al., 1995). L1 is also involved in integrin-mediated cell binding and migration through interaction with several RGD-binding integrins, i.e. α5β1, αvβ1, αvβ3 as well as the platelet integrin αIIbβ3 (Ruppert et al., 1995; Felding-Habermann et al., 1997; Blaess et al., 1998).

Similarly, cytoplasmic domain of L1 interacts with a variety of intracellular proteins such as kinases (e.g. casein kinase II, focal adhesion kinase) and adaptor molecules (e.g. ankyrin, AP-2), which modulate the association between L1 and the cytoskeleton (Gil et al., 2003; Bechara et al., 2008) and endosomal membrane systems (Kamiguchi et al.1998; Schaefer et al., 2002; Nakata et al., 2007), respectively.

Interactions between L1 and extracellular and intracellular binding partners not only mediate cell–cell adhesion, but are also involved in intracellular signaling cascades. One example, L1 potentiates neuronal cell migration to extracellular matrix proteins through β1 integrins and intracellular signaling to mitogen-activated protein (MAP) kinase (Thelen et al., 2002). Also, L1 promotes neurite outgrowth via activation of fibroblast growth factor (FGF) receptors and related second messenger cascades in fibroblasts stimulated with extracellular domain of L1 (Doherty et al., 1995).

1.4.3 Therapeutic potential of L1 in animal models of neurological disorders

L1 has been shown as helpful in ameliorating the negative symptoms in several rodent models of acute and chronic neurological disorders.

Intrathecal infusion of L1 fusion protein with a heavy chain of the human Ig (Fc) into the injured rat spinal cord promoted locomotor recovery and regeneration of corticospinal axons (Roonprapunt et al., 2003). L1-transfected embryonic stem cells as well as Schwann cells improved regeneration after spinal cord injury in mice (Chen et al., 2005; Lavdas et al., 2009). Expression of L1 in the spinal cord injured mouse via adeno-associated-virus (AAV) resulted in improved locomotor recovery, regrowth/sprouting and sparing of severed axons, and reduced reactive astrogliosis, by limiting astrocyte proliferation and migration, when injected both acutely and in a sub-chronic phase of injury (Chen et al., 2007; Lee et al., 2012). In a mouse model of Parkinson’s disease, embryonic stem cell-derived L1 overexpressing neural aggregates enhanced survival and migration of transplanted cells, differentiation into dopaminergic neurons, survival of endogenous dopaminergic neurons

and behavioral recovery (Cui et al., 2010). Neural stem cells expressing L1 upon differentiation into astrocytes promoted host–donor cell interactions when transplanted in a mouse model of Parkinson's disease (Ourednik et al., 2009). In a mouse model of Huntington's disease, transplanted L1 overexpressing embryonic stem cells showed preferential neuronal over glial cell differentiation, increased yield of γ-aminobutyric acid (GABA)-ergic neurons, concomitant with behavioral improvement (Bernreuther et al., 2006). Noteworthy in the context of AD is the observation that L1 increases the levels of choline acetyltransferase in the developing and injured central nervous system (Cui et al., 2011a; Lee et al., 2012).

1.5 APPPS1 mice – a model of cerebral amyloidosis

In this study APPPS1 mice described by Radde et al. (2006) were used as a transgenic model of parenchymal amyloidosis, with an early onset of amyloid deposition. These mice coexpress human APP and human PS1, each of them with FAD-linked mutation: double Swedish mutation KM670/671NL in APP and L166P in PS1. Both the PS1 and the APP constructs are under control of the Thy1 promoter, which provides high levels of neuron-specific transgene expression in the postnatal brain. Leucine to proline mutation at position 166 of PS1 is the most aggressive familial AD mutation so far identified, leading to disease onset as early as 24 years of age (Moehlmann et al, 2002; Bentahir et al, 2006). This mutation significantly increases Aβ42/40 ratio by decreasing Aβ40 production, while levels of Aβ42 remain unaffected (Bentahir et al, 2006). Human APP expression in APPPS1 mice is about three times that of endogenous mouse APP expression and is confined mainly to neurons in the neocortex, hippocampus and brain stem and to a lesser extent in the thalamus and striatum. The first amyloid plaques appear in the neocortex already at the age of 6 weeks. Global neuron loss is not present, but it is observed locally in dentate gyrus. Microgliosis and astroglyosis start with appearance of the first plaques. APPPS1 mice show only a minor memory deficit that coincides with significant amyloidosis in the hippocampus (at the age of 8 months). In summary, APPPS1 mice are a model of cerebral amyloidosis, and not directly of AD, as they do not show the tau pathology and significant neuronal loss. The advantages that make this mouse model valuable for investigation of mechanisms of cerebral amyloidosis are the early onset of amyloid pathology, C57BL/6J background known to reduce the variability in Aβ metabolism and deposition (Lehman et al, 2003) and no gender differences in Aβ level and amyloid deposition.

2. AIMS OF THE STUDY

In the present study, L1 was overexpressed in brains of a mouse model of Alzheimer's disease via adenoassociated virus (AAV). AAV-L1 or AAV-GFP, as a negative control, were injected into the hippocampus and occipital cortex of APPPS1 mice at three months of age, when the first histological abnormalities associated with amyloid deposition become apparent. Histological and biochemical analysis was performed four months after injection of the virus, at the time point when most brain areas have developed significant amyloidosis.

Aims of this study were to explore the effects of the overexpression L1 in a mouse brain with cerebral amyloidosis with regard to the main histopathological features of the brain affected with AD: amyloid plaque load, astrogliosis, microgliosis and neuronal and synaptic loss.

Another important aim of this study was to try to elucidate possible mechanisms by which L1 overexpression could affect the features of the disease mentioned above. These questions were approached by investigating interactions between L1 and APP and/or Aβ in different *in vitro* assays, such as *in vitro* aggregation assay of Aβ and direct and indirect binding studies, as well as the cell culture-based assays.

3. MATERIALS

3.1 Chemicals and supplies

All chemicals, reagents and kits were from the following companies: Abcam (Cambridge, UK); Amersham Pharmacia Biotech Europe (Freiburg, Germany); Anamed Elektrophorese (Groß-Bieberau/Rodau, Germany); Applied Biosystems (Darmstadt); Bayer (Leverkusen, Germany); Bio-Rad Laboratories (Munich, Germany); Calbiochem-Novabiochem (Bad Soden, Germany); Carl Roth (Karlsruhe, Germany); Cell Signaling Technology (Danvers, MA, USA); Chemicon via Millipore; Corning (Kaiserslautern, Germany); Covance (Princeton, NJ, USA); Dako (Hamburg, Germany); Dianova (Hamburg, Germany); eBioscience (San Diego, CA, USA); Eppendorf AG (Hamburg, Germany); GE Healthcare (Braunschweig, Germany); Gibco BRL Life Technologies (Karlsruhe, Germany); Greiner Bio-One (Solingen, Germany); Invitrogen (Karlsruhe, Germany); InVivo Biotech Services (Berlin, Germany); Jackson Immuno Research Laboratories Inc. (Suolk, UK) via Dianova; Macherey-Nagel (Duren, Germany); Merck (Darmstadt, Germany); Millipore (Schwalbach, Germany); PAA Laboratories (Colbe, Germany); Parke-Davis/Pfizer (Karlsruhe, Germany); Pierce/Perbio Science (Bonn, Germany); Pineda Antikörper-Service (Berlin; Germany); Promega (Mannheim, Germany); Roche Diagnostics (Mannheim, Germany); R&D Systems (Wiesbaden, Germany); Serva (Heidelberg, Germany); Sigma-Aldrich (Deisenhofen, Germany); Southern Biotechnology Associates (Eching, Germany); SRU Biosystems (Woburn, MA, USA); Synaptic Systems (Göttingen, Germany); Thermo Fischer Scientific (Ulm, Germany); Thermo Scientific (Bonn, Germany); Tocris Bioscience (Ellisville, MI, USA); Vector Laboratories (Burlingame, CA, USA); VWR International GmbH (Darmstadt); Wako Chemicals (Neuss, Germany);

3.2 Animals

Three-month-old transgenic male APPPS1 (C57BL/6J-TgN; Thy1-$APP_{KM670/671NL}$; Thy1-$PS1_{L166P}$) mice were obtained from a breeding colony at the University of Tübingen, Germany. These mice co-express human APP containing KM670/671NL mutation (Swedish double mutation) and human PS-1 with L166P mutation. The expression of transgenes is under the neuron-specific murine Thy-1 promoter element, which is active postnatally with maximum expression after postnatal day 14 (Luthi et al, 1997). The APPPS1 mice are generated on the C57BL/6J background as described in Radde et al., 2006. Briefly,

PS1(L166P) cDNA and APP751(KM670/671NL) cDNA were inserted into the pTSC21 vector which encodes the murine Thy1.2 expression cassette and Thy1-APPKM670/671NL and Thy1-PS1L166P constructs were digested from the vector, purified and coinjected into male pronuclei of C57BL/6J oocytes. Line 21 (APPPS1-21 mice) was selected for further analysis because it had high transgene expression levels, Both transgenes are integrated at the lower arm of chromosome 2 between 40 and 60 cM.

The wild-type C57BL/6J mice were obtained from the breeding colony at the central animal facility of the Universitätsklinikum Hamburg-Eppendorf.

L1-deficient (L1y/-) mice were generated by insertion of a tetracycline-controlled transactivator into the second exon of the L1 gene (Rolf et al., 2001). The L1y/− mice were males carrying the mutant allele of the X-chromosome-linked L1 gene. The wild-type (L1y/+) mice used as controls were male littermates of the L1y/− mice carrying the wild-type L1 allele. The L1 mutants were maintained on a 129SvJ/NMRI genetic background to improve breeding efficiency and attenuate some abnormal features seen in L1y/− mice bred on a C57BL/6J background such as overt hydrocephalus, low body mass (60–80% of L1y/+ mice), poor breeding and high mortality of the L1y/− offspring within the first 2 months after birth (Guseva et al., 2009).

All experiments were conducted in accordance with the “Principles of laboratory animal care" (NIH publication No. 86-23, revised 1985), as well as with German and European Community laws on the protection of experimental animals. The procedures used were approved by the responsible committee of the State of Hamburg. All animal treatments, data acquisition and analyses were performed in a blinded fashion.

3.2 Viral vectors

Viral vectors were provided by Dr. Sebastian Kügler, University of Göttingen, Germany. AAV5 vector was constructed to express L1 or GFP as described by Chen et al. (2007). AAV-5 serotype was used because of its high diffusion and transduction abilities (Peng et al., 2011). The genome of the AAV-L1 construct consists of the short version (530 bp) of the murine cytomegalovirus immediate early promoter (mCMV promoter) (Bett et al., 1994), the cDNA for murine L1 N-terminally tagged with the FLAG-epitope and the bovine growth hormone polyadenylation site. AAV-GFP construct contains woodchuck hepatitis post-transcriptional control element (WPRE) which stabilizes mRNA, resulting in a 2–10-fold higher rate of protein expression. This element is not contained in the AAV-L1 virus due to

vector size restrictions. The genome particles: transducing units ratio ranged from 25:1 to 35:1. The concentrations of the vectors were 3 x 10^9 transducing units/µl.

3.3 Plasmid vector

For transfection of HEK cells pcDNA3.1 plasmid containing full-length murine L1-cDNA (pcDNA3.1-L1 construct) was used (Kalus et al., 2003).

3.3 Cell lines

Human embryonic kidney cells (HEK293) stably transfected with KM670/671NL mutated APP (double Swedish mutation, APP_{sw}) and wild-type PS1 ($PS1_{wt}$) were a kind gift from Professor Harald Steiner, Ludwig Maximillian Universität, Munich, Germany (Citron et al., 1992; Moehlmann et al., 2002).

3.4 Antibodies

Characterized commercial antibodies against cell marker antigens were used for immunohistochemistry and immunofluorescence experiments. Table 3.1 provides information about these antibodies including commercial source, product number, and dilution used in this study. In addition, the following data are essential with regard to some of the antibodies specificities.

Anti-Aβ 6E10 mouse monoclonal antibody recognizes amino acid residues 1-16 of human Aβ. The epitope sequence is EFRHDS (amino acids 3-8 of Aβ). The antibody recognizes full-length APP band of 90-110 kDa, soluble APPα band of 100 kDa and 4 kDa band of Aβ (as well as its aggregates of different size). It does not react with mouse APP or Aβ.

Polyclonal antibodies against C-terminus and N-terminus of APP were raised in rabbit using synthetic peptides corresponding to the C-terminal of human APP_{695} (amino acids 676-695) and the N-terminal of human APP_{695} (amino acids 46-60) as antigens, respectively. These antibodies recognize both human and mouse APP.

Monoclonal mouse antibody against 2',3'-cyclic nucleotide 3'- phosphodiesterase (CNP-ase) is produced from hybridoma cells derived from mice immunized with purified human CNP-ase. In Western blot the antibody recognizes both CNP1 (46 kDa) and CNP2 (48 kDa) bands of the enzyme and in immunohistochemistry of brain sections selectively labels oligodendrocytes.

Monoclonal mouse anti-L1 172R antibody was raised against purified chick L1, and binds to the L1 cytoplasmic domain at about T1172 (adjacent to the YRSL sorting signal). Phosphorylation of either T1172 or Y1176 strongly inhibits binding of 74-5H7 to the L1 cytoplasmic domain.

Monoclonal rat anti-L1 clone 555 and anti-L1 clone 557 antibodies were purified from hybridoma culture supernatant. They are directed against the epitope between the second and third fibronectin type III domain (FnIII) (clone 555) and the N-terminus of the third FnIII repeat (clone 557) of L1. They both recognize 200 kDa, 140 kDa and 80 kDa bands in Western blot (Appel et al., 1995).

Monoclonal anti-NeuN IgG1 is produced from hybridoma cells (clone A60) derived from mice immunized with purified nuclei from mouse brain. The antibody recognizes 2-3 bands in the 46-48 kDa range (manufacturer's technical information).

Anti-neurofilament 200 is IgG fraction of antiserum produced in rabbit using purified neurofilament 200 from bovine spinal cord as immunogen. The antibody recognizes 200 kDa band in Western blot (manufacturer's technical information).

Monoclonal IgG1 anti-parvalbumin mouse antibody is produced from clone PARV-19 hybridoma cells derived by immunizing mice with purified frog muscle parvalbumin. It recognizes a single 12 kDa band on Western blot (manufacturer's technical information).

Polyclonal anti-S-100b antibody is produced by immunizing rabbits with S-100b isolated from cow brain. In Western blots this antibody labels several bands between 9 kDa and 13 kDa (manufacturer's technical data).

Polyclonal rabbit anti-VGAT antibody is raised against a synthetic peptide containing amino acid residues 75-87 of rat VGAT. It recognizes two bands of 57 kDa and 50 kDa on Western blots (manufacturer's technical data).

Secondary antibodies used in this study are listed in Table 3.2.

Antigen	Host	Code/clone	Application Dilution	Source
Actin	Mouse, monoclonal	ab8226	WB - 1:2,000	Abcam
Amyloid precursor protein (APP), β-amyloid (Aβ),	Mouse, monoclonal	Clone 6E10	IHC - 1:1,000 WB - 1:1,000	Covance
APP, N-terminus (APP-NT)	Rabbit	A8967	WB - 1:2,000	Sigma-Aldrich
APP, C-terminus (APP-CT)	Rabbit	A8717	WB - 1:2,000	Sigma-Aldrich
Cyclic nucleotide phosphatase (CNP)	Mouse, monoclonal	C5922 Clone 11-5B	IF - 1:1,000	Sigma-Aldrich
Glutamic acid decarboxylase 67 (GAD67)	Mouse, monoclonal	G5419 Clone K-87	WB - 1:1,000	Sigma-Aldrich
glial fibrillary acidic protein (GFAP)	Rabbit,	Z0334	IHC - 1:2,000 WB - 1:5,000	Dako Cytomation
Glyceraldehyde 3-phosphate dehydrogenase (GAPDH)	Mouse, monoclonal	CB1001 Clone 6C5	WB - 1:2,000	Millipore
Ionized calcium-binding adapter molecule 1 (Iba1)	Rabbit	019-19741	IHC - 1:1,500	Wako Chemicals
L1	Mouse, monoclonal	172R Clone 74-5H7	WB - 1:1,000	Covance
L1	Rat, monoclonal	Clone 555	IF - 2 µg/ml WB - 2 µg/ml IP - 2 µg/ml	InVivo Biotech
L1	Rat, monoclonal	Clone 557	WB - 2 µg/ml IP - 2 µg/ml	InVivo Biotech
Mac-2 (galectin-3)	Rat, monoclonal	14-5301 Clone M3/38	IHC - 1:500	e-Bioscience
Neurofilament 200	Rabbit	N4142	IF - 1:1,000	Sigma-Aldrich
S-100b	Rabbit	Z0311	IF - 1:500	Dako Cytomation
Vesicular inhibitory neurotransmitter transporter (VGAT)	Rabbit,	131 003	IF - 1:1000	Synaptic Systems

Table 3.1. Primary antibodies used in this study. IHC stands for immunohistochemistry, IF for immunofluorescence, IP for immunoprecipitation and WB for Western blot.

Host	Specificity	Conjugate	Application/ Dilution
Goat	anti-rabbit	Cy3	IF - 1:200
Goat	anti-mouse	Cy3	IF - 1:200
Donkey	anti-rat	Cy2	IF, ML - 1:200
Donkey	anti-rabbit	Cy-3	IF, ML - 1:200
Donkey	anti-rabbit	biotin	IHC - 1:200
Donkey	anti-mouse	biotin	IHC - 1:200
Donkey	anti-rat	biotin	IHC - 1:200
Donkey	anti-mouse	HRP	WB - 1:10,000
Donkey	anti-rat	HRP	WB - 1:10,000
Goat	anti-rabbit	HRP	WB - 1:10,000

Table 3.2. Secondary antibodies used in this study. All secondary antibodies were obtained from Dianova.

3.5 Protein constructs and peptides

Recombinant L1–Fc and CHL1–Fc containing the extracellular domain of mouse L1 and CHL1, respectively, fused to the Fc portion of human IgG were produced in eukaryotic expression system and purified as described (Chen et al., 1999). Being produced in a eukaryotic expression system (CHO cells), these protein constructs were glycosylated.

Immunoglobulin-like domains 1-6 (Ig1-6) and fibronectin type III homologous repeats 1-5 (Fn1-5), Fn1-2, Fn2-3 and Fn4-5 of L1 were produced as described (Appel et al., 1993; 1995). The Ig1-6 and Fn1-5 recombinant proteins were produced in a eukaryotic protein production system (CHO cells) and therefore they were normally N- and O-glycosylated, whereas the Fn1-2, Fn2-3 and Fn4-5 proteins were produced in *E. coli* and thus non-glycosylated.

Human Fc fragment was obtained from Dianova.

Synthetic human Aβ40 and Aβ42 peptides were from Tocris Bioscience and Thermo Fisher Scientific, respectively.

3.6 Cell culture reagents

Following reagents were used for human embryonic kidney (HEK) cell culture: Dulbecco's modified Eagle Medium (DMEM) with L-Glutamine, high glucose (4.5 g/l) (PAA); fetal calf serum (FCS), heat inactivated (PAA); Hanks´ BSS (HBSS) without Ca^{2+} and Mg^{2+} with phenol red (PAA); Penicillin-Streptomycin Solution, 100X (10,000 I.U. penicillin, 10,000

µg/mL; streptomycin, PAA); Trypsin/EDTA solution 1X (0.025% trypsin, 0.01% EDTA in phosphate buffered saline); DMSO, cell culture grade (Sigma Aldrich).

For transient transfection of HEK cells Fugene HD transfection reagent (Promega) was used.

4. METHODS

4.1 Surgical procedures

For surgery, mice were anaesthetized by intraperitoneal injections containing the mixture of ketamine (Ketanest® 100 mg per kg body weight, Parke-Davis/Pfizer) and xylazine (5 mg Rompun® per kg body weight, Bayer). The head was placed in a mouse stereotaxic frame (Stoelting Europe, Dublin, Ireland) and scull was exposed. Two holes for injections were drilled in the scull unilaterally in the right hemisphere using a dental drill (KaVo, Biberach/Riß, Germany). Mice received injections of AAV-L1 or AAV-GFP (1 µl solution/injection at the concentration of 3 x 10^9 transducing units/µl) using a Hamilton syringe unilaterally into the right hemisphere, with one injection targeted to the hippocampus and the other to the occipital cortex (Fig. 4.1). Coordinates for the injections were, according to the Mouse Brain Atlas (Franklin and Paxinos, 2007): hippocampus: -2 mm from Bregma, 1.5 mm from the midline, 1.5 mm deep; cortex: -3 mm from Bregma, 2 mm from the midline, 0.5 mm deep.

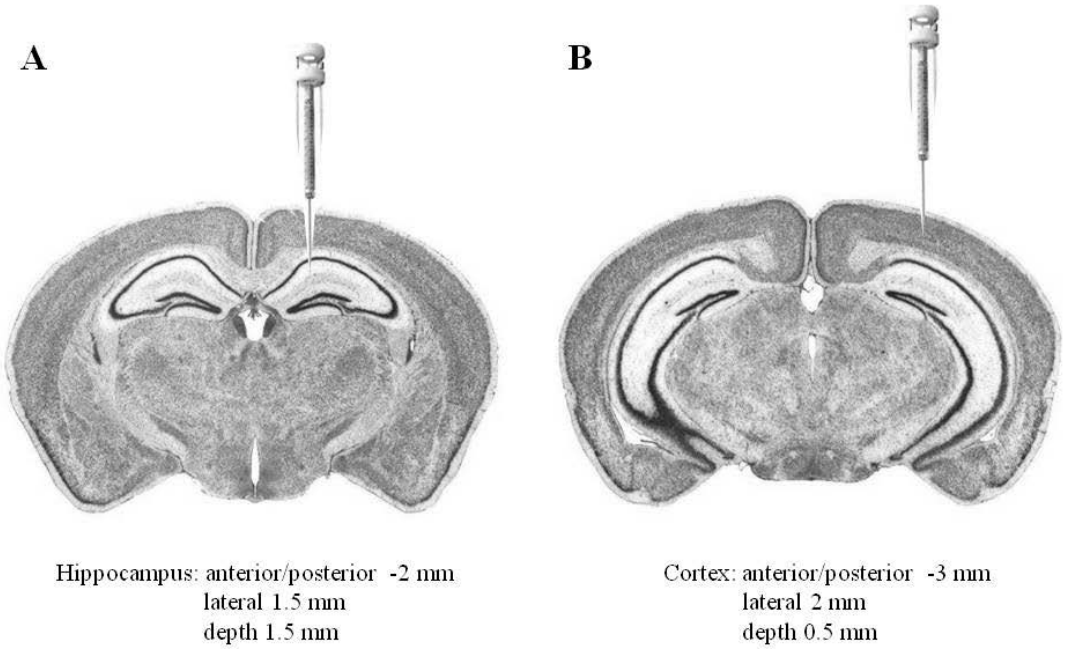

Figure 4.1. Sites of AAV-L1 and AAV-GFP injection. Nissl stained coronal sections of mouse brain showing approximate planes of injections in hippocampus (A) and occipital cortex (B). Images taken from digital brain atlas (http://www.hms.harvard.edu/research/brain/atlas.html).

After surgery, mice were kept in a heated room (37°C) for several hours to prevent hypothermia and thereafter singly housed in a temperature-controlled (22°C) room with water and standard food provided *ad libitum* for 4 months before being sacrificed for histological and biochemical experiments.

4.2 Histological methods

4.2.1 Tissue fixation and sectioning

Buffers and solutions:

0.2 M cacodylate buffer, pH7.3

To 0.4 M sodium cacodylate (Sigma-Aldrich) solution (42.8 g in 500 ml distilled water) 0.4 M HCl was added until pH reached 7.3 (approximately 34 ml required). The solution was filled up to 1000 ml with distilled water.

Cryoprotective solution

15 % sucrose in 0.1M cacodylate buffer, pH7.3

Fixative with cacodylate buffer:

4 % paraformaldehyde

0.1 % $CaCl_2$

0.1 M cacodylate buffer

pH7.3

Preparation: 40 g paraformaldehyde was added to 400 ml water in a glass flask and warmed up to 100°C in a water bath under constant stirring. After boiling started, 1 M NaOH was added slowly (drop by drop) until the milky suspension was cleared (at neutral pH). The solution was cooled to RT under running tap water and 500 ml 0.2 M sodium cacodylate buffer (pH7.3) and 1 g anhydrous $CaCl_2$ were added and pH was adjusted to 7.3. The solution was filled up to 1000 ml and filtered.

Mice were anaesthetized with a 16% solution of sodium pentobarbital (Narcoren, Merial, Hallbergmoos, Germany, 5 µl per g body weight, intraperitoneally). The animals were transcardially perfused with fixative for 15 min at room temperature (RT). Following perfusion, the brains were removed and postfixed in the same fixative overnight and placed in 15 % cryoprotective solution for 2 days, all at 4°C. Brains were then frozen by immersion for 2 min in 2-methyl-butane precooled to -25°C and stored in liquid nitrogen until sectioned.

Serial coronal sections of 25 µm thickness were cut in a cryostat (Leica CM3050, Leica Instruments, Nußloch, Germany) and collected on SuperFrost Plus glass slides (Roth). The sections were stored at −20°C.

4.2.2 Immunofluorescence

Buffers and solutions

Blocking solution	5 % normal goat or donkey serum 0.2% Triton X-100 0.02% sodium azide in PBS pH 7.3
Phosphate buffered saline (PBS)	137 mM NaCl 2,7 mM KCl 8 mM Na2HPO4 1,5 mM KH2PO4 pH 7.3
PBS-lambda-carrageenan solution	0.5% lambda-carrageenan (Sigma-Aldrich) 0.02% sodium azide in PBS
Sodium citrate solution	0.01 M sodium citrate pH9.0

In order to retrieve antigens in fixed tissue, water-bath antigen de-masking was performed by incubating sections in sodium citrate solution for 30 min at 80°C. For double-labeling with GFP and cell type-specific antibodies the temperature for antigen retrieval was lowered to 70°C in order to preserve GFP epifluorescence. Non-specific binding was blocked in blocking solution containing normal goat serum for 1 h at RT. Incubation with the primary antibody diluted as indicated in Table 3.1 in PBS-lambda-carrageenan solution, was carried out for 3 days at 4°C. After washing in PBS (3 x 15 min at RT), the appropriate fluorescently-labeled secondary antibody, diluted 1:200 in PBS-lambda-carrageenan solution, was applied for 2 h at RT in the dark. After a subsequent wash in PBS, cell nuclei were

stained for 10 min at RT with bis-benzimide solution (Hoechst 33258 dye, 5 µg/ml in PBS, Sigma-Aldrich). Finally, the sections were washed again, mounted in anti-quenching medium Fluoromount G (Southern Biotechnology Associates) and stored in the dark at 4°C. As a negative control instead of primary antibody sections were incubated with a normal (pre-immune) serum from the animal in which the primary antibody has been produced with the resulting lack of fluorescent signal. Additionally, L1 555 antibody was controlled by staining L1y/- brain sections, with the resulting lack of fluorescent signal. For double labeling sections were blocked in blocking solution containing normal donkey serum and incubated with the mixture of primary antibodies. Appropriate secondary antibodies preaddsorbed to eliminate cross-reactions with others species and with other immunoglobulin classes were used. To ensure for specificity of double immunofluorescent staining single primary antibodies were used with a mixture of secondary antibodies, which resulted in the lack of staining with the secondary antibody for which the primary antibody was omitted.

4.2.3 Immunohistochemistry

The avidin/biotin-peroxidase method with the diaminobenzidine (DAB) substrate as a chromogen was used to visualize Aβ, GFAP, Iba-1 and Mac-2 antibodies. Endogenous peroxidase activity was blocked in 0.3 % H_2O_2 in methanol for 30 min at RT, followed by water-bath antigen retrieval as described in chapter 4.2.2. Sections were then blocked in blocking solution containing normal goat or donkey serum in PBS for 1 h at RT and incubated in primary antibody overnight at 4°C. After washing in PBS (3 x 15 min at RT), biotinylated secondary antibody diluted 1:200 in PBS was applied for 1 h at RT. Sections were then washed again in PBS and incubated in ABC reagent (Vectastain Elite ABC Kit, Vector Laboratories) for 30 min at RT. Sections were then washed 3 x 5 min in PBS and staining was developed in peroxidase substrate solution (DAB, Vector Laboratories) until satisfying intensity, usually 2-4 min.

Prior to immunostaining for Aβ, sections were incubated in 70% formic acid for 30 min at RT to denature amyloid aggregates and expose the epitope within Aβ.

4.2.4 Congo red staining of amyloid plaques

Congophilic plaques were visualized using the Congo red kit (Sigma-Aldrich), according to the manufacturer's instructions. Brain sections were first incubated in alkaline sodium

chloride solution for 20 min at RT and then in alkaline Congo red solution for 20 min at RT. Both sodium chloride solution and Congo red solution are alcoholic solutions 80 % saturated with sodium chloride, and the latter contains 0.2 % of Congo red. Solutions were alkalized with sodium hydroxide solution (1% sodium hydroxide). All solutions were provided in the kit. Congo red staining was followed by GFAP, Iba-1 or Mac-2 immunohistochemistry as described above.

4.3 Microscopy and photographic documentation

Images were documented on an LSM 510 confocal microscope (Zeiss, Oberkochen, Germany) or an Axiophot 2 microscope equipped with a digital camera AxioCam HRC and AxioVision software (Zeiss) and processed for brightness and contrast using Adobe Photoshop CS5 software (Adobe Systems Inc., San Jose, CA).

4.3.1 Analysis of amyloid load

Amyloid plaque load was analyzed on brain sections immunostained for Aβ using Axiophot 2 microscope and Axiovision softvare. Following parameters were measured: area of sections of hippocampus and occipital cortex, number of Aβ-immunostained plaques in hippocampus and cortex, as well as area of single plaques cross-sections. Density of plaques was expressed as number of plaques per area.

4.3.2 Stereological analyses

The optical disector principle was used to estimate cell densities of GFAP-, S-100b-, Iba-1-, NeuN-, and parvalbumin-positive cells as described (Irintchev et al., 2005). The counts were performed on an Axioskop microscope (Zeiss) equipped with a motorized stage and Neurolucida software-controlled computer system (Microbrightfield, Colchester, VT). Sections were observed under low-power magnification (10× objective) with a 365/420 nm excitation/emission filter set (01, Zeiss, blue fluorescence). The nuclear staining allowed delineation of hippocampal and occipital cortical structures using the Neurolucida software. Every 10th section of the hippocampus and the occipital cortex were analyzed. Cell densities were estimated by counting nuclei of labeled cells within systematically randomly spaced optical disectors. The parameters for this analysis were: guard space depth 2 μm, base and height of the disector 3,600 μm^2 and 10 μm, respectively, distance between the optical disectors 60 μm, objective 40× Plan-Neofluar 40×/0.75. The same parameters were used for

the counting of granule cells except for the base of the disector and the space between disectors, which were 900 μm^2 and 90 μm, respectively. Area measurements were performed directly under the Zeiss Axiophot microscope using the Neurolucida software. Volumes of the hippocampus and the occipital cortex were calculated using Cavalieri's principle. Accumulations of Iba-1 and Mac-2 immunoreactive cells around Congo red positive plaques in the hippocampus were counted per section area.

4.3.3 Light-microscopic analysis of perisomatic terminals

Estimation of perisomatic puncta and area of principal cell bodies was performed as described (Morellini et al., 2010; Nikonenko et al., 2006). Stacks of images of 1 μm thickness were obtained from different hippocampal subfields in VGAT immunostained sections using an LSM 510 confocal microscope (Zeiss, 63x oil immersion objective, 1024×1024 pixel resolution). One image per cell at the level of the largest cell-body cross-sectional area was used to measure soma area and count individually discernible perisomatic puncta. Numbers of VGAT-positive puncta were normalized to the perimeter of the cell profile. At least 20 cells per hippocampus region were counted. All measurements were performed using Image Tool 2.0 software (University of Texas Health Science Center, San Antonio, TX).

4.4 Cell culture methods

4.4.1 Maintenance and long-term storage of HEK cells

Culture medium	DMEM
	10% FCS
	Penicillin-Streptomycin (1X)
	Geneticin (0.2 mg/ml)
	Zeocin (0.2 mg/ml).
Freezing medium	DMEM
	20% FCS
	10% DMSO

HEK293 cells stably transfected with APP with double Swedish mutation KM670/671NL and PS1 were cultivated at the temperature of 37˚C, 5% CO_2 and 90% relative humidity.

Medium was changed every second day and the cells were passaged approximately every four days.

For passaging, cells were washed with HBSS and then incubated with Trypsin-EDTA solution in the incubator for 2-3 min. Trypsin activity was then stopped by adding culture medium, the cells were centrifuged (5 min, 1,000 g, RT), resuspended in culture medium and split 1:5 - 1:10.

For long-term storage cells were grown to 70% confluency, detached by Trypsin-EDTA solution (as described above), and resuspended in freezing medium, in 1 ml aliquots containing 10^7 cells. Cells were then placed in containers with isopropanol and gradually frozen in -80˚C freezer. After 24 h they were transferred in liquid nitrogen tank.

When necessary, frozen cells were thawed in a 37˚C waterbath, resuspended in warm DMEM medium without selection antibiotics, centrifuged as described above and cultivated in culture medium without selection antibiotics until first passage.

4.4.2 Transient transfection of HEK cells

Transfection mixture:	2 µg DNA (pcDNA3.1-L1)
(*per well*)	6 µl Fugene HD (Promega)
	100 µl DMEM

For transient transfection, HEK cells at 50-70% confluency were detached by Trypsin-EDTA solution as described in 4.4.1., resuspended in culture medium and plated in 12-well plates at $2x10^5$ cells per well in 1 ml of culture medium. Immediately after plating transfection mixture was added to the medium. After 24 h conditioned medium was collected, cleared by centrifugation at 100,000 g at 4°C for 1 h and stored at -80°C until Western blot or ELISA analysis. Cells were collected and lysed in RIPA buffer for 1 h at 4°C. After that, cells were centrifuged at 10,000 g for 10 min and supernatants were saved at -20°C for Western blot analysis.

4.5 Biochemical methods

4.5.1 Preparation of brain homogenates

Buffers and solutions

RIPA buffer	50 mM Tris
	180 mM NaCl
	1% NP40
	1 mM sodium pyrophosphate
	pH 7.4
Tris buffered saline	20 mM Tris
(TBS)	137 mM NaCl
	pH 7.6

To analyze protein expression levels, mouse brains were homogenized in RIPA or TBS buffer containing protease inhibitor cocktail (Roche Diagnostics). Homogenates were cleared by centrifugation (1,000 g, 10 min, 4˚C) and protein concentration was measured by BCA test.

4.5.2 Determination of protein concentration

For the determination of the protein concentration in the brain homogenates, cell lysates and purified proteins, the BCA assay (bicinchoninic acid assay) Kit (Thermo Scientific) was used. 10 µl of the sample were placed on a microplate and incubated for 30 min at 37°C with 200 µl of the solution which was prepared according to the kit manual. Then the absorbance was measured at 562 nm wavelength by µQuantTM microplate spectrophotometer (Bio-Tek Instruments Inc., Winooski, Vermont, USA). The protein concentration was evaluated from the absorbance using a calibration curve.

4.5.3 SDS-PAGE (polyacrilamyde gel electrophoresis) and Western blot analysis

Buffers and solutions

Anode buffer (Tris-tricine PAGE)	0.2M Tris pH8.9 with HCl
Blocking buffer	4 % skimmed milk powder in PBST
Cathode buffer (Tris-tricine PAGE)	0.1M Tris 0.1M Tricine 0.1 % SDS (pH should be 8.25 without adjusting)
Gel buffer (Tris-tricine PAGE) 3X	3 M Tris 0.3 % SDS pH8.45 with HCl
PBS-T	0.05% Tween-20 in PBS
Running buffer	25 mM Tris 192 mM glycine 0.1 % SDS
SDS-PAGE sample buffer *(4x Laemmli buffer)*	200 mM Tris-Cl (pH6.8) 40% glycerol 8% SDS 0.4% bromophenol blue 5% (w/v) DTT or β-Mercaptoethanol
Stripping solution	3 % glacial acetic acid 0.5 M NaCl
Transfer buffer	25 mM Tris 192 mM glycine 20% methanol

Component	Stacking gel	Resolving gel	Resolving gel

	4%	10%	12%
30% Acrylamide-Bis (29:1)	0.5 ml	2.67 ml	3.2 ml
dH_2O	2.10 ml	2.23 ml	1.7 ml
1 M Tris-HCl pH8.8	-	3 ml	3 ml
1 M Tris-HCl pH6.8	0.38 ml	-	-
10 % SDS	40 µl	80 µl	80 µl
10 % APS	15 µl	15 µl	15 µl
TEMED	6 µl	6 µl	6 µl
Total volume	3 ml	8 ml	8 ml

Table 4.1. Composition of Tris-glycine polyacrylamide gels. Gel dimensions were: height 6 cm, width 6.5 cm, and thickness 1 mm.

Component	Stacking gel 4%	Resolving gel 10%	Resolving gel 12%
30% Acrylamide-Bis (29:1)	0.5 ml	2.5 ml	3 ml
dH_2O	2.32 ml	2.5 ml	2 ml
Gel buffer 3X	0.93 ml	2.5 ml	2.5 ml
10 % APS	15 µl	15 µl	15 µl
TEMED	6 µl	6 µl	6 µl
Total volume	3.75 ml	7.5 ml	7.5 ml

Table 4.2. Composition of Tris-tricine polyacrylamide gels. Gel dimensions were: height 6 cm, width 6.5 cm, and thickness 1 mm.

Preparation of samples for Western blot analysis is described in chapters 4.5.1 and 4.4.2. Appropriate amounts of brain homogenates were mixed with sample buffer and heated at 95˚C for 5 min. The samples were electrophoretically resolved on 10 or 12% Tris-glycine SDS polyacrylamide gels (Table 4.1). Molecular weight standards were Precision Plus Protein All Blue Standards (BioRad). The samples were then transferred onto 0.2 µm polyvinylidene difluoride (PVDF, Millipore) membrane for 2 h at 90 V. Membrane was then blocked in blocking buffer for 1 h at RT and probed with primary antibody overnight at 4˚C or for 1-2 h at RT. After that, membrane was washed 6 times for 5 min in PBST and incubated with appropriate HRP-coupled secondary antibody (Dianova). After washing, proteins were visualized using ECL reagent (Amersham) on BioMax film (Kodak), or

detected by LAS 4000 Mini camera (GE Healthcare). Chemiluminescence was quantified using TINA 2.09 software (University of Manchester, UK).

Cell lysates or conditioned media from cultured HEK cells were prepared for analysis the same way as brain homogenates, resolved on 10 or 12% Tris-glycine SDS polyacrylamide gels (Table 4.2) using tricine-based anode and cathode running buffers.

For analysis of Aβ42 aggregates, precast gradient 10-20% Tris-tricine gels (Anamed Elektrophorese) and tricine-based anode and cathode running buffers were used.

In order to remove antibodies for multiple antigen detection, membranes were incubated with stripping solution for 20 min at RT. Stripped membranes were neutralized by washing shortly in 0.1 M Tris-HCl pH8.0, washed in PBST, blocked and incubated with another primary antibody.

4.5.4 Immunoprecipitation

Homogenates from adult mouse brains were prepared in RIPA buffer containing complete protease inhibitor cocktail (Roche Diagnostics), lysed for 40 min at 4°C and centrifuged for 5 min at 14000g at 4°C. Supernatants containing 1 mg of total protein were brought to the volume of 1 ml with RIPA buffer and cleared with protein A-magnetic beads (Dynabeads, Invitrogen) for 1 h at 4°C. After that samples were incubated with corresponding antibodies or non-specific control Ig for 1 h at 4°C, followed by precipitation with protein A-magnetic beads overnight at 4°C. The beads were then washed 3 times with RIPA buffer, 2 times with PBS and boiled in sample buffer. Eluted material was used for Western blot analysis.

4.5.5 ELISA measurement of Aβ

4 months after AAV-L1 injection (as described in 4.1), injected and contralateral control brain hemispheres were isolated, frozen in liquid nitrogen and stored at -80°C until used for analysis of Aβ content by ELISA. The samples were produced in a three-step extraction. In the first step, soluble TBS fraction of Aβ was extracted. The brain hemispheres were homogenized in 1 ml TBS (4.5.1) containing protease inhibitors (Roche) per 150 mg wet weight tissue. Following centrifugation (350,000 g, 30 min, 4°C), supernatant containing soluble Aβ was removed and stored at -80°C until use. The pellet was resuspended in 2% SDS in TBS with protease inhibitors using the same volume as in the first step, and then homogenized and centrifuged as described. The supernatant (SDS fraction) was removed and the pellet was extracted with 70% formic acid (FA) in water. FA fraction was cleared by

centrifugation (10000 g, 10 min, 4°C). The levels of Aβ40 and Aβ42 in different fractions were measured using Aβ x-40 and x-42 ELISA kits (Human/Rat β Amyloid (40) ELISA Kit Wako II and Human/Rat β Amyloid (42) ELISA Kit Wako, high-sensitive; Wako, Osaka, Japan) according to the manufacturer's instructions. Briefly, 100 µl of standards and samples were applied per well of 96-well microplate precoated with capture BNT77 antibody. Both standards and samples were diluted in Standard and Sample Diluent (SSD). Dynamic range of the assay was 1-100 pmol/l for Aβ40 and 0.2-20 pmol/l for Aβ42. For the measurement of Aβ40 fractions were diluted in the following way: TBS fraction 3x, SDS fraction 300x, and FA fraction was first neutralized by 20x dilution in 1M Tris Base and then additionally diluted 500x in SSD. Dilutions for Aβ42 measurement were 30x for TBS, 2000x for SDS and 2000x for neutralized FA fraction. All samples were tested in duplicates. Plates were sealed and refrigerated overnight. After washing 5 times with wash solution, 100 µl of HRP-conjugated detection antibody solution ($BA27(Fab')_2$ for Aβ40 and BC05(Fab') for Aβ42) per well was applied and the plate was incubated at 4°C for 2 h in Aβ40 assay or 1 h for Aβ42 assay. Plate was then washed again 5 times with washing solution, and 100 µl tetramethylbenzidine (TMB) solution was added per well, starting the HRP reaction at room temperature. The reaction was stopped after 30 min with 100 µl stop solution and the absorbance was read at 450 nm using µQuantTM microplate spectrophotometer (Bio-Tek InstrumentsInc., Winooski, Vermont, USA). All the components of the assay were provided in the kit.

4.5.6 Chemokine (C-C motif) ligand 2 ELISA

For chemokine (C-C motif) ligand 2 (CCL2) ELISA, the above described TBS soluble fractions were used. The protein concentration was quantified with the BCA assay kit (Pierce, Rockford, IL) and the CCL2 levels were measured using CCL2 ELISA Kit (Mouse CCL2 ELISA Ready-SET-Go!, eBioscience) according to the manufacturer's instructions. First, Corning Costar 9018 plate was coated with 100 µl of capture antibody diluted in coating buffer (provided in the kit) per well, overnight at 4˚C. Plate was then washed 3 times with wash buffer (PBS with 0.05% Tween-20) and blocked with 200 µL assay diluent (provided in the kit) per well at room temperature for 1 hour. Standards were diluted in assay diluent to create standard curve range 15 - 2000 pg/mL. 100 µL of standards and samples were added in duplicates to the appropriate wells and the plate was incubated overnight at 4°C, followed by washing 3 times. 100 µL of detection antibody diluted in assay diluent was

added per well, the plate was incubated at room temperature for 1 hour and washed 3 times. After that, 100 µL/well of avidin-HRP (provided in the kit) diluted in assay diluent was added, the plate was incubated at room temperature for 30 min and washed 5 times. Substrate solution (TMB, provided in the kit) was then added (100 µL per well) and the plate incubated at room temperature for 15 min. The reaction was stopped with 50 µL of stop solution (1M H_3PO_4) per well and the plate was read at 450 nm using µQuantTM microplate spectrophotometer (Bio-Tek InstrumentsInc.).

4.5.7 *In vitro* Aβ42 aggregation

The Aβ42 peptide was prepared for the aggregation assay according to Stine et al. (2011). Aβ42 was dissolved in hexafluoroisopropanol (HFIP) in order to break beta-sheet structures and ensure that most Aβ is present as monomer. 1 mM Aβ42 solution was prepared by adding 1 ml HFIP to 4.5 mg of Aβ42 powder. After the peptide was completely dissolved, solution of Aβ42 in HFIP was incubated at room temperature for at least 30 min more and then aliquoted in 50 µl aliquots containing 225 µg Aβ42. Microcentrifuge tubes were left open under the fume hood overnight in order to allow HFIP to evaporate. Dried peptide was stored at −20°C. Dimethyl sulfoxide (DMSO) was used to solubilize dry peptide and 5 mM Aβ42 DMSO stock was prepared by adding 10 µL of DMSO to 225 µg Aβ42 and sonicating the solution for 10 min in a bath sonicator. 100 µM Aβ42 solution was then prepared by adding phenol red-free Dulbecco's Modified Eagle Medium (DMEM) and incubated for 2 days at 37°C in the presence of 1 µM L1-Fc or CHL1-Fc in order to test oligomer formation. After incubation, the samples were analyzed by Western blot. Briefly, samples containing 1µg Aβ42 were boiled in sample buffer, separated on 10-20% Tris-Tricine gels (Anamed) by SDS –PAGE, transferred onto PVDF membrane and probed with 6E10 antibody against Aβ.

4.5.8 Label-free binding assay (BIND assay)

BIND assay was used to test whether L1 and Aβ peptides interact directly. BIND® technology (SRU Biosystems) is a label-free assay technology that enables detection of a variety of biomolecular interactions, ranging from small drug-like molecules binding detection to cell-based assays. BIND uses optical biosensors based on photonic crystals to measure the kinetic adsorption of biomolecular materials through their greater dielectric permittivity at optical wavelengths compared to water (Cooper, 2002). Biosensors are produced with a proprietary nanostructured optical grating (narrowband guided-mode

resonance reflectance filter) that is incorporated within each well of standard 96-, 384- and 1536-well microplates.

Upon illumination with broadband light the optical grating reflects only a narrow range of wavelengths of light, called Peak Wavelength Value or PWV. When a biomolecule or cell binds to the biosensor surface or immobilized target on the sensor surface, this reflected wavelength increases; conversely, detachment of a molecule is observed as a decrease in PWV (Cunningham et al., 2004). Real time binding can be detected by measuring PWV shift over time, which is directly proportional to the mass of the bound molecule. This allows detection of protein–protein interactions without labeling of proteins, thereby minimizing side effects und unspecific binding.

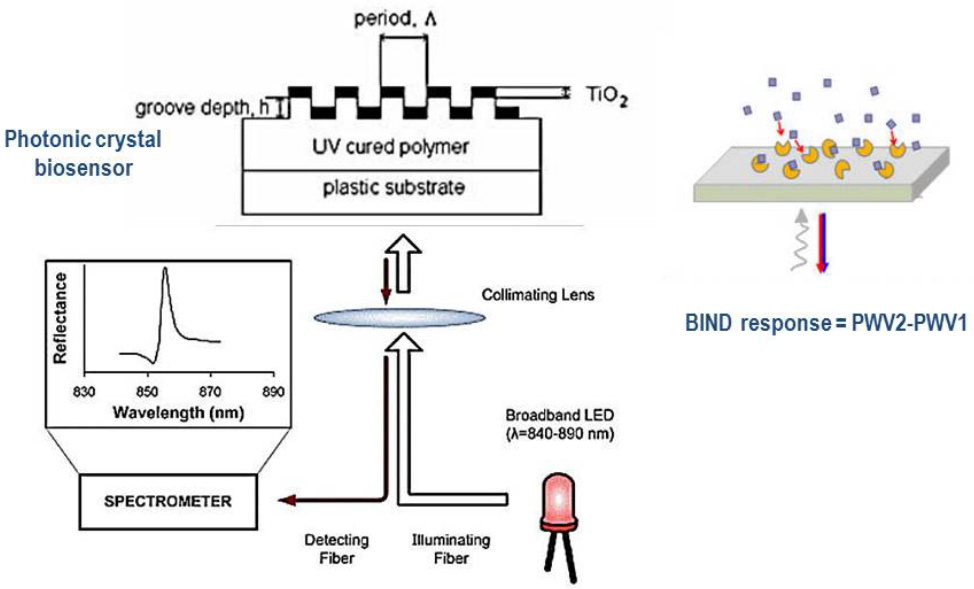

Figure 4.2. Optical path of BIND Reader. Schematic representation TiO_2 grating and path of light signal. BIND response is a difference in peak wavelength value (PWV) associated with a binding event.

384-well plates with TiO_2 surface (SRU Biosystems) were washed three times with Dulbecco's PBS containing Ca^{2+} and Mg^{2+} (PBS^+) (PAA Laboratories) and coated overnight at 4°C with 250 ng of Aβ40 or Aβ42 peptide per well. Wells were then washed three times with PBS^+ and PWV shift was measured on BIND PROFILER reader (SRU Biosystems) to control for sufficient coating of proteins. Wells were then blocked with 2% bovine serum albumin (BSA) in PBS^+ for 3 h at room temperature. After three washes with PBS^+, PWV shift was determined, and different concentrations of ligands in PBS^+ were added to the wells. L1-Fc and CHL1-Fc constructs, Fc fragment, immunoglobulin domains (Ig1-6) and

fibronectin type III domains (Fn1-5, Fn1-2, Fn2-3 and Fn4-5) were used at concentrations 0.1 µM, 0.5 µM, and 1 µM. Binding of ligands to substrate-coat protein or peptide was measured every 30 s for maximally 60 min. Values obtained from wells without ligands were set as background and subtracted from values obtained with ligand solution. All ligands were tested in triplicates.

4.6 Statistical analysis

All numerical data are presented as group mean values with standard deviations (SD). Statistical tests used for comparisons are indicated in the figure legends, and the threshold value for acceptance of differences was 5%. Analyses were performed using the SYSTAT 9 software package (SPSS, Chicago, IL, USA).

5. RESULTS

To analyze the effects of L1 overexpression on amyloid-induced pathology in APPPS1 mice, AAV serotype 5 was used to deliver L1 into the brain. The AAV-L1 construct is designed to drive L1 expression under the control of the murine cytomegalovirus immediate-early promoter and has already been successfully used to overexpress L1 in the spinal cord of mice (Chen et al., 2007; Lee et al., 2012). AAV-L1 and AAV-GFP construct as a control were injected unilaterally into the hippocampus and occipital cortex of 3-month-old APPPS1 mice and the brains were analyzed 4 months after injection.

5.1 AAV - mediated transduction of the occipital cortex and hippocampus

5.1.1 AAV-GFP transduction reveals preference of AAV5 for neurons and astrocytes

For quantitative determination of cellular targets of AAV-mediated gene transfer in the brain, a preliminary experiment was performed in our laboratory (Christian Müller, doctoral thesis). Since L1 is expressed at the cell surface of neuronal cell bodies and non-myelinated axons, it is difficult to estimate the number of transduced cells. Therefore, GFP was used as a reporter for transduction, being under the control of the same universal promoter that drives the L1 expression. AAV-GFP was injected into the occipital cortex and hippocampus of four 3-month-old wild-type C57BL/6J mice, using the stereotaxic coordinates described in the Methods section. Mice were sacrificed one month after virus injection and their brains were analyzed for GFP expression. Using cell type-specific markers for neurons (NeuN), astrocytes (S-100b), oligodendrocytes (CNPase) and microglial cells/macrophages (Iba-1), most of the GFP-transduced cells were identified as neurons or astrocytes. A small percentage of the transduced cells were oligodendrocytes, which is in accordance with their low relative numbers in the gray matter in comparison to neurons and astrocytes. Microglial cells/macrophages expressing GFP could not be detected. Since approximately 90% of all GFP-expressing cells were neuronal and astroglial cells, it is likely that these cells, as the most numerous and possibly most susceptible cells to AAV5 viral transduction, are the ones that convey the effects of the transduced genes. Importantly, one month after virus injection the stereologically determined overall numbers of transduced cells were relatively large (2,389 ± 384 cells in the total hippocampus, and 1,289 ± 291 cells in the total occipital cortex) and transduced cells were almost exclusively detected in the injected brain hemispheres.

5.1.2 Expression of L1 in neurons and astrocytes after AAV-L1 transduction is confirmed in L1-deficient mice

Although AAV-GFP transduction showed significant numbers of transduced cells, it was necessary to confirm that AAV-mediated expression of L1 in neurons and astrocytes is achieved. As already mentioned in the previous chapter, as L1 is expressed at the cell surface of neuronal cell bodies and non-myelinated axons it would be difficult to observe increase in the expression in wild-type mice. Therefore, AAV-L1 was injected into the occipital cortex and hippocampus of 3-month-old L1-deficient mice. One month later, animals were sacrificed and double immunostainings were performed to identify L1-transduced neurons and astrocytes. Neurons were co-labeled with monoclonal antibody 555 against L1 (L1-555) and an antibody against neuron-specific intermediate filament (neurofilament) (Fig. 5.1A-C). Astrocytes were co-labeled with antibody 555 and the astrocyte-specific marker S-100b (Fig. 5.1D-F).

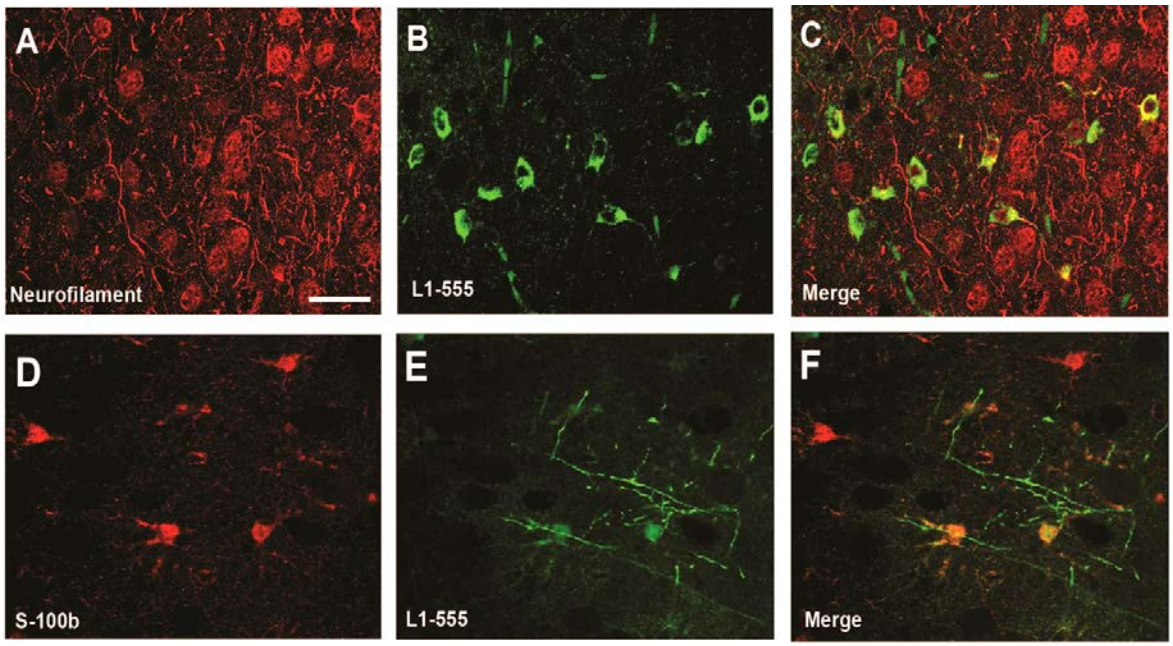

Figure 5.1. L1 expression in L1-deficient mice after AAV-L1 transduction. Double immunostainings for L1 and the neuronal marker neurofilament (A-C) or the astrocyte marker S100b (D-F) show L1 expression in neurons and astrocytes of L1-deficent mice one month after AAV-L1 injection into the hippocampus and the occipital cortex. Scale bar: 20 µm.

The results of the immunostainings showed that one month after AAV-L1 injection into the hippocampus and occipital region of the brain, L1 protein expression could be confirmed in neurons and astrocytes (Fig. 5.1).

5.1.3 AAV-L1 transduction increases levels of L1 expression in APPPS1 mice

To confirm that AAV-L1 transduction leads to the increased L1 protein levels in APPPS1 mice, immunoblot analysis was performed. Four months after injection approximately 20% higher levels of L1 protein could be detected in homogenates of AAV-L1 injected hemispheres, when compared to the levels of L1 in the homogenates of corresponding non-injected contralateral hemispheres (Fig. 5.2A, B).

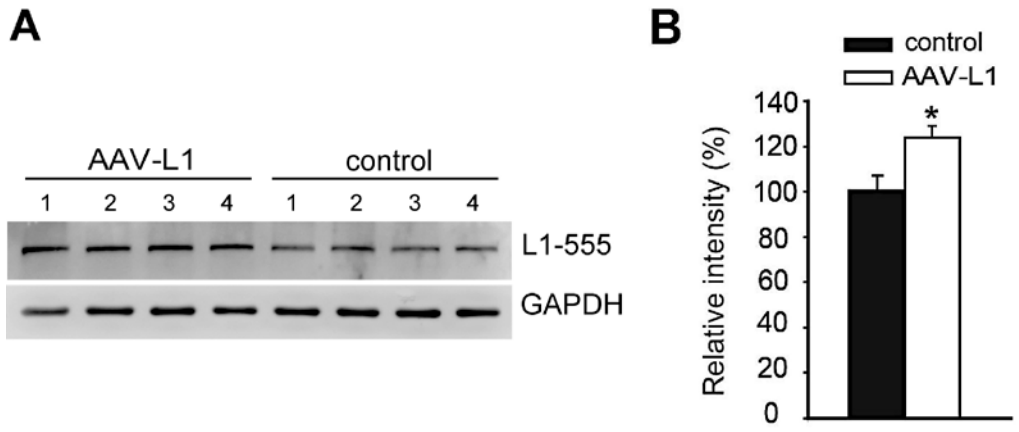

Figure 5.2. L1 overexpression in APPPS1 mice 4 months after AAV-L1 transduction. (A) Representative immunoblot showing L1 expression in AAV-L1 injected hemispheres and non-injected contralateral (control) hemispheres of APPPS1 mice 4 months after injection. Lanes marked with the same number show L1 expression in different hemispheres from the same brain. (B) Quantification of the immunoblot shown in (A). L1 levels are normalized to the GAPDH levels. Data are presented as mean + standard deviation. Asterisk indicates $p < 0.05$, one-way ANOVA with Tukey's *post hoc*; n = 4 mice/group.

5.2 Analysis of the amyloid plaque load and Aβ content in AAV-L1 injected APPPS1 mice

One of the most important aims of this study was to address the question whether AAV-L1 injections into APPPS1 mouse brains affects amyloid plaque formation. As described in the Methods section, APPPS1 mice were unilaterally injected with AAV-L1 or AAV-GFP into the hippocampus and occipital cortex at 3 months of age. 4 months later - at 7 months of age, when they show significant cerebral amyloidosis (Radde et al., 2006), animals were sacrificed for histological and biochemical analyses of plaque load.

5.2.1 Injection of AAV-L1 reduces amyloid plaque load

To visualize plaques, Aβ immunostaining was performed on spaced-serial sections from AAV-L1 and AAV-GFP transduced brains. At the age of 7 months, APPPS1 mice had developed a significant plaque load in the hippocampus and neocortex (Fig. 5.3A, B). Plaque load was measured as the percentage of area covered with Aβ-stained plaques in the hippocampus and occipital cortex. This was done by measuring areas of single plaques; that way changes in number of plaques and their average size could also be estimated. The total area covered by plaques was smaller in the injected (ipsilateral) hemisphere of mice transduced with AAV-L1 than in the non-injected (contralateral) hemisphere (Fig. 5.3C). This reduction was mostly due to a lower overall number of plaques (Fig. 5.3D) in the ipsilateral hemisphere of mice injected with AAV-L1, but smaller average plaque size also contributed to this effect (Fig. 5.3E). In animals injected with AAV-GFP, there was no reduction in any of the measured parameters (Fig. 5.3C-E), indicating that the damage to the tissue caused by the injection or the effect of AAV was not the cause for the observed difference in plaque load in AAV-L1 injected animals.

To rule out that any of the observed changes in plaque load and density were due to changes in overall APP expression due to L1 transduction, APP levels were determined in homogenates of injected and contralateral control brain hemispheres by Western blot analysis. For this experiment an antibody against the N-terminus of APP, which detects both mouse and human APP was used. Similar levels of APP were found in L1 transduced and control hemispheres (Fig. 5.4).

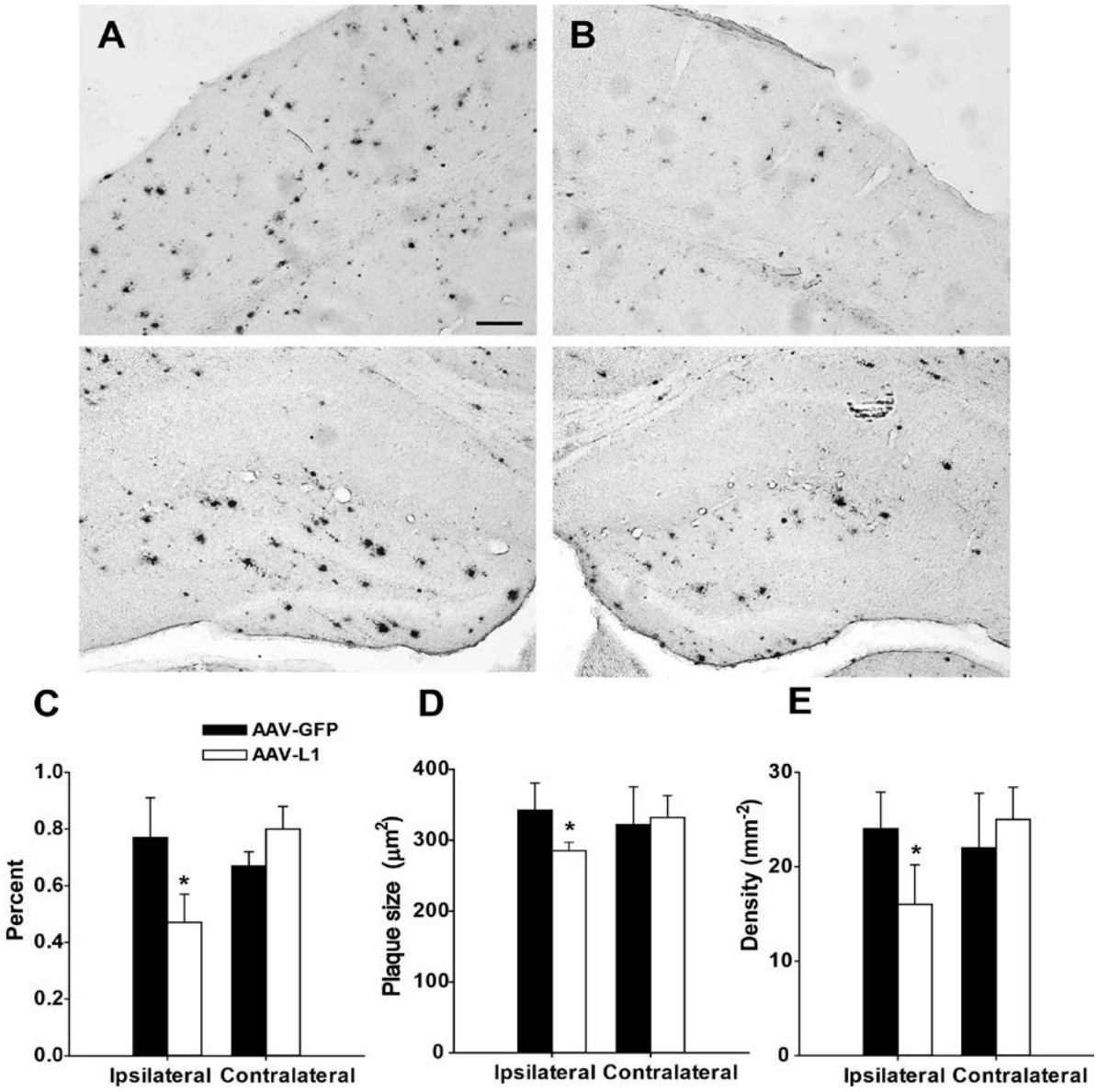

Figure 5.3. Injection of AAV-L1 reduces the amyloid plaque load in APPPS1 mice. (A, B) Representative micrographs of Aβ-stained occipital cortices (upper panels) and hippocampi (lower panels) of AAV-L1 non-injected (A) and injected (B) hemispheres. Scale bar: 200 µm. (C-E) Percentage of Aβ - stained plaque-covered area (C), average plaque size (D) and number of plaques per area (E) in the hippocampus and occipital cortex are reduced in the AAV-L1 injected (ipsilateral) hemispheres compared to the non-injected (contralateral) hemispheres and to the AAV-GFP injected brains. Data are presented as mean + standard deviation. Asterisks indicate $p < 0.05$, two way ANOVA with Tukey's *post hoc*; n = 4 mice/group.

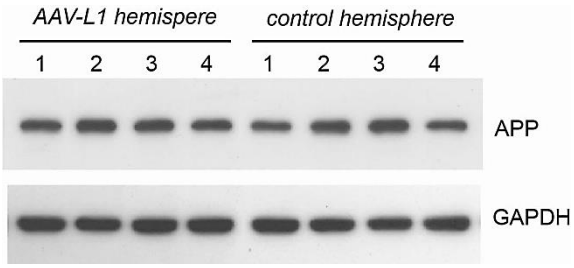

Figure 5.4. AAV-L1 transduction does not affect APP expression in APPPS1 mice. Representative immunoblot showing full length APP expression in AAV-L1 injected hemispheres and contralateral-control hemispheres. Antibody against the N-terminus of APP, which recognizes both human and mouse APP was used. Lanes marked with the same number show APP expression in different hemispheres from the same brain. GAPDH immunoblot is shown as a loading control.

5.2.2 AAV-L1 injection reduces soluble Aβ42 peptide levels and the Aβ42/40 ratio in APPPS1 mice

Total amounts of Aβ, as well as the ratio of the longer to shorter Aβ species, specifically Aβ42/40 ratio, influence amyloid deposition and plaque formation. Therefore, to evaluate whether the effects of AAV-L1 injection on plaque load seen by histological analysis may be due to L1-mediated changes in Aβ, Aβ42 and Aβ40 levels, the abundance of these peptides was determined by ELISA. For that purpose AAV-L1 injected and contralateral control hemispheres were subjected to the extraction (solubilization) of Aβ. Three fractions of different solubility were analyzed. Tris buffered saline (TBS) saline soluble fraction was obtained as a supernatant after centrifugation of TBS brain homogenate. This fraction contains soluble species of Aβ, monomers and oligomers, which represent only a small fraction of brain Aβ. The Aβ fraction soluble in anionic detergent SDS contains variable amounts of already deposited Aβ, depending on the age of animals. The Aβ fraction soluble only in 70 % formic acid (FA) contains most of the brain Aβ, which is deposited in a highly insoluble form, and therefore can only be extracted with an extremely harsh treatment such as incubation in 70 % formic acid.

As shown in Figure 5.5A, the amount of Aβ40 in the soluble TBS fraction was similar in injected and control hemispheres, whereas there was a moderate reduction of soluble Aβ42 in the injected hemisphere. Notice that this fraction contains a very small percentage of total Aβ. In the SDS fraction the content of both Aβ40 and Aβ42 did not differ between hemispheres (Fig 5.5B). The FA fraction (Fig 5.5C) contained the vast majority of total Aβ (Fig 5.5D) and showed similar contents of Aβ40 in injected and control hemispheres, while the amounts of Aβ42, although not significantly lower, had a strong tendency towards

reduction in the injected hemispheres. Importantly, the ratio between levels of Aβ42 and Aβ40 was significantly reduced in the AAV-L1 injected hemispheres compared with the control hemispheres (Fig. 5.5E).

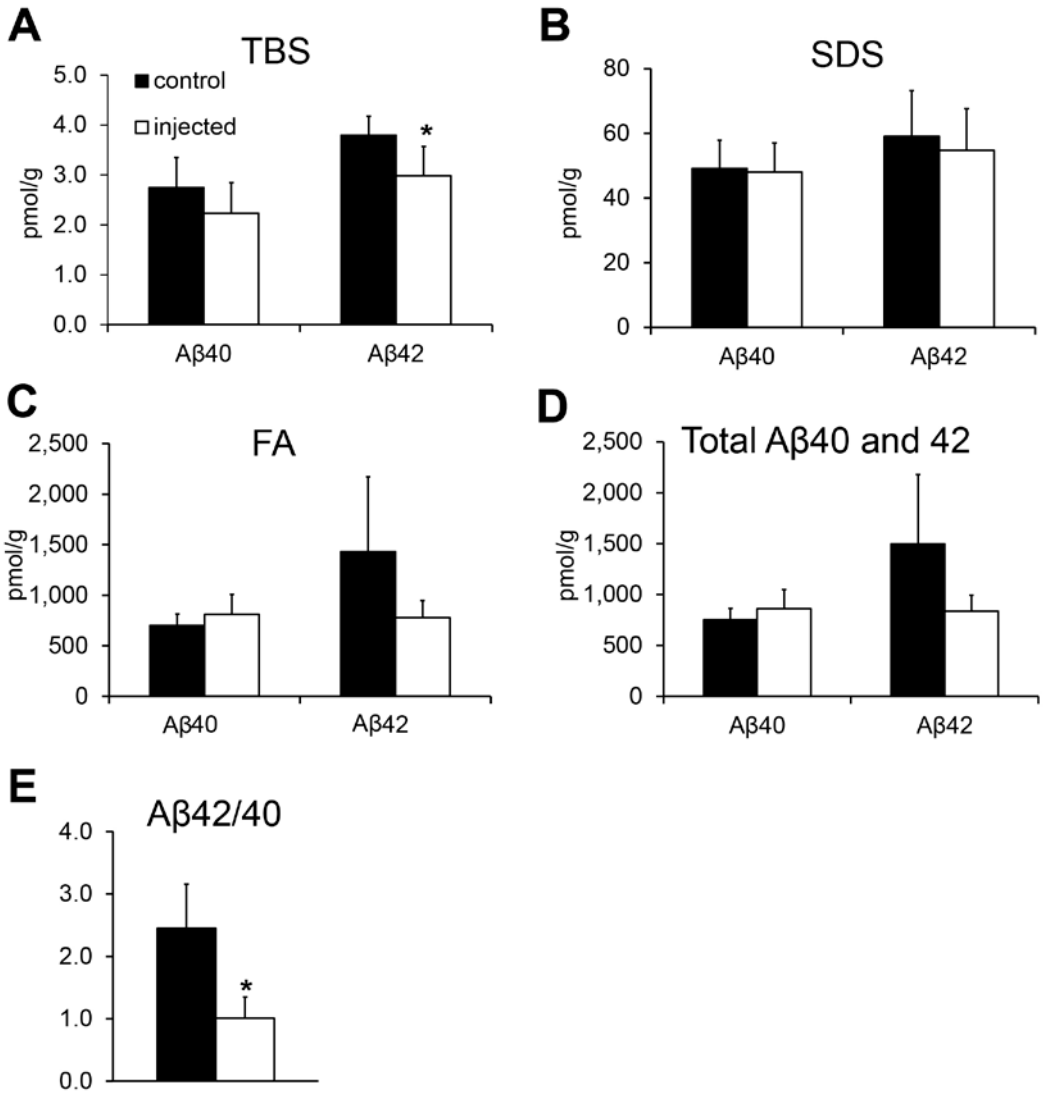

Figure 5.5. Injection of AAV-L1 reduces soluble amyloid β42 peptide levels and total Aβ42/40 ratio in APPPS1 mice. Levels of Aβ40 and Aβ42 in the TBS fraction (A), SDS fraction (B) and FA fraction (C), as well as levels of total Aβ40 and Aβ42 (D) in AAV-L1 injected and control hemispheres are shown. Notice that the FA fraction contains most of the total Aβ40. The level of soluble Aβ42 in TBS is reduced (A), and there is a tendency towards reduction of FA/total Aβ42 (C, D) in the injected hemisphere. Aβ levels are expressed in pmol/g brain wet weight. Ratio of total Aβ42/40 in injected hemispheres is reduced compared to control hemisphere (E). Data are presented as mean + standard deviation. Asterisks indicate $p < 0.05$, one-way ANOVA with Tukey's *post hoc*; n = 4 mice/group.

Next, the levels of full length APP and Aβ monomers, dimers and oligomers were determined in homogenates of AAV-L1 injected and control hemispheres by Western blot analysis (Fig. 5.6). Antibody 6E10 specific for human Aβ sequence was used to detect the expression of the transgenic APP, as well as Aβ monomers, dimers and oligomers generated from it. In line with the previous results shown in Fig. 5.4, levels of human APP were comparable between the AAV-L1 injected and control hemispheres (Fig 5.6). Levels of Aβ, however, varied between the brains (notice low Aβ levels in brain number 4, Fig. 5.6), and it seemed that there was a small reduction in Aβ monomer and dimer levels in the injected hemisphere in three out of four brains (brains 1-3, Fig. 5.6).

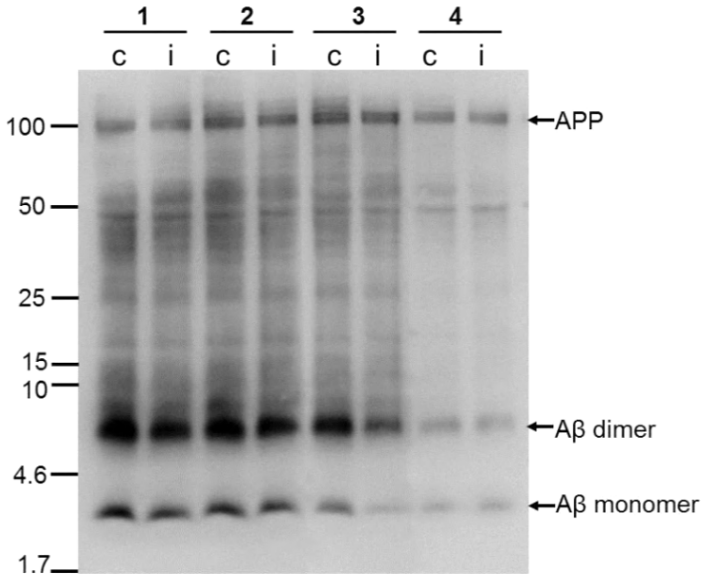

Figure 5.6. Western blot analysis of AAV-L1 injected and control hemispheres (6E10 antibody). Numbers designate different brains, and lanes loaded with samples from the control and injected hemispheres are marked with *c* and *i* respectively. The expression of APP is similar in different brains and no difference between the hemispheres is detectable. The Aβ monomer and dimer levels seem to show a tendency towards reduction in injected hemispheres. Notice lower levels of Aβ (monomer, dimer, and oligomers) in brain number 4.

5.3. Effects of AAV-L1 transduction on astrogliosis

Astrogliosis is a prominent feature of AD and plays an important role in the pathology of the disease. In APPPS1 mice, astrogliosis starts with the onset of plaques deposition (Radde et al., 2006). Having in mind that AAV-L1 injection leads not only to transduction of neurons, but also to transduction of astrocytes (Chapter 5.1), it was important to determine whether this ectopic expression of L1 in astrocytes affected astrogliosis.

5.3.1 Injection of AAV-L1 reduces astrogliosis in APPPS1 mice

To evaluate numbers of astrocytes, APPPS1 brain sections were immunostained for glial fibrillary acidic protein (GFAP) as an astrocyte marker (Fig. 5.7A,B) and used for stereological estimation of the numerical density of astrocytes. Density of GFAP-positive astrocytes was approximately 25% lower in the AAV-L1 injected hippocampi and approximately 20% lower in the AAV-L1 injected occipital cortices than in the control AAV-GFP injected hemispheres (Fig. 5.7C) indicating a reduction in astrogliosis in AAV-L1 injected brains.

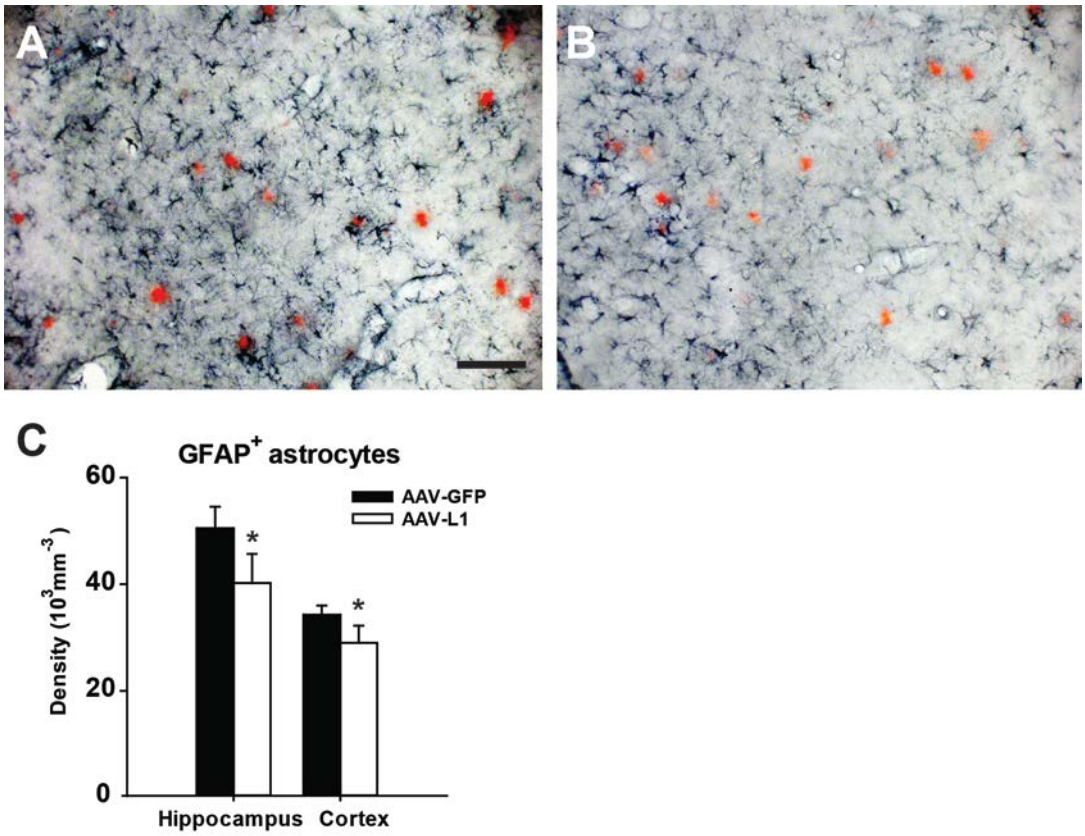

Figure 5.7. Injection of AAV-L1 reduces astrogliosis and GFAP expression in APPPS1 mice. (A, B) Representative bright field micrographs of immunostaining for GFAP combined with Congo red amyloid staining in AAV-L1 (A) and AAV-GFP (B) injected hippocampus. Scale bar: 50 μm. (C) Densities of astrocytes immunostained for GFAP are lower in the hippocampus and occipital cortex of mice injected with AAV-L1 versus those injected with AAV-GFP. Data are presented as mean + standard deviation. Asterisks indicate $p < 0.05$, one-way ANOVA with Tukey's *post hoc*; n = 4 mice/group.

5.3.2 Injection of AAV-L1 reduces levels of GFAP expression

To confirm the results obtained for the GFAP expression by immunohistological examination, and to assess overall amount of GFAP in astrocytes, Western blot analysis was performed. Tissue of combined occipital cortex and hippocampus from the AAV-L1 and AAV-GFP injected hemispheres were evaluated for GFAP protein levels (Fig. 5.8A). Densitometric analysis showed approximately 25% lower GFAP levels in AAV-L1 compared with AAV-GFP injected hemispheres (Fig. 5.8B). Combined with the observed reduction of approximately 25% in the number of GFAP-positive astrocytes, this reduction in GFAP expression can be contributed to the reduction in number of astrocytes, rather than reduced GFAP expression in single cells.

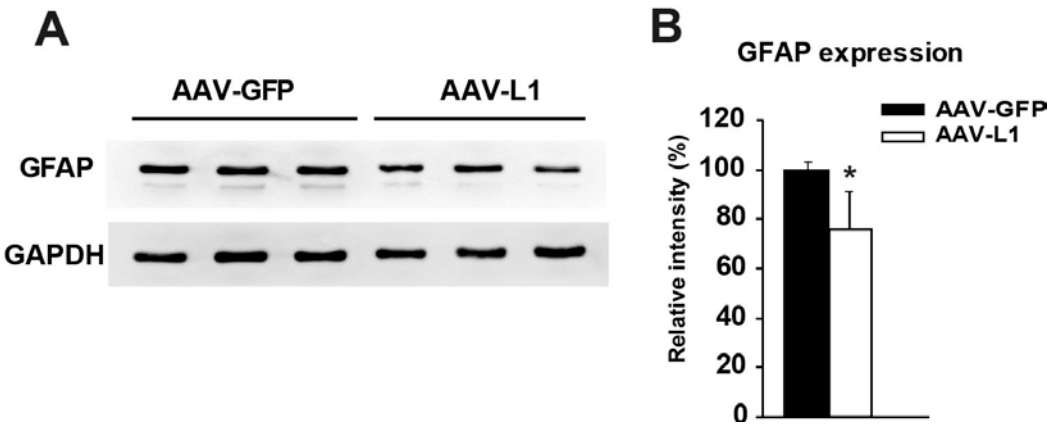

Figure 5.8. Injection of AAV-L1 reduces GFAP expression in APPPS1 mice. (A) Representative immunoblots showing GFAP expression in the hippocampus of AAV-GFP and AAV-L1 injected mice. (B) Quantitative analysis of the immunoblot shown in (A). Data are presented as mean + standard deviation. Asterisks indicate $p < 0.05$, one-way ANOVA with Tukey's *post hoc*.

5.4 Effects of AAV-L1 transduction on microgliosis

Inflammation plays an important role in AD pathology; therefore it was important to determine whether AAV-L1 injections would lead to alterations in the inflammatory response to neurodegeneration in APPPS1 mice. To this end cells involved in the inflammatory response in the brain were counted, namely astrocytes (see above), and microglia/macrophages.

The density of Iba-1 immunoreactive cells (Fig 5.9A,B), which identify the microglial cell/macrophage lineage including both quiescent and activated microglia, was estimated by stereological analysis in AAV-L1 and AAV1-GFP injected mice. The density of microglial

cells/macrophages was similar in the two experimental groups, both in the hippocampus and occipital cortex, indicating that AAV-L1 injections did not alter microglial cell proliferation and cell death, or recruitment of macrophages from blood vessels in response to amyloid plaque formation in APPPS1 mice (Fig. 5.9C). The morphology of Iba-1 positive cells was also similar in brains of APPPS1 mice injected with AAV-L1 and AAV-GFP (compare Figs. 5.9A and 5.9B), both showing signs of microglial activation such as enlarged cell bodies and shortened clumpy processes.

Microglia/macrophages accumulate around amyloid plaques and have been described to be important for plaque maintenance and clearance (Bolmont et al., 2008). Therefore the numbers of such clusters of Iba-1-positive cells were counted, but no difference was found between the AAV-L1 and AAV-GFP injected hippocampi (Fig. 5.9D). However, the average number of Iba-1-positive cells in a cluster was higher in AAV-L1 than in AAV-GFP injected hemispheres (Fig. 5.9D).

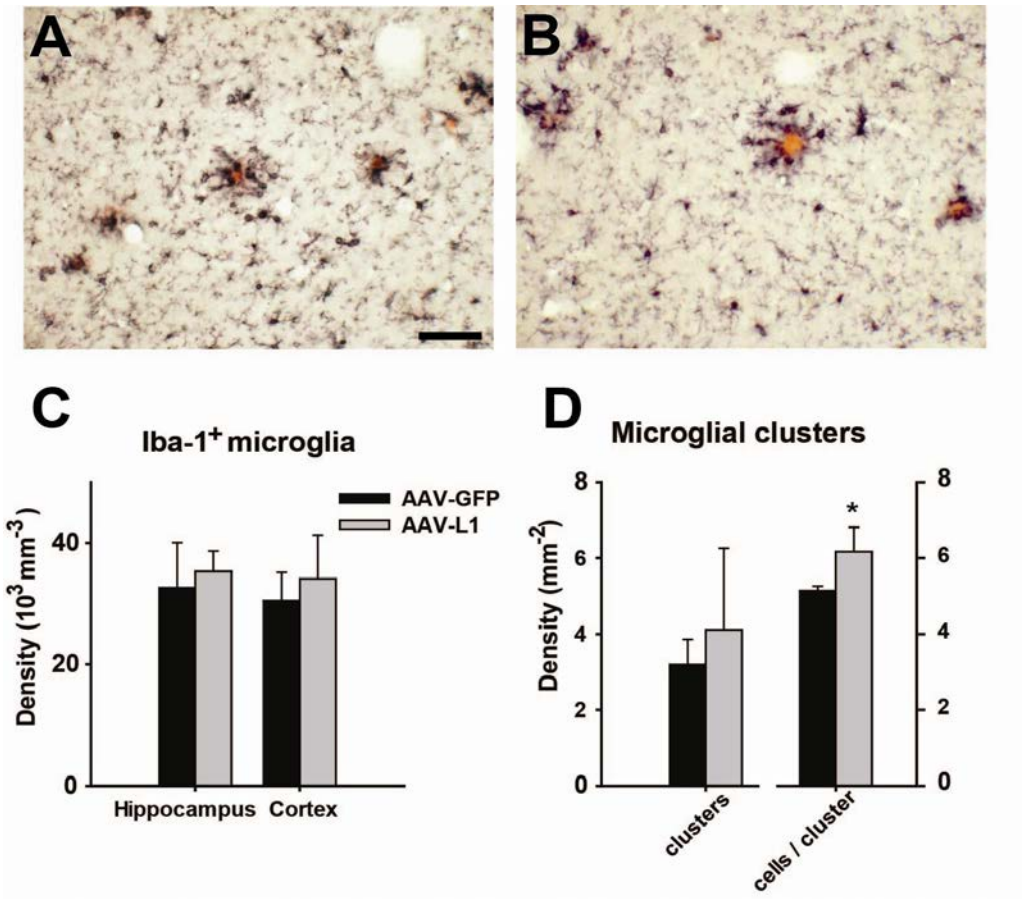

Figure 5.9. Injection of AAV-L1 does not affect microgliosis, but influences microglial aggregation in APPPS1 mice. Representative bright field micrographs of combined Congo red and immunohistochemical staining for the microglial/macrophage marker Iba-1 in the hippocampi of mice injected with AAV-L1 (A) and

AAV-GFP (B). Scale bar: 50 µm. (C) Densities of Iba-1-positive (Iba-1+) cells are not different in the hippocampus and occipital cortex of mice injected with AAV-L1 compared with AAV-GFP injected mice. (D) Number of microglial clusters per mm^2 (profile density) and average number of microglial cells per cluster in the hippocampi of mice injected with AAV-L1 or AAV-GFP. Data are presented as mean + standard deviation. Asterisk indicates $p < 0.05$, one-way ANOVA with Tukey's *post hoc*; n = 4 mice/group.

In order to further characterize the microglia clustering around plaques, immunostaining for Mac-2, a marker of actively phagocyting microglia (Rotshenker, 2009) was performed. Virtually all Mac-2-positive cells were found around the Congo red stained plaques, with only rare single cells not contacting the plaques (Fig. 5.10). However, there was no difference in the number of Mac-2-positive cells in the clusters around the plaques between the AAV-L1 (3.71 ± 1.49 cells/cluster) and AAV-GFP (3.28 ± 1.11 cells/cluster) injected hippocampi. It is notable that the numbers of Mac-2-positive cells around plaques were much lower compared to Iba-1-positive cell numbers. Additionally, some plaques were not contacted by Mac-2-positive cells, in both AAV-L1 and AAV-GFP injected brains, with no significant difference in the number of those plaques between the groups.

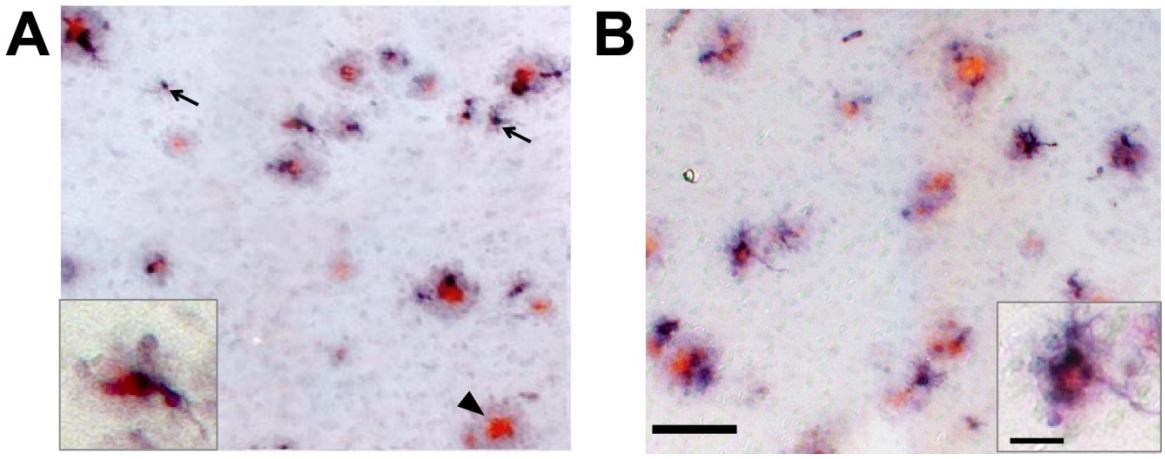

Figure 5.10. Mac-2-positive microglia surround amyloid plaques. (A, B) Representative bright field micrographs of Mac-2 immunostaining combined with Congo red staining for amyloid deposits. Mac-2-positive microglia in the AAV-L1 injected (A) and control hemisphere (B) are almost exclusively present around plaques. Representative micrographs of Mac-2-positive microglia clusters surrounding Congo red-stained plaque are shown in insets. Rare Mac-2-positive cells not are contacting plaques (A, marked with arrows) and some plaques are not surrounded with Mac-2positive microglia (A, marked with arrowheads). Scale bars: 50 µm and 20 µm (insets).

In the view of increased Iba-1-positive microglia/macrophage clustering around congophilic plaques, it seemed reasonable to examine levels of the C-C motif ligand 2 (CCL2) chemokine. In the nervous system CCL2 is produced by both microglia and astrocytes and belongs to the group of inducible or inflammatory chemokines, which are expressed in various pathological conditions and play an essential role in migration of leukocytes to the nervous system. CCL2 and its receptor CCR2 have been implicated in the recruitment of monocytes/macrophages during different neuroinflammatory processes (Ransohoff, 2002). In AD brain CCL2 is upregulated (Hickman and El Khoury, 2010) and it has been reported that CCL2 deficiency leads to the impaired microglial accumulation and accelerated disease progression in an AD mouse model (Kiyota et al., 2013).

However, when TBS brain extracts were analyzed by CCL2-specific ELISA, no difference was found in CCL2 levels between the AAV-L1 injected hemisphere and the contralateral, non-injected control hemisphere (Fig. 5.11).

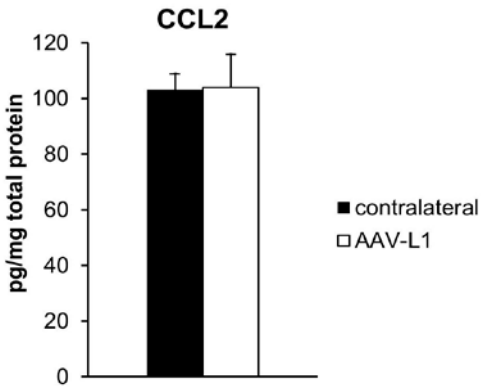

Figure 5.11. Levels of CCL2 chemokine are not altered in AAV-L1 injected hemispheres. Levels of CCL2 were measured in TBS homogenates of AAV-L1 injected and contralateral hemispheres by means of CCL2 specific ELISA. No differences were detected ($p > 0.05$; one-way ANOVA with Tukey's *post hoc*; n = 4 mice/group).

5.5 Effects of AAV-L1 transduction on parvalbumin-positive subpopulation of interneurons and inhibitory synapses in the hippocampus

5.5.1 Normal numbers of parvalbumin-positive interneurons in APPPS1 mice

Although global neuronal loss is not present in APPPS1 mice at the age of 8 months, neuron cell death is observed in the dentate gyrus (Radde et al., 2006). Additionally, loss of different classes of interneurons, among others parvalbumin-positive interneurons, was observed in the olfactory cortex of a similar APP/PS1 double transgenic mouse model (Saiz-Sanchez et

al., 2013). Therefore, parvalbumin-positive interneurons in the hippocampus, as a population of neurons susceptible to various modes of stress, including amyloid toxicity, were analyzed in this study, with the aim to determine if their numbers are decreased in APPPS1 mice, and if so, whether the loss can be rescued by L1 transduction. For that purpose, numbers of parvalbumin-immunostained interneurons in hippocampi of wild-type C57BL/6J mice, as well as AAV-L1 and AAV-GFP injected hippocampi of APPPS1 mice were estimated stereologically. Surprisingly, no difference was found between the genotypes (Fig. 5.12). Congruently, injection of either of the AAV constructs had no effect on number of parvalbumin-positive interneurons.

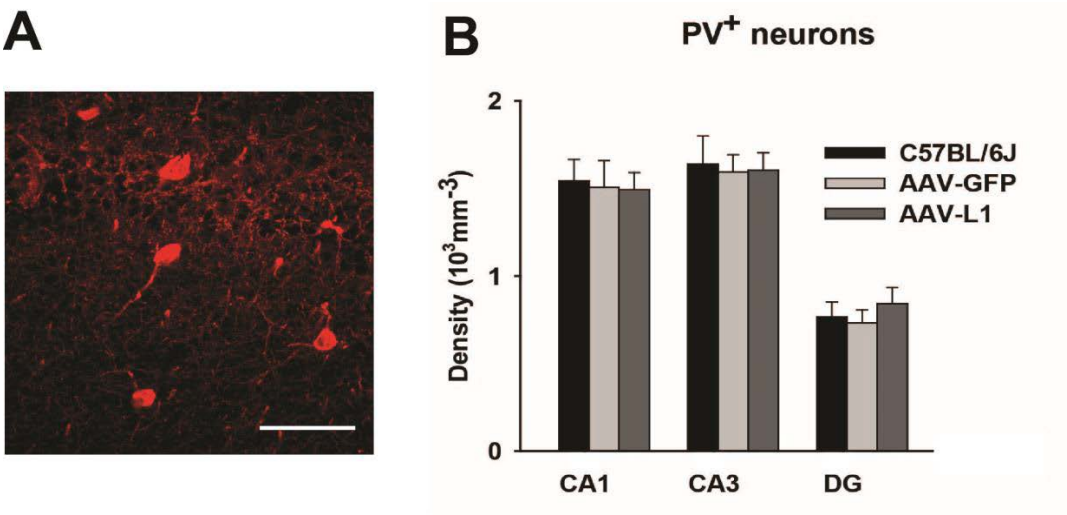

Fig 5.12. Hippocampal parvalbumin-positive interneurons are not dying in APPPS1 mice. (A) Representative image of parvalbumin-immunostained interneurons in hippocampus. Scale bar: 50 µm. (B) Densities of hippocampal parvalbumin-positive interneurons are not different between wild-type C57BL/6J mice and AAV-L1 or AAV-GFP injected APPPS1 mice. Data are presented as mean + standard deviation, statistical difference was tested by two-way ANOVA with Tukey's *post hoc*; n = 4 mice/group.

5.5.2 Injection of AAV-L1 ameliorates loss of inhibitory perisomatic synapses on CA1 and CA3 pyramidal cells in APPPS1 mice

Synapse loss is the strongest correlate of cognitive decline in AD, and synapses are an attractive therapeutic target due to their plastic nature that allows potential recovery (Terry et al., 1991). L1 has been suggested to play a role in maturation and stabilization of reinnervating axons during the repair process after injury of the adult mouse hippocampus and spinal cord (Jucker et al., 1996; Lee et al., 2012). Furthermore, L1-deficient mice have decreased numbers of hippocampal perisomatic inhibitory synapses, implicating a positive regulatory role of L1 in synaptic plasticity (Saghatelyan et al., 2004). Therefore, the density

of inhibitory synaptic terminals on cell bodies of principal neurons in the hippocampus was examined using the pre-synaptic marker VGAT and quantitative confocal microscopic analysis (Morellini et al., 2010). Additionally, although loss of parvalbumin-positive interneurons was not observed in APPPS1 mice (Chapter 5.5.1), the possibility that their synapses were lost was tested by combining VGAT and parvalbumin immunostainings (Fig. 5.13A). APPPS1 mice had fewer perisomatic terminals surrounding pyramidal cell bodies in the CA1 and CA3 hippocampal regions compared to aged-matched wild-type controls, whereas perisomatic inhibitory synaptic input to the dentate gyrus (DG) was similar to that in age-matched wild-type mice (Fig. 5.13B). Both parvalbumin-positive and parvalbumin-negative synapses were reduced in numbers, to a similar extent. More inhibitory terminals, including both parvalbumin-positive and parvalbumin-negative synapses, were seen in the CA1 and CA3 regions of AAV-L1 injected mice than in AAV-GFP injected mice, whereas AAV-L1 injection did not change the number of terminals in the DG (Fig. 5.13B). Thus, AAV-L1 injections reduced the loss of perisomatic inhibitory terminals in the CA1 and CA3 regions of APPPS1 mice compared to AAV-GFP injections. Since APPPS1 mice do not show neuronal cell loss at the age of 7 months, the loss of perisomatic synaptic terminals can be considered as the first functionally significant structural parameter of neurodegeneration connected to amyloid deposition in these mice.

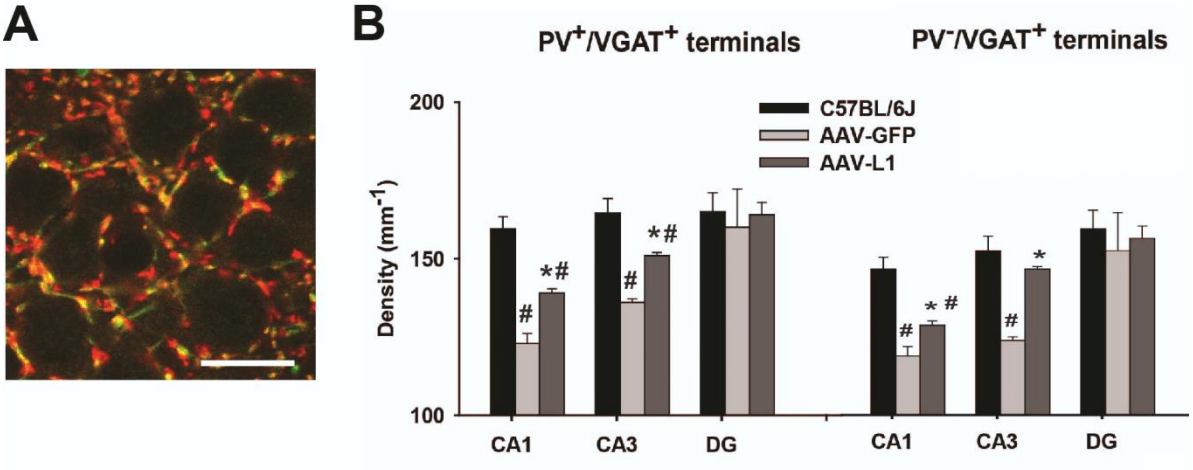

Figure 5.13. Injection of AAV-L1 reduces the loss of perisomatic inhibitory terminals on pyramidal neurons in the hippocampus of APPPS1 mice. (A) Representative confocal micrograph of VGAT-(red) and parvalbumine (yellow)-immunostained perisomatic puncta around CA3 pyramidal neurons in the hippocampus of a mouse injected with AAV-GFP. Scale bar: 10 µm. (B) Numbers of parvalbumine-positive/VGAT-positive ($PV^+/VGAT^+$) and parvalbumin-negative/VGAT-positive ($PV^-/VGAT^+$) perisomatic terminals per mm (linear density) in the CA1, CA3 and dentate gyrus (DG) of the hippocampus of wild-type C57BL/6J mice, and APPPS1 mice injected with AAV-L1 and AAV-GFP. Data are presented as mean + standard deviation.

Asterisks indicate difference between the treatments, pound signs indicate difference between the genotypes, $p < 0.05$, two-way ANOVA with Tukey's *post hoc*; n = 4 mice/group.

To further assess if there was a global loss of GABA activity in the APPPS1 mice, as well as generalized synaptic deficit, brain homogenates from wild-type C57BL6/J and APPPS1 mice were analyzed by Western blot to determine the amount of the GABA synthesizing enzyme glutamic acid decarboxylase 67 (GAD67) and general pre-synaptic marker, synapsin I. The results indicate that there is no generalized loss of either GAD67 or synapsin I in APPPS1 mice, strengthening the hypothesis that the detected loss of parvalbumin-positive and parvalbumin-negative inhibitory synapses in the Amon's horn of the hippocampus represent specific localized early structural evidence of neurodegeneration in APPPS1 mice.

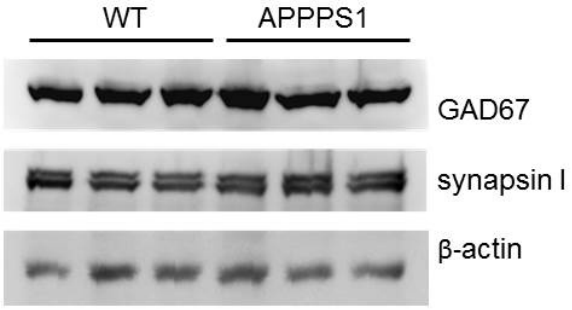

Figure 5.14. Expression of GAD67 and synapsin I in APPPS1 mice. Western blot showing similar levels of expression of glutamic acid decarboxylase 67 (GAD67) and synapsin I in brain homogenates from APPPS1 mice and age-matched wild-type mice.

5.6 L1 binds to Aβ peptides and reduces Aβ42 aggregation *in vitro*

5.6.1 Aβ42 aggregation *in vitro* is reduced by L1-Fc, but not by CHL1-Fc

To gain an insight into the mechanism(s) underlying the beneficial effects of L1 in reducing plaque load in the brain, as shown by immunohistochemistry and ELISA (Chapter 5.2), an *in vitro* approach was used.

The observed amyloid plaque reducing effect of L1 injections was difficult to explain according to current knowledge. Thus, we hypothesized that L1 may bind directly to amyloid precursor protein and/or to its cleavage products, the Aβ peptides. The ectodomain of membrane-attached L1, as well as the shed ectodomain, containing Ig-like and FnIII-like domains, are the parts of L1 exposed to the extracellular space where Aβ peptides are released. Therefore the influence of the extracellular domain of L1 in form of the L1-Fc fusion protein on Aβ aggregation was determined in an *in vitro* amyloid aggregation assay.

Aβ42 peptide was incubated in cell culture medium for 48 h at 37°C in the presence of L1-Fc fusion protein, or CHL1-Fc as a control. Under these conditions, the levels of Aβ42 peptide mono-, tri- and tetramers were increased upon L1-Fc treatment, whereas the higher molecular weight Aβ42 aggregates (molecular weight of 40 kDa and more) were markedly reduced in the presence of L1-Fc (Fig. 5.15). This indicates that L1 shows an anti-aggregation effect on Aβ42, probably by binding it and thus reducing amount of peptide available to aggregation. Aβ42 was used in this assay because it aggregates at much higher rates compared to Aβ40, and it is considered that "seeding" of the plaques starts with this species, whereas Aβ40 is deposited at later stages of plaque formation.

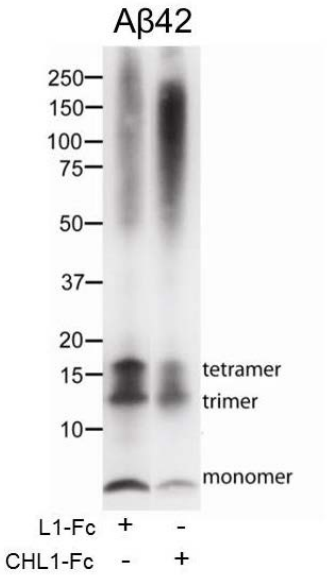

Figure 5.15. L1-Fc reduces Aβ42 aggregation *in vitro*. Immunoblot showing aggregation of Aβ42 peptide *in vitro* in the presence of L1-Fc or CHL1-Fc. Aβ42 (100 µM) was incubated for 2 days in cell culture medium at 37°C, in the presence of L1-Fc or CHL1-Fc (1 µM each).

5.6.2 L1 directly and specifically binds to Aβ40 and Aβ42 peptides

In order to examine if this anti-aggregation effect of L1 is a result of a direct interaction between L1 and Aβ, a BIND assay was used to determine if the extracellular domain of L1 binds to Aβ40 and Aβ42 peptides. This method is an alternative to ELISA, and it allows label-free approach to direct protein-protein interactions. When proteins bind to the immobilized ligand and the plate is exposed to light of the full spectrum, the wavelength of the reflected light shifts towards higher wavelengths and this wavelength shift is a direct measure for the amount of bound ligand. Aβ40 or Aβ42 peptide was immobilized in 396-

well plate with titan oxide (TiO) surface and L1-Fc was added as TiO surface plates were coated with Aβ40 or Aβ42 peptide and L1-Fc was added as a soluble ligand. CHL1-Fc and Fc were used as negative controls. Time course of binding of L1-Fc, CHL1-Fc and Fc in three different concentrations (0.1 µM, 0.5 µM and 1 µM) to immobilized Aβ40 and Aβ42 is shown in Fig. 5.16A-F. Peak wavelength (PWV) shift in pm (picometers) was measured. Concentration dependent binding of L1-Fc to both Aβ40 and Aβ42 was observed, while CHL1-Fc and Fc did not bind to either Aβ40 or Aβ42. PWV shift 30 min after addition of 1µM L1-Fc, CHL1-Fc or Fc to the Aβ-coated plate is shown in Fig. 5.16G, H.

To narrow down the region of L1 responsible for binding, parts of the L1 ectodomain containing only immunoglobulin domains 1-6 (Ig1-6) or fibronectin type III homologous repeats 1-5 (Fn1-5) of L1 were tested for binding to immobilized Aβ40 and Aβ42, as described above. Results showed that Fn1-5 domains bind to both Aβ40 and Aβ42, while Ig1-6 domains did not bind to Aβ40 or Aβ42 (Fig. 5.17).

To define more specifically the binding region within the Fn1-5, Fn1-2, Fn2-3 and Fn4-5 domains were tested in the same assay. Binding was shown for the Fn1-2 and Fn2-3 domains, but not for the Fn4-5 domain (Fig. 5.18). This suggests that binding to Aβ is possibly mediated by the Fn2 domain, as it is contained in both Fn1-2 and Fn2-3. However, binding of Fn1 and Fn3 domains is equally possible.

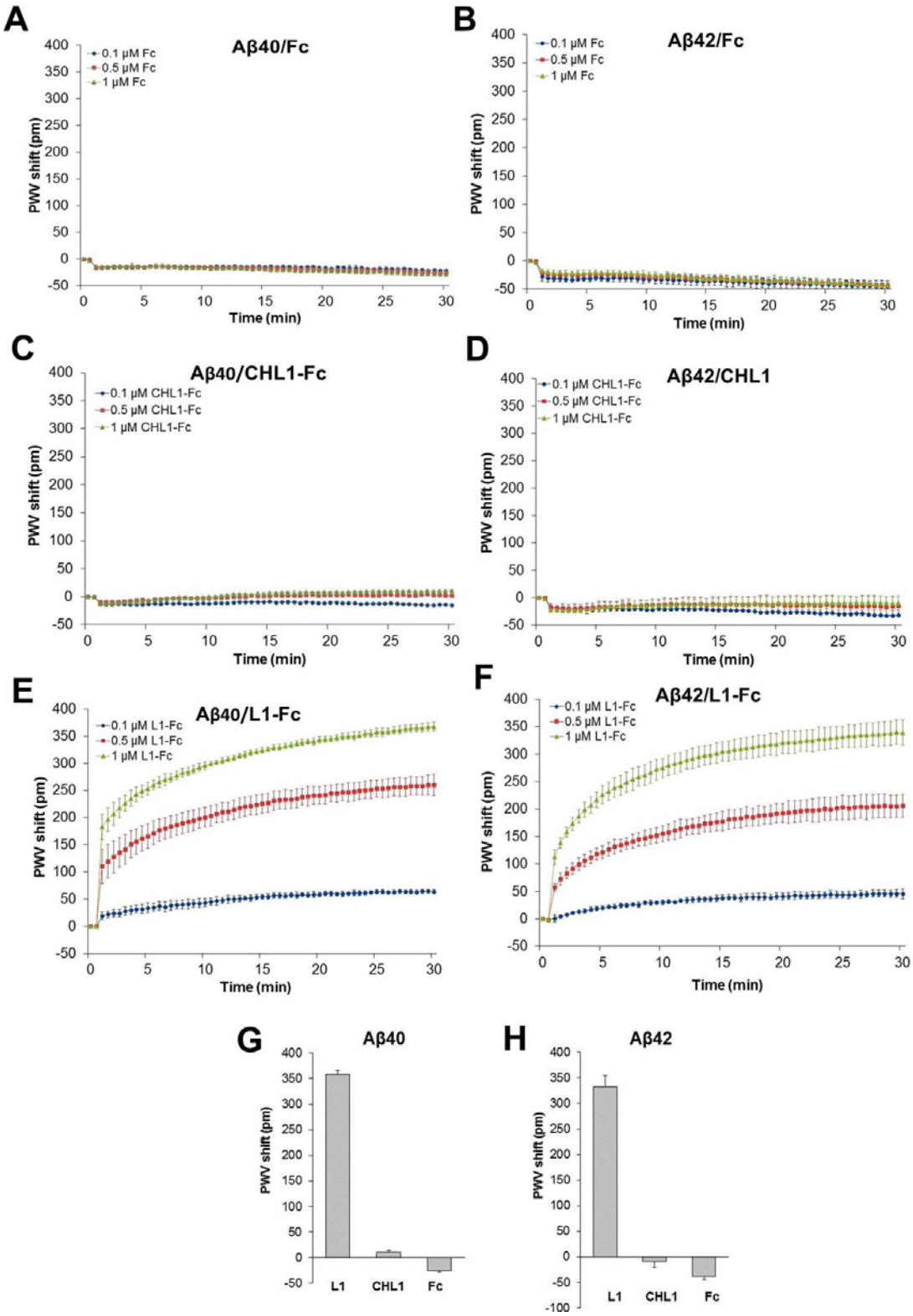

Figure 5.16. The extracellular domain of L1, but not of CHL1 binds to Aβ40 and Aβ42. The time course of the concentration-dependent binding of Fc (A, B), CHL1-Fc (C, D) and L1-Fc (E, F) to Aβ40 and Aβ42 is shown by the label-free binding assay using substrate-coated Aβ peptides and different concentrations (0.1 µM, 0.5 µM and 1 µM) of soluble Fc, CHL1-Fc and L1-Fc. (G, H) PWV shift 30 min after application of the highest concentration of L1-Fc, CHL1-Fc and Fc. Data are presented as mean ± standard deviation (A-F) and mean + standard deviation (G, H). All experiments were performed in triplicates.

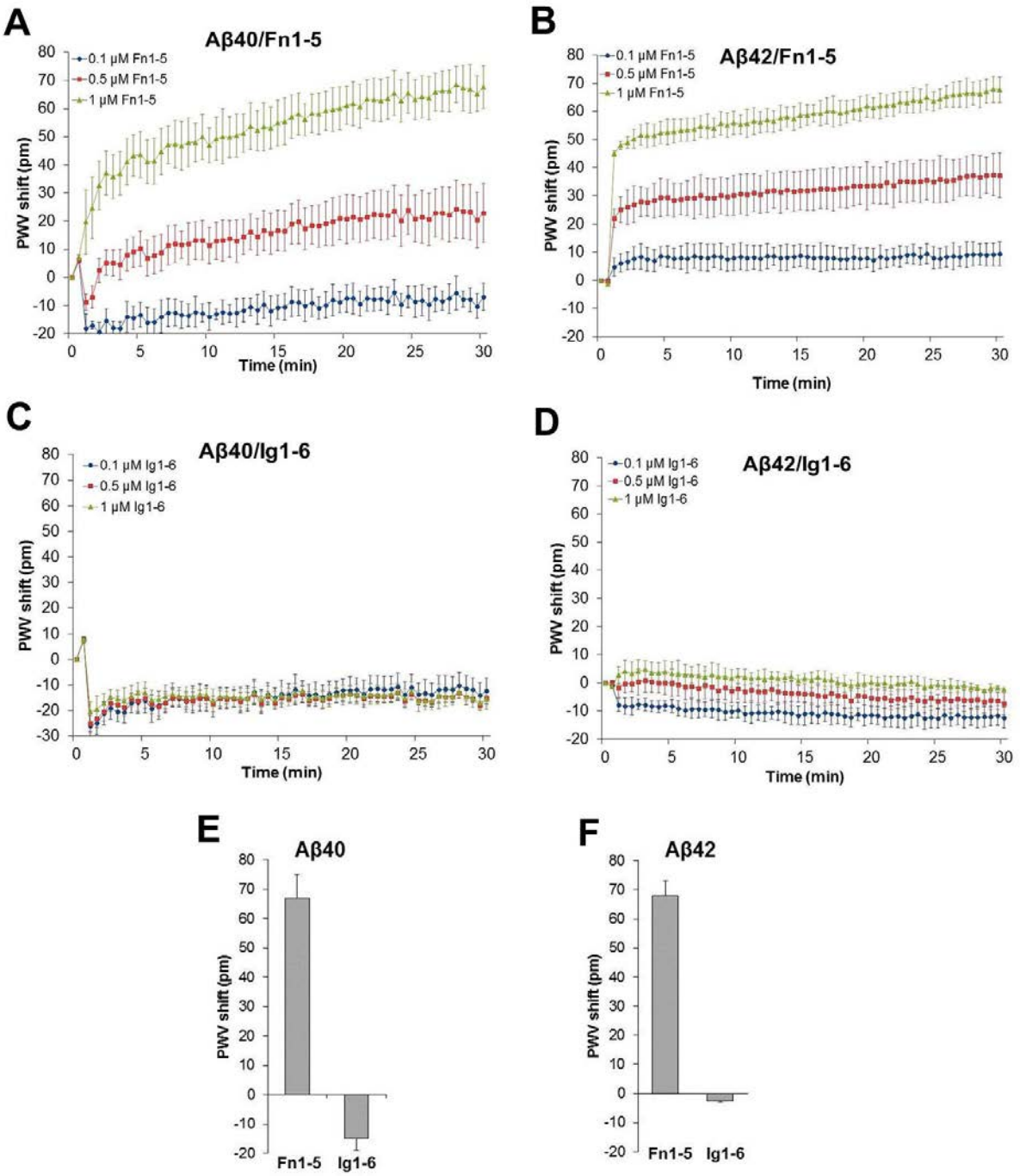

Figure 5.17. F**ibronectin type III homologous repeats 1-5 (Fn1-5), but not immunoglobulin-like domains 1-6 (Ig1-6) of L1 bind to Aβ40 and Aβ42.** The time course of the concentration-dependent binding of Fn1-5 (A, B) and Ig1-6 (C, D) to Aβ40 and Aβ42 is shown by the label-free binding assay using substrate-coated Aβ peptides and different concentrations (0.1 µM, 0.5 µM and 1 µM) of soluble Fn1-5 and Ig1-6. (E, F) PWV shift 30 min after application of the highest concentration of Fn1-5 and Ig1-6. Data are presented as mean ± standard deviation (A-D) and mean + standard deviation (E, F). All experiments were performed in triplicates.

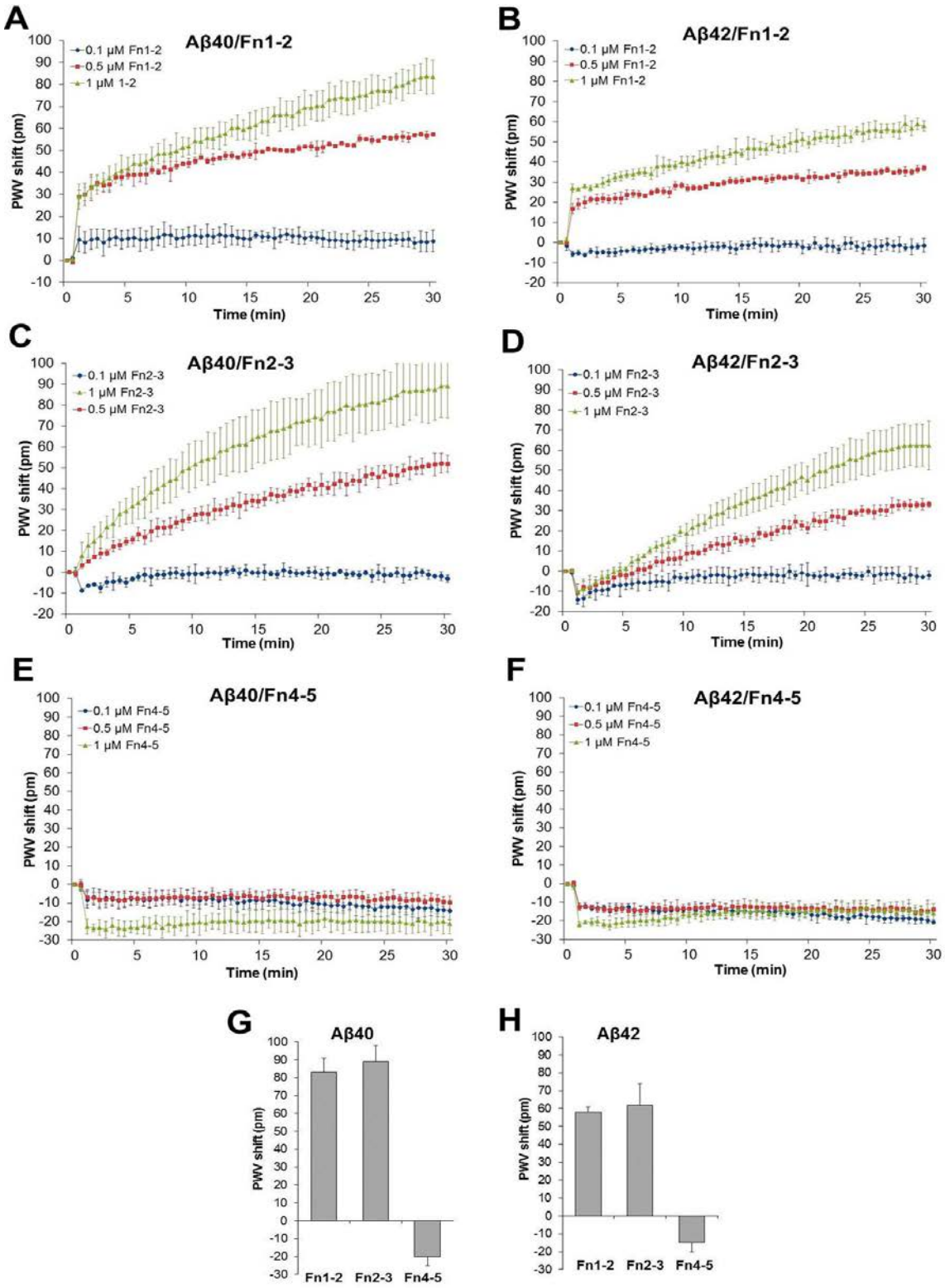

Figure 5.18. F**ibronectin type III homologous repeats Fn1-2 and Fn2-3, but not Fn4-5 of L1 bind to Aβ40 and Aβ42.** The time course of the concentration-dependent binding of Fn1-2 (A, B), Fn2-3 (C, D) and Fn4-5 (E, F) to Aβ40 and Aβ42 is shown by the label-free binding assay using substrate-coated Aβ peptides and different concentrations (0.1 µM, 0.5 µM and 1 µM) of soluble Fn1-2, Fn2-3 and Fn4-5. (G, H) PWV shift 30 min after application of the highest concentration of Fn1-2, Fn2-3 and Fn4-5. Data are presented as mean ± standard deviation (A-F) and mean + standard deviation (G, H). All experiments were performed in triplicates.

5.7 L1 is cleaved by γ-secretase but this does not interfere with APP processing

5.7.1 Cleavage of L1 by γ-secretase is increased in APPPS1 mice

It has been described that L1 is cleaved in its ectodomain to generate soluble fragments of different size, which are released into the extracellular space, and the transmembrane fragments containing membrane-proximal parts of the ectodomain, transmembrane region and the intracellular domain. Cleavage by trypsin, plasmin, or proprotein convertase PC5a generates a soluble extracellular 140 kDa fragment and an 80-kDa transmembrane fragment (Sadoul et al., 1988; Nayeem et al., 1999; Silleti et al., 2000; Kalus et al., 2003), while cleavage by an yet unidentified serine protease produces an extracellular 135 kDa fragment and a transmembrane 70 kDa fragment (Lutz et al., 2012). It has also been reported that L1 is processed by γ-secretase in cancer cells (Riedle et al., 2009).

Since APPPS1 mice overexpress PS1 with mutation which causes partial loss of the γ-secretase function (affecting Aβ42 but not Aβ40 generation), it was important to analyze L1 processing, especially by γ-secretase, in this mouse. Western blot analysis of brain homogenates of APPPS1 mice and wild-type (C57BL6/J) mice using the antibody 172-R, which recognizes the intracellular domain of L1, revealed several bands corresponding to full-length L1 and different membrane spanning fragments: 70 kDa and 80 kDa fragments, and a band that probably corresponds to a 28 kDa fragment (Fig. 5.19). Levels of the full length L1 were similar in both genotypes, whereas a significant reduction in the amount of 70 kDa and 80 kDa fragments could be observed in the APPPS1 brains compared to wild-type mice. In addition, increased levels of the 28 kDa γ-secretase cleavage product (Riedle et al., 2009) were observed in APPPS1 mice. This result indicates that in APPPS1 mice cleavage of the 70 kDa L1 fragment is increased, probably due to PS1 overexpression, and that processing of L1 is not negatively affected by the L166P mutation in PS1.

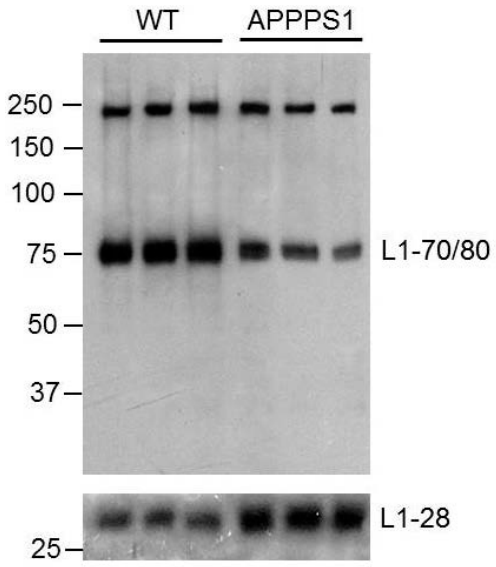

Figure 5.19. Processing of the 70 kDa L1 fragment is increased in APPPS1-21 mice brains and lead to enhanced generation of the 28 kDa L1 fragment. Brain homogenates of wild-type and APPPS1-21 mice were analyzed by Western blot using the monoclonal antibody 172-R directed against the intracellular domain of L1. The amount of the 70 kDa L1 fragment (L1-70) is decreased and the amount of the γ-secretase product of 28 kDa (L1-28) is increased in APPPS1 mice compared to amounts of the same fragments in wild-type mice. Levels of full-length L1 are similar in both genotypes.

5.7.2 Co-immunoprecipitation of L1 and APP

As L1 and APP are both transmembrane proteins present in the similar cell compartments, most notably in the synapse, and both can be cleaved by γ-secretase, it is conceivable that that L1 might interact with APP or γ-secretase and thus interfere with binding of APP to the γ-secretase complex. To determine if L1 interacts with APP co-immunoprecipitation experiments were performed. Brain homogenate from APPPS1 mice was incubated with different antibodies specific for APP or L1. APP-specific antibodies used were polyclonal APP-NT antibody against the N-terminus, polyclonal APP-CT antibody against the C-terminus and monoclonal 6E10 antibody against an epitope within the Aβ sequence. The following L1-specific antibodies were used: monoclonal L1-555 antibody against the epitope between the second and third FnIII domain, monoclonal L1-557 against the epitope at the N-terminus of the third FnIII domain and polyclonal antibody against the extracellular part of L1. As shown in Figure 5.20, APP could be pulled from the brain homogenate with polyclonal antibody against L1 as detected with antibodies specific for the N- or C-terminus of APP, but not with monoclonal 6E10 antibody. In the L1 immunoprecipitates no Aβ could be detected using monoclonal 6E10 antibody. In contrast, APP could not be co-precipitated

with 555 and 557 monoclonal antibodies against L1, which recognize epitopes within the FnIII-like domains 2 and 3 of L1, suggesting that binding of antibodies 555 and 557 to L1 masks the domain of L1 that interacts with APP. Furthermore, L1 could not be co-precipitated with any of the APP antibodies.

These results indicate that APP and L1 might interact, either directly or indirectly, possibly via the FnIII domains of L1. Unpublished data from our laboratory (Dr. Gabriele Loers) provide the evidence that the interaction might be direct and independent from the Aβ sequence, as extracellular domains of APP and L1 coupled to the human Fc-fragment were shown to bind to each other in the BIND assay.

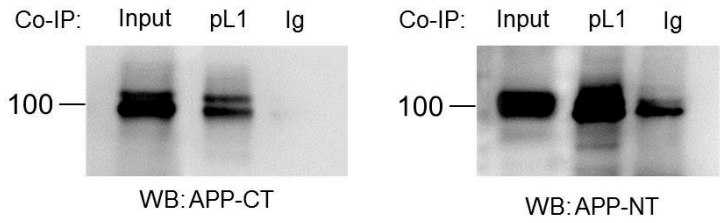

Figure 5.20. APP co-precipitates with L1. Immune rabbit serum against L1 (pL1) was used for immunoprecipitation of molecules interacting with L1 from brain homogenate of APPPS1 mice. Non-immune serum served as a control (Ig). APP could be detected in the immunoprecipitates by Western blot using the antibody against C-terminus of APP (APP-CT, panel on the left) and the N-terminal APP antibody (APP-NT, panel on the right).

5.7.3 L1 does not compete with APP for binding to the γ-secretase complex

Results of co-immunoprecipitation experiments indicate that APP and L1 might interact. This interaction might be direct or indirect, through PS1 or other components of the γ-secretase. Thus, L1 competing with APP for binding to PS1 could be a mechanism by which L1 affects APP processing and Aβ generation. To test this hypothesis, HEK cells stably transfected with human APP carrying Swedish mutation APP (APP_{sw}) and human wild-type PS1 ($PS1_{wt}$) were used. As these cells do not express L1 endogenously, they were transfected with a plasmid containing the cDNA sequence of full length L1 (pcDNA3.1-L1), and APP processing as well as Aβ production were evaluated 24 h after transfection. Efficacy of transfection was determined in cell lysates by Western blot and high levels of L1 expression were detected (Figure 5.21A, upper panel). Cell lysates were analyzed by Western blot to determine levels of full length APP and the 99-amino acid C-terminal fragment of APP

(CTF-99), which is a substrate for the γ-secretase. Neither APP nor CTF-99 levels were altered by L1 expression (Fig. 5.21A), suggesting that L1 did not interfere with APP processing by γ-secretase. Additionally, levels of soluble APP (sAPPα) generated by α-secretase in the conditioned medium from both transfected and non-transfected cells were the same. This result indicates that the production and transport of APP to the cell surface were not affected by L1, as the α-secretase pathway is the dominant way of APP ectodomain shedding. However, when Aβ40 and Aβ42 levels in conditioned medium were analyzed by ELISA, significantly lower levels of both Aβ40 and Aβ42 were detected in the medium from cells transfected with L1 compared to non-transfected cells (Fig. 5.21B). Although this finding alone could suggest a decreased Aβ generation, having in mind that the levels of APP and CTF-99 were not affected by transfection of L1, and that L1 binds to Aβ peptides (Chapter 5.6.2), it seems more likely that this reduction is a consequence of the large amounts of soluble L1 fragments in the medium of transfected cells, which bind Aβ peptides thus making them inaccessible to ELISA detection.

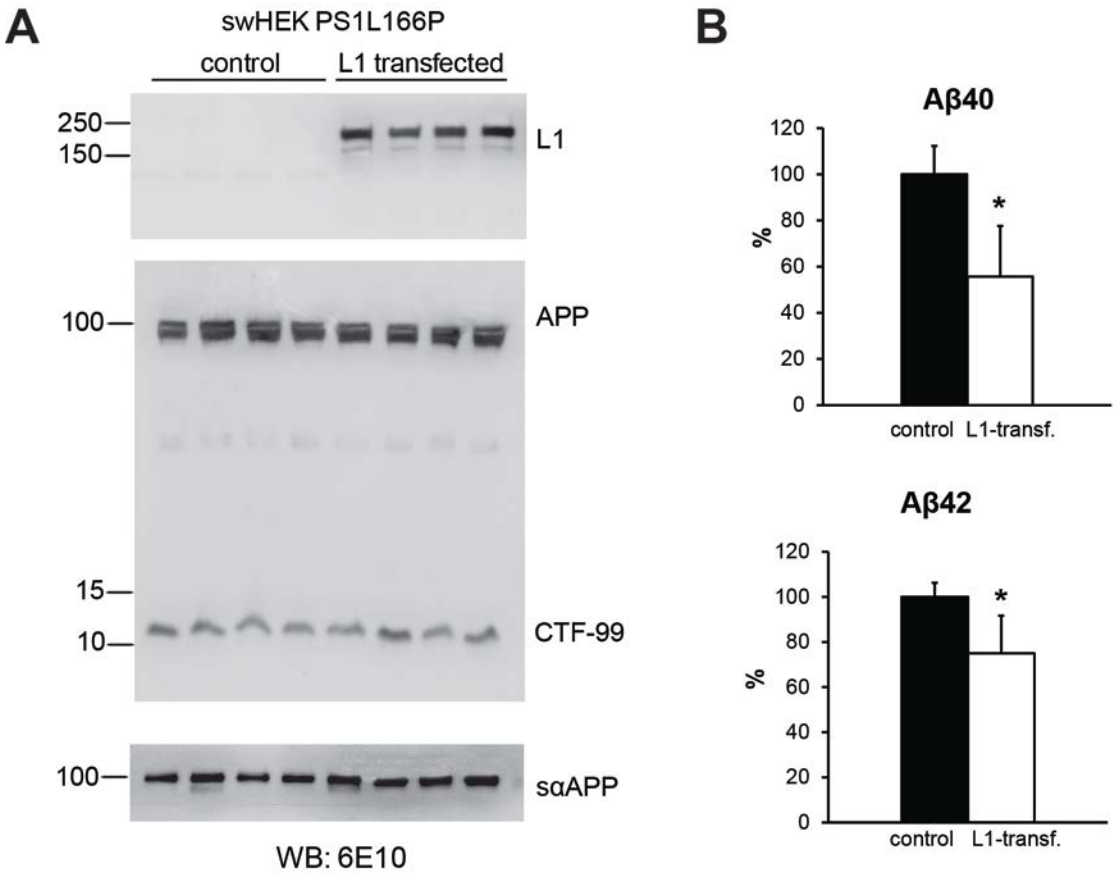

Figure 5.21. APP processing is not affected in HEK-APP$_{sw}$/PS1$_{wt}$ cells transiently transfected with L1. HEK cells stably transfected with human APP carrying Swedish mutation and human wild-type PS1 (HEK-APP$_{sw}$/PS1$_{wt}$) were transiently transfected with a plasmid containing the cDNA of murine L1. High levels of L1

expression in cell lysates of transfected cells were confirmed by Western blot using L1-172R antibody (A, top panel). Expression of full length APP and CTF-99 in cell lysates, as well as levels of soluble APP (sαAPP) in conditioned medium were not affected by L1 transfection (A, middle and bottom panel). (B) Amounts of both Aβ40 and Aβ42 were significantly reduced in conditioned medium from transfected cells, compared to non-transfected cells. Asterisks indicate $p < 0.05$, one-way ANOVA with Tukey's *post hoc*, n=4 samples/group.

6. DISCUSSION

6.1 L1 binds to β-amyloid peptides and reduces formation of amyloid plaques

A significant novel finding in this study is that L1 overexpression leads to a reduction in amyloid load in APPPS1 mouse model of cerebral amyloidosis. Decrease in the plaque size and number was observed in the hippocampus and occipital cortex four months after the AAV-L1 injection. This can be explained by another significant finding of this study – the ability of the extracellular domain of L1 to bind to Aβ peptides, shown by a label free binding assay. In this assay, the extracellular domain of L1 bound to Aβ40 and Aβ42 with a similar affinity, whereas the extracellular domain of the close homolog of L1 (CHL1) did not bound, confirming the specificity of L1-Aβ interaction. Within the complex extracellular domain of L1, the binding site(s) for Aβ could be narrowed down to the first three FnIII domains, as construct containing the first and second FnIII domain, as well as construct containing the second and third FnIII domains bound to Aβ. The anti-aggregational effect of L1 has been shown in an *in vitro* Aβ42 aggregation assay, in which Aβ42 incubated with the extracellular domain of L1 formed less oligomers compared to incubation with the extracellular domain of CHL1. This finding can explain the reduction in plaque size and number *in vivo*, as Aβ42 is the species that initiates plaque formation. It should be noted that the recombinant Fn1-2 and Fn2-3 proteins were produced in bacteria, and therefore not glycosylated, indicating that binding of the first three FnIII domains to Aβ depends on their protein sequence and not on the attached carbohydrates. On the other hand, binding of the recombinant L1-Fc and Fn1-5, which were produced in a eukaryotic system and thus glycosylated, indicates that the carbohydrates, which are normally present on L1 *in vivo*, do not interfere with the interaction between L1 and Aβ.

Although histological evaluation of the plaque load showed decreased plaque development as a consequence of L1 transduction, Aβ content determined by ELISA analysis did not show reduction of total Aβ amount in the injected hemisphere. This can be explained by the fact that histological analysis was confined to localized parts of the brain directly affected by AAV-L1 injection. On the other hand, ELISA was performed on extracts from whole hemispheres and therefore the effect of AAV-L1 injection could easily be “diluted” by the high production of Aβ outside of cortex and hippocampus. Nevertheless, a decrease of soluble Aβ42 was observed, and, as has been already mentioned, that alone is enough to slow down plaque formation. Additionally, a strong tendency towards reduction of overall Aβ42 levels was noticed, as well as a reduction of the Aβ42/40 ratio, suggesting that AAV-

L1 injection improved the clearance of Aβ42. Although the affinities of L1 were similar for binding to Aβ40 and Aβ42, the effect on Aβ42 can be explained by the higher production of Aβ42 in APPPS1 mice, compared to the Aβ40 production (Radde et al., 2006). Additionally, as Aβ42 aggregates rapidly into oligomers, it is possible that L1 binds Aβ42 oligomers and thus helps their clearance. Aβ40, on the other hand would mostly be available as a monomer (as it aggregates very slowly and deposits only in the already existing plaques), and therefore its clearance would be slower than that of Aβ42.

When discussing the effects of L1 overexpression on the plaque load the time point for the AAV-L1 injection and the dynamics of plaque deposition have to be taken into account. In APPPS1 mice the first amyloid plaques appear in the neocortex already at 6 weeks of age, whereas in the hippocampus amyloid deposition starts in the dentate gyrus at the age of 2–3 months. Progression of amyloidosis is rather fast and by the age of 8 months the entire forebrain is covered with plaques (Radde et al., 2006). The AAV-L1 was injected at the age of 3 months and it takes at least 2-3 weeks to reach the maximal levels of L1 expression (Chen et al., 2007), and the age of 4 months significant plaque load is already developed in APPPS1 mice. Therefore, it could be expected that earlier time point of the injection would have more pronounced effect on plaque formation. This would, however, therapeutically be not as relevant, since AD patients are commonly diagnosed at the stage when amyloid plaques are already developed.

Several other mechanisms could also contribute to the L1-mediated plaque reduction. For example, it is possible that by reducing astrocyte proliferation, L1 modifies astrocytic Aβ secretion and/or increases Aβ uptake by astrocytes, thus reducing extracellular accumulation of Aβ. Since L1 increases angiogenesis (Hall et al., 2004; Friedli et al., 2009) it is also conceivable that providing a better blood supply would enhance neuroprotection. It is interesting in this context that L1 reduces the efficiency of the blood-brain barrier and may thus contribute to clearance of Aβ from the brain to the vasculature (Wang et al., 2006) in a delicate balance between drainage and infiltration of components of the immune system. Another possible protective role of L1 in AD stems from its potential for decreasing neural cell proliferation and, thus, preventing cell cycle activity (Bernreuther et al., 2006; Dihne et al., 2003; Guseva et al., 2011). Cell cycle re-entry has been emphasized as a major player in the damage to neurons caused by Aβ in AD, and in other forms of neurodegeneration (Herrup, 2010; Varvel et al., 2008; Wu et al., 2011).

Additionally, it has been reported that the cleavage of the intracellular domain of L1 and its nuclear translocation, important for L1-mediated signalling, are due to a PS-1 dependent γ-secretase activity in human carcinoma cells (Riedle et al., 2009) and this study has shown that the γ-secretase mediated proteolytic cleavage of L1 is increased in APPPS1 mice (Lutz et al., 2012). The possibility that L1 overexpression leads to saturation of γ-secretase activity leading to reduced Aβ secretion has been ruled out by the experiment with transient expression of L1 in a cell line which does not express L1 endogenously, but is stably transfected to express human APP and PS1. The results of this experiment showed that L1 expression did not alter levels of C-terminal fragment of APP, which is a substrate for γ-secretase, and therefore a reliable indicator of the γ-secretase APP processing. Furthermore, it has recently been demonstrated that L1 and CHL1 are cleaved by the β-site amyloid precursor protein-cleaving enzyme BACE1 (Zhou et al., 2012). It is possible that L1 cleavage fragments play a role in AD pathology (Lutz et al., 2012).

6.2 The effect of L1 on astrogliosis and inflammation

The extent of reactive astrogliosis and levels of accumulated Aβ in astrocytes have been shown to correlate with the severity of AD-associated tissue damage (Nagele et al., 2004; Simpson et al., 2010), and in APPPS1 mice astrogliosis occurs simultaneously with plaque deposition and microgliosis. Furthermore, evidence obtained from cultures containing astrocytes and neurons argues in favor of a detrimental effect of astrocyte–Aβ interactions on neuronal viability (Allaman et al., 2010; Paradisi et al., 2004). Internalization of the aggregated form of Aβ by astrocytes has been observed to profoundly affect their metabolic phenotype, both in terms of energy consumption and oxidative stress, resulting in an overall degeneration-promoting role in AD pathology (Allaman et al., 2010). L1 is known for its ability to reduce astrogliosis and astrocytic differentiation in several experimental paradigms, including transplantation of L1 overexpressing neural stem cell into mice with spinal cord injury and Parkinson's disease symptoms (Cui et al., 2010; Cui et al., 2011b) and AAV-L1 injection into spinal cord injured mice (Chen et al., 2007; Lee et al., 2012). Interestingly, L1 overexpressed by neural stem cells under the human GFAP promoter and transplanted into injured mouse spinal cords reduced astrocytic differentiation of stem cells, but did not affect astrogliosis after injury, indicating that ectopic expression of L1 in host astrocytes is relevant to reduce astrogliosis (Xu et al., 2011).). This is further supported by an observation that in mice that transgenically overexpress L1 in neurons astrocytic reaction to spinal cord injury is

not altered (Jakovcevski et al., 2013). A previous study on AAV-mediated L1 overexpression in the injured spinal cord showed that L1 reduces GFAP expression, most likely by homophilic L1-L1 binding and subsequent signal transduction in L1-expressing host astrocytes (Chen et al., 2007). This notion was further corroborated by *in vitro* analyses showing that ectopic L1 expression in host astrocytes reduces their proliferation, migration and process formation (Chen et al., 2007). In the present study a reduction in numbers of GFAP-positive astrocytes and a decrease in GFAP expression were observed, which is likely due to a similar mechanism, since AAV-mediated gene transfer targets also astrocytes. However, despite the finding that neuronal overexpression of L1 does not influence activity and proliferation of astrocytes in spinal cord injury, the possibility that it can affect astrogliosis in AD cannot be excluded, as spinal cord injury and AD are, besides similarities in inflammatory response, different neuropathological entities. Although it is not clear whether decreased astrogliosis is linked to a decrease in plaque formation, our observation suggests a less severe astrocytic reaction upon application of L1.

Brain inflammation is another important hallmark of AD pathology (Herrup, 2010; Weiner and Frenkel, 2006; Wyss-Coray, 2006). In predepositing APPPS1 mice neuroinflamation is not present, and they do not differ in microglia number from non-transgenic control mice. Microgliosis starts with the appearance of the first plaques, with the activated Iba1-positive microglia clustering around amyloid deposits. By the age of 7-8 months transgenic mice show a threefold increase in microglia number (Radde et al., 2006; Djogo et al., 2013).

In the present study, L1 overexpression did not affect numbers or activation of microglial cells/macrophages in APPPS1 mice. This finding was unexpected since L1-overexpressing neural stem cell aggregates were shown to reduce numbers of microglial cells/macrophages following spinal cord injury (Cui et al., 2011b). Several reasons may account for this apparent lack of effect on inflammation. First, AAV5-mediated gene transfer does not target microglial cells/macrophages. It is, therefore, conceivable that L1 would not affect these in the AD model used. Second, analysis did not include parameters of CNS inflammation other than number of microglial cells/macrophages, such as cytokine secretion, pro-inflammatory T-lymphocytes and activity of reactive astrocytes, which could be altered by L1 application, in view of a reduced astrogliosis. Finally, although there is firm evidence that inflammatory response is involved in AD pathology, it is not clear whether this response is beneficial or detrimental during the pathological process. On the one hand, microglial cells/macrophages play a role in Aβ clearance (Bolmont et al., 2008), but on the other hand a detrimental role

via cytokine secretion has been suggested based on epidemiological data, implicating a lower risk for AD in long-term users of non-steroidal anti-inflammatory drugs (NSAIDs) (Wyss-Coray, 2006). However, NSAIDs are not useful in AD patients with developed amyloid pathology. Ultrastructural studies have shown that microglia clustered around plaques is ineffective in phagocytosis of amyloid (Wisniewski et al., 1989). Interestingly, in the same AD mouse model used in this study, near complete microglia ablation did not affect formation and maintenance of Aβ plaques (Grathwohl et al., 2009). Additionally, it has been recently demonstrated in two mouse models of AD that important functions of microglia, directed process motility and phagocytic activity, are impaired upon the onset of amyloid deposition (Krabbe et al., 2013); this impairment could be reversed by reducing amyloid burden. In line with this reduced ability of microglia to ingest amyloid is the observation of this study that only some of the microglial cells around amyloid plaques are positive for Mac-2, marker of phagocytic microglial activity.

Within the time-frame studied, L1 overexpression does not change the number of Iba-1-positive cells, but affects their distribution around amyloid plaques. However, it remains to be seen whether this change in distribution is biologically significant, as the number of actively phagocytic Mac-2-positive microglia/macrophages present around the plaques was not affected by L1 overexpression. It is important in this context that levels of the CCL2 chemokine were not different between the AAV-L1 injected and control hemispheres. CCL2 is important inflammatory chemokine and it is upregulated in both microglia and astrocytes in AD, but it seems that its production was not affected by reduced number of astrocytes after AAV-L1 injection.

6.3 Functional considerations – the neuroprotective effect of L1

Global neocortical neuron loss is not apparent up to 8 months of age in APPPS1 mice, but local neuron loss in the dentate gyrus is observed (Radde et al., 2006). Therefore, it is not surprising that they show only subtle behavioral phenotype - impairment in working memory present at the age of 8 months, which coincides with significant amyloidosis in the hippocampus (Radde et al., 2006). In line with this observation is electrophysiological evidence for impaired long-term potentiation in CA1 *in vivo* at the same age (Gengler et al., 2010). However, loss of parvalbumin-positive interneurons was reported in the olfactory cortex of a similar APP/PS1 double transgenic mouse model (Saiz-Sanchez et al., 2013) and electrophysiological deficits in PV-positive cortical interneurons were found (Verret et al.,

2012). Additionally, selective vulnerability of PV-positive interneurons has been documented under different experimental conditions, including epilepsy (Schwaller et al., 2004), global ischemia (Meade et al., 2000), IL6 overexpression (Samland et al., 2003) and ketamine exposure (Behrens et al., 2008). In this study parvalbumin-positive interneurons were quantified in the hippocampus, but no loss was observed.

Since the early symptoms of AD pathogenesis are thought to occur at synapses, and loss of dendritic spines and synaptic contacts is commonly seen in AD mouse models (Terry et al., 1991; Wei et al., 2010), it was not surprising that significantly reduced numbers of inhibitory perisomatic terminals in hippocampal CA1 and CA3 regions, compared with age-matched wild-type controls, were found in this study. Interestingly, this loss was not observed in the dentate gyrus. Importantly, L1 overexpression reduced loss of perisomatic inhibitory terminals in the CA1 and CA3 regions of the hippocampus, which is on a functional level the most noteworthy effect of L1 overexpression in APPPS1 mice, indicating a potentially important functional contribution of L1 to prevention of neurodegeneration. This beneficial contribution of L1 is not surprising, considering the previously reported effects of L1 as a survival factor for neurons as well as promoter of neurite elongation and synaptic plasticity both *in vitro* and *in vivo* (Chen et al., 1999; Cui et al., 2010; 2011b; Dihne et al., 2003; Guseva et al., 2011; Lee et al., 2012; Nishimune et al., 2005).

Although behavioral consequences of L1 were not investigated in this study, previous studies with L1 in nervous system disease models support the notion that significant morphological improvements are coupled with behavioral benefits (Chen et al., 2007; Cui et al., 2010; Lee et al., 2012).

6.4 Conclusion

Late-onset (sporadic) AD is the most common form of dementia in humans over the age of 65 and affects more than 50% of individuals older than 85. Advances in medicine as well as improved social and environmental conditions, are expanding life expectancy with significant numbers living well into their 80s and 90s. Since the incidence and prevalence of AD and other dementias increase with age, the number of people with these conditions is also expected to grow rapidly unless new therapeutic approaches are available to prevent, or at least delay the onset of disease. AD has an intricate and not yet fully understood pathology that demands a complex therapeutic approach (Herrup, 2010).

This study presents evidence that AAV-mediated overexpression of L1 in neurons and astrocytes improves amyloid pathology in a mouse model of AD. Potentially therapeutically relevant effects of L1 overexpression in an AD mouse model include the reduction of amyloid plaque load, decreased astrogliosis and better preservation of inhibitory synaptic terminals on pyramidal cell bodies in the hippocampus. These beneficial effects of L1 are probably mediated via multiple mechanisms, including its previously described neurotrophic effect, a reduction of astrocyte activation, as well as the novel finding reported here that L1 binds specifically to Aβ and reduces Aβ aggregation. This renders future non-viral L1 application in the form of either a recombinant extracellular domain, L1 function mimicking peptides or in form of small organic compounds that functionally mimic L1 epitopes, possibly in conjunction with other curative treatments. Small peptide mimetics of glycans like polysialic acid have been used to promote regeneration after injury of the spinal cord and femoral nerve (Mehanna et al., 2009; 2010). Moreover, a peptide containing the N-terminus of the third FnIII domain of L1 was shown to bind to Aβ40 and Aβ42 in a dose-dependent manner (Dr. Gabriele Loers, unpublished data).

Applications of such L1 constructs into the brain - via slowly releasing synthetic hydrogels, nanoparticles, organic biomaterials such as alginate, or encapsulated L1 recombinant construct expressing cells - are currently feasible approaches to bypass the blood brain barrier (He et al., 2012). In addition, such direct applications into the nervous system would circumvent potential pitfalls of L1 application with unknown consequences of its functions outside the nervous system, where L1 is also expressed.

It is noteworthy that AAVs are now used in clinical trials worldwide, so AAV might also become a plausible method of L1 delivery in patients (Grieger et al., 2012).

Strategies directed towards reduction of amyloid deposition or clearance cannot cure fully developed AD, as the loss neurons and their circuitries cannot be reversed. However, recent advances in diagnostics, such as PET imaging of fibrillar amyloid-beta using Pittsburgh compound B (Cohen et al., 2012), allow for detection of fibrillar Aβ deposition in vivo and thus enables early or perhaps preclinical detection of disease and accurate distinction of AD from other dementias in patients presenting with mild or atypical symptoms. That gives hope for more successful treatment strategies as the intervention could be made before massive neurodegeneration had happened. Well-timed treatment could at least postpone or slow down the disease progression. However, two key questions are still without answer. First is to what extent should Aβ production be lowered, or amyloid clearance facilitated, to mediate

a therapeutic disease-modifying effect, and second, at what stage of the disease would an amyloid-β-directed therapeutic approach show clinical efficacy. However, L1 or L1-function mimicking compounds, in addition to the anti-aggregation effect are also neuroprotective and therefore well suited to be potential candidates for therapy.

7A. SUMMARY

Alzheimer's disease (AD) is a devastating neurodegenerative disorder and the most common cause of elderly dementia. One of the main histopathological features of AD diseased brain are amyloid plaques, depositions made of β-amyloid peptide (Aβ), derived from β-amyloid precursor protein (APP).

The neural cell adhesion molecule L1 is an adhesion molecule of the Ig superfamily which plays an important role in neuronal development. Several studies showed that L1 overexpression has the potential to reduce degenerative processes and to improve recovery in animal models of traumatic injury and neurodegenerative disorders. Interestingly, increased levels of L1 were shown in the cerebrospinal fluid of AD patients. In light of these findings, this study was focused on investigating the possibility that L1 might ameliorate some characteristic cellular and molecular parameters associated with the disease in APPPS1 mouse model of AD. APPPS1 mice overexpress mutated forms of human APP (KM670/671NL, "Swedish" mutation) and human presenilin-1 (PS1, L166P mutation) under the control of a neuron-specific promoter and have rapid progression of cerebral amyloidosis. Three-month-old mice received an injection of adeno-associated virus encoding the neuronal isoform of full-length L1 (AAV-L1) or, as negative control, green fluorescent protein (AAV-GFP) into the hippocampus and occipital cortex of one brain hemisphere. Four months after virus injection, the mice were analyzed for histological and biochemical parameters of AD.

L1 was found to be overexpressed in neurons and ectopically expressed in astrocytes, while no expression was detected in microglia/macrophages and oligodendrocytes. Histological analysis revealed decreased Aβ plaque load in AAV-L1 injected. Reduced levels of soluble Aβ42, and lower Aβ42/40 ratio were detected by ELISA in AAV-L1 injected hemispheres compared with the contralateral hemisphere of the same brain. AAV-L1 injection reduced astrogliosis, but had no effect on numbers of Iba1-positive microglial cells/macrophages, which falls in line with observed pattern of transduction. However, numbers of microglial cells/macrophages in clusters around plaques were increased in AAV-L1 injected mice. To explain this, CCL2 chemokine levels were tested, but no difference was found. Additionally, when analyzed with marker for active phagocytic microglia/macrophages, Mac-2 (galectin-3), numbers of cells were significantly lower and did not show a difference in clustering. An important finding of this study was that AAV-L1 injected mice had increased densities of inhibitory synaptic terminals on pyramidal cells in the hippocampus when compared with AAV-GFP injected controls.

To analyze/discover the molecular mechanism that may underlie the lower amyloid load in AAV-L1 injected mice, we tested two possibilities: 1) L1 binds Aβ and thus affects Aβ aggregation, or 2) L1 competitively reduces APP processing and therefore Aβ secretion, being a substrate for PS1, the same enzyme involved in Aβ generation. The first possibility was explored in a label-free binding assay. Concentration dependent binding of the extracellular domain of L1, but not of the close homolog of L1 (CHL1) to Aβ40 and Aβ42 was seen, with the fibronectin type III homologous repeats 1-3 of L1 mediating this effect. Also, *in vitro* aggregation assay showed reduced aggregation of Aβ42 the presence of the extracellular domain of L1 but not in the presence of CHL1. Competitive binding of L1 to PS1 as a cause of reduced APP processing was investigated in a cell line expressing human APP and PS1. Upon transfection with L1 there was no change in APP expression or processing, which suggests that L1 does not interfere with these processes.

The combined observations indicate that L1, when overexpressed in neurons and glia, reduces several histopathological hallmarks of AD in mice, probably by reduction of Aβ aggregation, ectopic L1 expression in astrocytes and protection of synapses. L1 thus appears to be a candidate molecule to ameliorate the pathology of AD.

7B. ZUSAMMENFASSUNG

Die Alzheimer´sche-Krankheit ist eine verheerende neurodegenerative Erkrankung und die häufigste Ursache von Demenz bei älteren Menschen. Eines der wichtigsten histopathologischen Merkmale, das sich in Gehirnen von Patienten mit Morbus Alzheimer finden lässt, sind Amyloid-Plaques, Ablagerungen von β-Amyloid-Peptid (Aß) welches aus dem β-Amyloid-Vorläuferprotein („Amyloid-Precursor-Protein“, APP) entsteht.

Das neurale Zelladhäsionsmolekül L1 ist ein Adhäsionsmolekül der Immunglobulin-Superfamilie, welches eine wichtige Rolle in der neuronalen Entwicklung spielt. Mehrere Studien haben gezeigt, dass die Überexpression von L1 zur Reduktion von degenerativen Prozessen und zur Regeneration von traumatischen Verletzungen und neurodegenerativen Störungen in Tiermodellen führt. Interessanterweise wurde im Liquor von Patienten die an Morbus Alzheimer leiden eine erhöhte Menge an löslichen L1 Proteinfragmenten nachgewiesen. In Anbetracht dieser Ergebnisse wurde in dieser Studie die Möglichkeit überprüft, ob L1 einige der charakteristischen zellulären und molekularen Parameter, die mit der Krankheit im APPPS1 Mausmodell der Alzheimer´schen-Krankheit assoziert sind, verbessert. APPPS1 Mäuse überexprimieren mutierte Formen von humanem APP (KM670/671NL, "Schwedische" Mutation) und menschlichem Presenilin-1 (PS1, L166P-Mutation) unter der Kontrolle eines Neuron-spezifischen Promotors und haben eine schnell fortschreitende zerebrale Amyloidose. Drei Monate alte Mäuse erhielten eine Injektion eines Adeno-assoziierten Virus, welcher die neuronale Isoform des L1 (AAV-L1) kodiert, oder, als Negativkontrolle, grün fluoreszierendes Protein (AAV-GFP) in den Hippocampus und okzipitalen Kortex einer Gehirnhälfte. Vier Monate nach der Virus-Injektion wurden die Mäuse für histologische und biochemische Parameter der Alzheimer´schen-Krankheit analysiert.

Injektion von AAV-L1 führte in Neuronen zu einer Überexpression von L1 und zu einer ektopischen Expression von L1 in Astrozyten, wohingegen keine Expression von L1 in Mikroglia/Makrophagen und Oligodendrozyten festgestellt werden konnte. Die histologische Analyse zeigte eine verringerte Aß Plaque Belastung in AAV-L1 injizieren Gehirnen. Mittels ELISA wurden in AAV-L1 injiziert Hemisphären reduzierte Mengen von löslichem Aß42 Peptid und ein niedrigeres Aβ42/40 Verhältnis im Vergleich mit der kontralateralen Hemisphäre des gleichen Gehirns festgestellt. AAV-L1 Injektion reduzierte die Astrogliose, hatte aber keinen Einfluss auf die Zahl der Iba1-positiven Mikrogliazellen/Makrophagen. Dies ist im Einklang mit dem beobachteten Muster der L1-Transduktion. Allerdings war die

Anahl von Mikrogliazellen/Makrophagen in den Anhäufungen um die Plaques in AAV-L1 injizierten Mäusen erhöht. Um dies zu erklären, wurden die Mengen an CCL2 Chemokin bestimmt, aber es wurde kein Unterschied in den CCL2-Mengen zwischen den AAV-L1 injizierten Hemisphären und den Kontrollhemisphären gefunden. Wenn darüber hinaus die Zahl der aktiv phagozytierenden Mikroglia/Makrophagen (Mac-2, Galektin-3 positive Zellen) untersucht wurde, war die Anzahl von Mac-2 positiven Zellen signifikant niedriger, aber es zeigten sich keine Unterschiede in der Anhäufung dieser Zellen. Eine wichtige Erkenntnis dieser Studie war, dass AAV-L1 injizierte Mäuse im Vergleich mit AAV-GFP injizierten Kontrolltieren eine höhere Dichte von hemmenden Synapsen auf Pyramidenzellen im Hippokampus aufweisen.

Zwei mögliche molekularen Mechanismen, die die niedrige Amyloid-Belastung in AAV-L1 injizierten Mäusen erklärten, wurden von mir getestet: 1) L1 bindet Aß und wirkt somit auf die Aß-Aggregation, oder 2) L1 reduziert die APP-Prozessierung und Aß-Sekretion L1 ist ebenfalls ein Substrat für PS1, das gleiche Enzym welches an der Aß-Bildung beteiligt ist. Die erste Möglichkeit wurde in einem markierungsfreien Bindungs-„Assay“ getestet. Eine konzentrationsabhängige Bindung der extrazellulären Domäne von L1, nicht aber der des „Close Homolog of L1“ (CHL1), an Aβ40 und Aß42 konnte gezeigt werden. Diese Bindung wurde von den Fibronektin-Typ-III homologen Wiederholung 1-3 in der extrazelluären Domäne von L1 vermittelt. Auch im *in vitro*-Aggregations-Versuch wurde in Anwesenheit der extrazellulären Domäne von L1eine reduzierte Aggregation von Aß42 Peptiden gezeigt. Die kompetitive Bindung von L1 an PS1 als Ursache verminderter APP-Prozessierung wurde in einer Zelllinie die humanes APP und PS1 exprimiert untersucht. Nach Transfektion mit L1 gab es keine Veränderung in der APP-Expression oder Prozessierung, was darauf hindeutet, dass L1 nicht in diese Prozesse eingreift. Die Beobachtungen zeigen, dass L1, wenn es in Neuronen und Glia überexprimiert wird, mehrere histopathologische Kennzeichen der Alzheimer´schen Erkrankungbei Mäusen reduziert. Dies erfolgt wahrscheinlich durch Reduktion von Aß-Aggregation, ektopische L1 Expression in Astrozyten und Schutz der Synapsen. L1 scheint daher ein interessanter Kandidat, für Behandlung der Alzheimer´schen Krankheit und zur Verbesserung der Alzheimer Pathologie zu sein.

8. REFERENCES

Abe K, Tanzi RE, Kogure K. Selective induction of Kunitz-type protease inhibitor domain-containing amyloid precursor protein mRNA after persistent focal ischemia in rat cerebral cortex. Neurosci Lett 1991; 125:172-4.

Albert MS. Changes in cognition. Neurobiol Aging 2011; 32:58-63.

Allaman I, Gavillet M, Bélanger M, Laroche T, Viertl D, Lashuel HA et al. Amyloid-beta aggregates cause alterations of astrocytic metabolic phenotype: impact on neuronal viability. J Neurosci 2010; 30:3326–38.

Annaert W, De Strooper B. Presenilins: molecular switches between proteolysis and signal transduction. Trends Neurosci 1999; 22:439-43.

Andersen K. Gender Differences in the Incidence of AD and Vascular Dementia: The EURODEM Studies. EURODEM Incidence Research Group. Neurology 1999; 53:1992–7.

Andersen OM, Reiche J, Schmidt V, Gotthardt M, Spoelgen R, Behlke J et al. Neuronal sorting protein-related receptor sorLA/LR11 regulates processing of the amyloid precursor protein. Proc Natl Acad Sci USA 2005; 102:13461-6.

Appel F, Holm J, Conscience JF, Schachner M. Several extracellular domains of the neural cell adhesion molecule L1 are involved in neurite outgrowth and cell body adhesion. J Neurosci 1993; 13:4764-75.

Appel F, Holm J, Conscience JF, von Bohlen und Halbach F, Faissner A, James P, et al. Identification of the border between fibronectin type III homologous repeats 2 and 3 of the neural cell adhesion molecule L1 as a neurite outgrowth promoting and signal transducing domain. J Neurobiol 1995; 28:297-312.

Arai T, Ikeda K, Akiyama H, Shikamoto Y, Tsuchiya K, Yagishita S et al. Distinct isoforms of tau aggregated in neurons and glial cells in brains of patients with Pick's disease, corticobasal degeneration and progressive supranuclear palsy. Acta Neuropathol 2001; 101:167–73.

Arai H, Lee VMY, Messinger ML, Greenberg BD, Lowery DE, Trojanowski JQ. Expression patterns of β-amyloid precursor protein in neural and nonneural human tissues from AIzheimer's disease and control subjects. Ann Neurol 1991; 30:686-93.

Asou H, Miura M, Kobayashi M, Uyemura K. The cell adhesion molecule L1 has a specific role in neural cell migration. Neuroreport 1992; 3:481-4.

Baek SH, Ohgi KA, Rose DW, Koo EH, Glass CK, Rosenfeld MG. Exchange of N-CoR corepressor and Tip60 coactivator complexes links gene expression by NF-kappaB and beta-amyloid precursor protein. Cell 2002; 110:55-67.

Bard F, Cannon C, Barbour R, Burke RL, Games D, Grajeda H et al. Peripherally administered antibodies against amyloid beta-peptide enter the central nervous system and reduce pathology in a mouse model of Alzheimer disease. Nat Med 2000; 6:916–9.

Barrow CJ and Zagorski MG. Solution structure of beta-peptide and its constituent fragments: relation to amyloid deposition. Science 1991; 253:179-82.

Bartsch U, Kirchhoff F, Schachner M. Immunohistological localization of the adhesion molecules L1, N-CAM, and MAG in the developing and adult optic nerve of mice. J Comp Neurol 1989; 284:451-62.

Baumeister R, Leimer U, Zweckbronner I, Jakubek C, Grünberg J, Haass C. Human presenilin-1, but not familial Alzheimer's disease (FAD) mutants, facilitate *Caenorhabditis elegans* Notch signalling independently of proteolytic processing. Genes Funct 1997; 1: 149–59.

Bechara A, Nawabi H, Moret F, Yaron A, Weaver E, Bozon M et al. FAK-MAPK-dependent adhesion disassembly downstream of L1 contributes to semaphorin3A-induced collapse. EMBO J 2008; 27:1549–62.

Beher D, Hesse L, Masters CL, Multhaup G. Regulation of amyloid protein precursor (APP) binding to collagen and mapping of the binding sites on APP and collagen type I. J Biol Chem 1996; 271:1613-20.

Behrens MM, Ali SS, Dugan LL. Interleukin-6 mediates the increase in NADPH-oxidase in the ketamine model of schizophrenia. J Neurosci 2008; 28:13957-66.

Bentahir M, Nyabi O, Verhamme J, Tolia A, Horré K, Wiltfang J et al. Presenilin clinical mutations can affect γ-secretase activity by different mechanisms. J Neurochem 2006; 96:732–42.

Bermejo-Pareja F, Benito-León J, Vega S, Medrano MJ, Román GC. Incidence and subtypes of dementia in three elderly populations of central Spain. J Neurol Sci 2008; 264:63–72.

Bernreuther C, Dihné M, Johann V, Schiefer J, Cui Y, Hargus G et al. Neural cell adhesion molecule L1-transfected embryonic stem cells promote functional recovery after excitotoxic lesion of the mouse striatum. J Neurosci 2006; 26:11532-9.

Blaess S, Kammerer RA, Hall H. Structural analysis of the sixth immunoglobulin-like domain of mouse neural cell adhesion molecule L1 and its interactions with alpha(v)beta3, alpha(IIb)beta3, and alpha5beta1 integrins. J Neurochem 1998; 71:2615-25.

Blennow K, de Leon MJ, Zetterberg H. Alzheimer's disease. Lancet 2006; 368:387-403.

Blessed G, Tomlinson BE, Roth M. The association between quantitative measures of dementia and of senile change in the cerebral grey matter of elderly subjects. Br J Psychiatry 1968; 114:797-811.

Bolmont T, Haiss F, Eicke D, Radde R, Mathis CA, Klunk WE et al. Dynamics of the microglial/amyloid interaction indicate a role in plaque maintenance. J Neurosci 2008; 28:4283-92.

Bouras C, Hof PR, Giannakopoulos P, Michel JP, Morrison JH. Regional distribution of neurofibrillary tangles and senile plaques in the cerebral cortex of elderly patients: A quantitative evaluation of a one-year autopsy population from a geriatric hospital. Cereb Cortex 1994; 4:138–50.

Braak H, Braak E. Neuropathological stageing of Alzheimer-related changes. Acta Neuropathol 1991; 82:239-59.

Braak H, Thal DR, Ghebremedhin E, Del Tredici K. Stages of the pathologic process in Alzheimer disease: Age categories from 1 to 100 years. J Neuropathol Exp Neurol 2011; 70:960–9.

Bu G, Cam J, Zerbinatti C (2006). LRP in amyloid-beta production and metabolism. Ann N Y Acad Sci 2006; 1086:35-53.

Buée L, Bussière T, Buée-Scherrer V, Delacourte A, Hof PR. Tau protein isoforms, phosphorylation and role in neurodegenerative disorders. Brain Res Brain Res Rev 2000; 33:95–130.

Bush AI, Multhaup G, Moir RD, Williamson TG, Small DH, Rumble B et al. A novel zinc(II) binding site modulates the function of the beta A4 amyloid protein precursor of Alzheimer's disease. J Biol Chem 1993; 268:16109-12.

Buxbaum JD, Koo EH and Greengard P. Protein phosphorylation inhibits production of Alzheimer amyloid beta/A4 peptide. Proc Natl Acad Sci USA 1993; 90:9195-8.

Buxbaum JD, Liu KN, Luo Y, Slack JL, Stocking KL, Peschon JJ et al. Evidence that tumor necrosis factor alpha converting enzyme is involved in regulated alpha-secretase cleavage of the Alzheimer amyloid protein precursor. J Biol Chem 1998; 273:27765-7.

Cai XD, Golde TE, Younkin SG. Release of excess amyloid beta protein from a mutant amyloid beta protein precursor. Science 1993; 259:514-6.

Cai H, Wang Y, McCarthy D, Wen H, Borchelt DR, Price DL et al. BACE1 is the major beta-secretase for generation of Abeta peptides by neurons. Nat Neurosci 2001; 4:233–4.

Cairns NJ, Bigio EH, Mackenzie IR, Neumann M, Lee VM Hatanpaa KJ et al. Neuropathologic diagnostic and nosologic criteria for frontotemporal lobar degeneration: Consensus of the Consortium for Frontotemporal Lobar Degeneration. Acta Neuropathol (Berl) 2007; 114:5–22.

Castellano JM, Kim J, Stewart FR, Jiang H, DeMattos RB, Patterson BW et al. Human apoE isoforms differentially regulate brain amyloid-β peptide clearance. Sci Transl Med 2011; 3(89):89ra57.

Cao X, Sudhof TC. A transcriptionally active complex of APP with Fe65 and histone acetyltransferase Tip60. Science 2001; 293:115-20.

Cao X, Sudhof TC. Dissection of APPdependent transcriptional transactivation. J Biol Chem 2004; 279:24601-11.

Chang S, Rathjen FG, Raper JA. Extension of neurites on axons is impaired by antibodies against specific neural cell surface glycoproteins. J Cell Biol 1987;104:355-62.

Chen J, Bernreuther C, Dihné M, Schachner M. Cell adhesion molecule L1-transfected embryonic stem cells with enhanced survival support regrowth of corticospinal tract axons in mice after spinal cord injury. J Neurotrauma 2005; 22:896-906.

Chen J, Wu J, Apostolova I, Skup M, Irintchev A, Kügler S et al. Adeno-associated virus-mediated L1 expression promotes functional recovery after spinal cord injury. Brain 2007; 130:954-69.

Chen S, Mantei N, Dong L, Schachner M. Prevention of neuronal cell death by neural adhesion molecules L1 and CHL1. J Neurobiol 1999; 38:428-39.

Chen Y, Liu W, McPhie DL, Hassinger L, Neve RL. APP-BP1 mediates APP-induced apoptosis and DNA synthesis and is increased in Alzheimer's disease brain. J Cell Biol 2003; 163:27-33.

Chen Y, Bodles AM, McPhie DL, Neve RL, Mrak RE, Griffin WS. APP-BP1 inhibits Abeta42 levels by interacting with Presenilin-1. Mol Neurodegener 2007; 2:3.

Clark M J, Gagnon J, Williams AF, Barclay AN. MRC OX-2 antigen: A lymphoid/neuronal membrane glycoprotein with a structure like a single immunoglobulin light chain. EMBO J 1985; 4:113-8.

Cohen AD, Rabinovici GD, Mathis CA, Jagust WJ, Klunk WE, Ikonomovic MD. Using Pittsburgh Compound B for in vivo PET imaging of fibrillar amyloid-beta. Adv Pharmacol 2012; 64:27-81.

Cohen NR, Taylor JSH, Scott LB, Guillery RW, Soriano P, Furley AJW. Errors in corticospinal axon guidance in mice lacking the neural cell adhesion molecule L1. Curr Biol 1998; 8:26–33.

Corder EH, Saunders AM, Strittmatter WJ, Schmechel DE, Gaskell PC, Small GW et al. Gene dose of apolipoprotein E type 4 allele and the risk of Alzheimer's disease in late onset families. Science 1993; 261:921-3.

Corder EH, Saunders AM, Risch NJ, Strittmatter WJ, Schmechel DE, Gaskell PC Jr et al. Protective effect of apolipoprotein E type 2 allele for late onset Alzheimer disease. Nat Genet 1994; 7:180-4.

Coulson EJ, Paliga K, Beyreuther K, Masters CL. What the evolution of the amyloid protein precursor supergene family tells us about its function. Neurochem Int 2000; 36:175–84.

Cooper MA. Optical biosensors in drug discovery. Nat Rev Drug Discovery 2002; 1: 515–28.

Cunningham BT, Li P, Schulz S, Lin B, Baird C, Gerstenmaier J et al. Label-free assays on the BIND system. J Biomol Screen 2004; 9:481– 90.

Cui Y-F, Hargus G, Xu J-C, Schmid JS, Shen Y-Q, Glatzel M et al. Embryonic stem cell-derived L1 overexpressing neural aggregates enhance recovery in Parkinsonian mice. Brain 2010; 133:189-204.

Cui X, Weng YQ, Frappé I, Burgess A, Girão da Cruz MT et al. The cell adhesion molecule L1 regulates the expression of choline acetyltransferase and the development of septal cholinergic neurons. Brain Behav 2011a; 1:73-86.

Cui Y-F, Xu J-C, Hargus G, Jakovcevski I, Schachner M, Bernreuther C. Embryonic stem cell-derived L1 overexpressing neural aggregates enhance recovery after spinal cord injury in mice. PLoS ONE 2011b; 6:e17126.

Dahme M, Bartsch U, Martini R, Anliker B, Schachner M, Mantei N. Disruption of the mouse L1 gene leads to malformations of the nervous system. Nat Genet 1997; 17:346–9.

Daigle I, Li C. apl-1, a Caenorhabditis elegans gene encoding a protein related to the human beta-amyloid protein precursor. Proc Natl Acad Sci USA 1993; 90:12045–9.

Davies L, Wolska B, Hilbich C, Multhaup G, Martins R, Simms G et al. A4 amyloid protein deposition and the diagnosis of Alzheimer's disease: Prevalence in aged brains determined by immunocytochemistry compared with conventional neuropathologic techniques. Neurology 1988; 38:1688–93.

Dawson GR, Seabrook GR, Zheng H, Smith DW, Graham S, O'Dowd G et al. Age-related cognitive deficits, impaired long-term potentiation and reduction in synaptic marker density in mice lacking the beta-amyloid precursor protein. Neuroscience 1999; 90:1–13.

Delrieu J, Ousset PJ, Caillaud C, Vellas B. 'Clinical trials in Alzheimer's disease': immunotherapy approaches. J Neurochem 2012; 120(Suppl 1):186–93.

Demyanenko GP, Shibata Y, Maness PF. Altered distribution of dopaminergic neurons in the brain of L1 null mice. Brain Res Dev Brain Res 2001; 126:21-30.

Demyanenko GP, Tsai AY, Maness PF. Abnormalities in neuronal process extension, hippocampal development, and the ventricular system of L1 knockout mice. J Neurosci 1999; 19:4907–20.

De Strooper B, Annaert W, Cupers P, Saftig P, Craessaerts K, Mumm JS et al. A presenilin-1-dependent gamma-secretase-like protease mediates release of Notch intracellular domain. Nature 1999; 398:518-22.

De Strooper, B. and Annaert, W. Proteolytic processing and cell biological functions of the amyloid precursor protein. J Cell Sci 2000; 113:1857-70.

De Strooper B. Loss-of-function presenilin mutations in Alzheimer disease. Talking point on the role of presenilin mutations in Alzheimer disease. EMBO Rep 2007; 8:141–6.

De Strooper B. Proteases and proteolysis in Alzheimer disease: a multifactorial view on the disease process. Physiol Rev 2010; 90:465–94.

Dihne M, Bernreuther C, Sibbe M, Paulus W, Schachner M. A new role for the cell adhesion molecule L1 in neural precursor cell proliferation, differentiation, and transmitter-specific subtype generation. J Neurosci 2003; 23:6638-50.

Dimitrov M, Alattia JR, Lemmin T, Lehal R, Fligier A, Houacine J et al. Alzheimer's disease mutations in APP but not γ-secretase modulators affect epsilon-cleavage-dependent AICD production. Nat Commun 2013; 4:2246.

Doherty P, Williams E, Walsh FS. A soluble chimeric form of the L1 glycoprotein stimulates neurite outgrowth. Neuron 1995; 14:57-66.

Doody RS, Raman R, Farlow M, Iwatsubo T, Vellas B, Joffe S et al. A phase 3 trial of semagacestat for treatment of Alzheimer's disease. N Engl J Med 2013; 369:341-50.

Eckman CB, Mehta ND, Crook R, Perez-tur J, Prihar G, Pfeiffer E et al. A new pathogenic mutation in the APP gene (I716V) increases the relative proportion of A beta 42(43). Hum Mol Genet 1997; 6:2087-9.

Faissner A, Kruse J, Nieke J, Schachner M. Expression of neural cell adhesion molecule L1 during development, in neurological mutants and in the peripheral nervous system. Brain Res 1984; 317:69-82.

Farrer LA, Cupples LA, Haines JL, Hyman B, Kukull WA, Mayeux R et al. Effects of age, sex, and ethnicity on the association between apolipoprotein E genotype and Alzheimer disease. A meta-analysis. APOE and Alzheimer Disease Meta Analysis Consortium. JAMA 1997; 278:1349-56.

Farzan M, Schnitzler CE, Vasilieva N, Leung D, Choe H. BACE2, a beta -secretase homolog, cleaves at the beta site and within the amyloid-beta region of the amyloid-beta precursor protein. Proc Natl Acad Sci USA 2000; 97:9712-7.

Felding-Habermann B, Silletti S, Mei F, Siu CH, Yip PM, Brooks PC et al. A single immunoglobulin-like domain of the human neural cell adhesion molecule L1 supports adhesion by multiple vascular and platelet integrins. J Cell Biol 1997; 139:1567-81.

Fischer G, Künemund V, Schachner M. Neurite outgrowth patterns in cerebellar microexplant cultures are affected by antibodies to the cell surface glycoprotein L1. J Neurosci. 1986 Feb;6(2):605-12.

Forloni G, Demicheli F, Giorgi S, Bendotti C, Angeretti N. Expression of amyloid precursor protein mRNAs in endothelial, neuronal and glial cells: modulation by interleukin-1. Mol Brain Res 1992; 16:128-134.

Franklin K, Paxinos G. The Mouse Brain in Stereotaxic Coordinates. San Diego: Academic Press; 2007.

Friedli A, Fischer E, Novak-Hofer I, Cohrs S, Ballmer-Hofer K, Schubiger PA et al. Grünberg J. The soluble form of the cancer-associated L1 cell adhesion molecule is a pro-angiogenic factor. Int J Biochem Cell Biol 2009; 41:1572-80.

Gengler S, Hamilton A, Hölscher C. Synaptic plasticity in the hippocampus of a APP/PS1 mouse model of Alzheimer's disease is impaired in old but not young mice. PLoS ONE 2010; 5:e9764.

Giambarella U, Yamatsuji T, Okamoto T, Matsui T, Ikezu T, Murayama Y et al. G protein betagamma complex-mediated apoptosis by familial Alzheimer's disease mutant of APP. EMBO J 2007; 16:4897-907.

Gianni D, Zambrano N, Bimonte M, Minopoli G, Mercken L, Talamo, F et al. Platelet-derived growth factor induces the beta-gamma-secretase-mediated cleavage of Alzheimer's amyloid precursor protein through a Src-Rac-dependent pathway. J Biol Chem 2003; 278:9290-7.

Gil OD, Sakurai T, Bradley AE, Fink MY, Cassella MR, Kuo JA et al. Ankyrin binding mediates L1CAM interactions with static components of the cytoskeleton and inhibits retrograde movement of L1CAM on the cell surface. J Cell Biol 2003; 162:719-30.

Glenner GG and Wong CW. Alzheimer's disease: initial report of the purification and characterization of a novel cerebrovascular amyloid protein. Biochem Biophys Res Commun 1984a; 120:885-90.

Glenner GG and Wong CW. Alzheimer's disease and Down's syndrome: sharing of a unique cerebrovascular amyloid fibril protein. Biochem Biophys Res Commun 1984b; 122:1131-5.

Goate A, Chartier-Harlin MC, Mullan M, Brown J, Crawford F, Fidani L et al. Segregation of a missense mutation in the amyloid precursor protein gene with familial Alzheimer's disease. Nature 1991; 349:704-6.

Goedert M. Tau protein and neurodegeneration. Semin Cell Dev Biol 2004; 15:45-9.

Goldgaber D, Lerman MI, McBride WO, Saffiotti U, Gajdusek DC. Isolation, characterization, and chromosomal localization of human brain cDNA clones coding for the precursor of the amyloid of brain in Alzheimer's disease, Down's syndrome and aging. J Neural Transm 1987; Suppl. 24: 23-8.

Grathwohl SA, Kälin RE, Bolmont T, Prokop S, Winkelmann G, Kaeser SA et al. Formation and maintenance of Alzheimer's disease β-amyloid plaques in the absence of microglia. Nat Neurosci 2009; 12:1358-60.

Greenberg SM, Qiu WQ, Selkoe DJ, Ben-Itzhak A, Kosik KS. Amino-terminal region of the beta-amyloid precursor protein activates mitogen-activated protein kinase. Neurosci Lett 195; 198:52-56.

Grieger JC, Samulski RJ. Adeno-associated virus vectorology, manufacturing, and clinical applications. Methods Enzymol 2012; 507:229-54.

Guénette S, Chang Y, Hiesberger T, Richardson JA, Eckman CB, Eckman EA et al. Essential roles for the FE65 amyloid precursor protein-interacting proteins in brain development. EMBO J 2006; 25:420-31.

Guseva D, Angelov DN, Irintchev A, Schachner M. Ablation of adhesion molecule L1 in mice favours Schwann cell proliferation and functional recovery after peripheral nerve injury. Brain 2009; 132:2180-95.

Guseva D, Zerwas M, Xiao M-F, Jakovcevski I, Irintchev A, Schachner M. Adhesion molecule L1 overexpressed under the control of the neuronal Thy-1 promoter improves myelination after peripheral nerve injury in adult mice. Exp Neurol 2011; 229:339-52.

Hall H, Djonov V, Ehrbar M, Hoechli M, Hubbell JA. Heterophilic interactions between cell adhesion molecule L1 and alphavbeta3-integrin induce HUVEC process extension in vitro and angiogenesis in vivo. Angiogenesis 2004; 7:213-23.

Hardy J. Amyloid, the presenilins and Alzheimer's disease. Trends Neurosci 1997; 20:154-9.

Hardy J. A hundred years of Alzheimer's disease research. Neuron 2006; 52:3-13.

Hardy J, Duff K, Hardy KG, Perez-Tur J, Hutton M. Genetic dissection of Alzheimer's disease and related dementias: amyloid and its relationship to tau. Nat Neurosci 1998; 1:355-8.

Hardy JA, Higgins GA. Alzheimer's disease: the amyloid cascade hypothesis. Science 1992; 256:184-5.

Hardy J, Selkoe DJ. The amyloid hypothesis of Alzheimer's disease: progress and problems on the road to therapeutics. Science 2002; 297:353-6.

Harold D, Abraham R, Hollingworth P, Sims R, Gerrish A, Hamshere ML et al. Genome-wide association study identifies variants at CLU and PICALM associated with Alzheimer's disease. Nat Genet 2009; 41:1088-93.

Hass MR, Yankner BA. A {gamma}-secretase-independent mechanism of signal transduction by the amyloid precursor protein. J Biol Chem 2005; 280:36895-904.

He X, Knepper M, Ding C, Li J, Castro S, Siddiqui M et al. Promotion of spinal cord regeneration by neural stem cell-secreted trimerized cell adhesion molecule L1. PLoS ONE 2012; 7:e46223.

Heber S, Herms J, Gajic V, Hainfellner J, Aguzzi A, Rulicke T et al. Mice with combined gene knock-outs reveal essential and partially redundant functions of amyloid precursor protein family members. J Neurosci 2000; 20:7951-63.

Hebert LE, Scherr PA, Bienias JL, Bennett DA, Evans DA. Alzheimer Disease in the US population: Prevalence Estimates Using the 2000 census. Arch Neurol 2003; 60:1119–22.

Hebert SS, Serneels L, Tolia A, Craessaerts K, Derks C, Filippov MA et al. Regulated intramembrane proteolysis of amyloid precursor protein and regulation of expression of putative target genes. EMBO Rep 2006; 7:739-45.

Hendriks L, van Duijn CM, Cras P, Cruts M, Van Hul W, van Harskamp F et al. Presenile dementia and cerebral haemorrhage linked to a mutation at codon 692 of the beta-amyloid precursor protein gene. Nat Genet 1992; 1:218-21.

Herms J, Anliker B, Heber S, Ring S, Fuhrmann M, Kretzschmar H et al. Cortical dysplasia resembling human type 2 lissencephaly in mice lacking all three APP family members. EMBO J 2004; 23:4106–15.

Herreman A, Hartmann D, Annaert W, Saftig P, Craessaerts K, Serneels L et al. Presenilin 2 deficiency causes a mild pulmonary phenotype and no changes in amyloid precursor protein processing but enhances the embryonic lethal phenotype of presenilin 1 deficiency. Proc Natl Acad Sci USA 1999; 96:11872–7.

Herreman A, Van Gassen G, Bentahir M, Nyabi O, Craessaerts K, Mueller U et al. Gamma-secretase activity requires the presenilin-dependent trafficking of nicastrin through the Golgi apparatus but not its complex glycosylation. J Cell Sci 2003; 116:1127–36.

Herrup K. Reimaging Alzheimer's disease – an age-based hypothesis. J Neurosci 2010; 30:16755-62.

Hickman SE, El Khoury J. Mechanisms of mononuclear phagocyte recruitment in Alzheimer's disease. CNS Neurol Disord Drug Targets 2010; 9:168-73.

Ho A, Südhof TC. Binding of F-spondin to amyloid-beta precursor protein: a candidate amyloid-beta precursor protein ligand that modulates amyloid-beta precursor protein cleavage. Proc Natl Acad Sci USA 2004; 101:2548-53.

Hoe HS, Tran TS, Matsuoka Y, Howell BW, Rebeck GW. DAB1 and Reelin effects on amyloid precursor protein and ApoE receptor 2 trafficking and processing. J Biol Chem 2006a; 281:35176-85.

Hoe HS, Tran TS, Matsuoka Y, Howell BW, Rebeck GW. DAB1 and Reelin effects on amyloid precursor protein and ApoE receptor 2 trafficking and processing. J Biol Chem 2006b; 281:35176-85.

Hollingworth P, Harold D, Sims R, Gerrish A, Lambert JC, Carrasquillo MM et al. Common variants at ABCA7, MS4A6A/MS4A4E, EPHA1, CD33 and CD2AP are associated with Alzheimer's disease. Nat Genet 2011; 43:429-35.

Holmes C, Boche D, Wilkinson D, Yadegarfar G, Hopkins V, Bayer A et al. Long-term effects of Abeta42 immunisation in Alzheimer's disease: follow-up of a randomised, placebo-controlled phase I trial. Lancet 2008; 372:216–23.

Hortsch M. Structural and functional evolution of the L1 family: are four adhesion molecules better than one? Mol Cell Neurosci 2000; 15:1-10.

Hutton M, Lendon CL, Rizzu P, Baker M, Froelich S, Houlden H et al. Association of missense and 5'-splice-site mutations in tau with the inherited dementia FTDP-17. Nature 1998; 393:702-5.

Imbimbo BP, Solfrizzi V, Panza F. Are NSAIDs useful to treat Alzheimer's disease or mild cognitive impairment? Front Aging Neurosci 2010; 2. pii:19.

Irintchev A, Rollenhagen A, Troncoso E, Kiss JZ, Schachner M. Structural and functional aberrations in the cerebral cortex of tenascin-C deficient mice. Cereb Cortex 2005; 15:950-62.

Ittner MC, Götz J. Amyloid-β and tau--a toxic pas de deux in Alzheimer's disease. Nat Rev Neurosci 2011; 12:65-72.

Iwatsubo T, Odaka A, Suzuki N, Mizusawa H, Nukina N, Ihara Y. Visualization of A-beta42(43) and A-beta40 in senile plaques with end-specific monoclonals: evidence that an initially deposited species is A-beta42(43). Neuron 1994; 13:45-53.

Jacob J, Haspel J, Kane-Goldsmith N, Grumet M. L1 mediated homophilic binding and neurite outgrowth are modulated by alternative splicing of exon 2. J Neurobiol 2002; 51:177–189.

Jakovcevski I, Siering J, Hargus G, Karl N, Hoelters L, Djogo N et al. Close homologue of adhesion molecule L1 promotes survival of Purkinje and granule cells and granule cell migration during murine cerebellar development. J Comp Neurol 2009; 513:496-510.

Jakovcevski I, Djogo N, Hölters LS, Szpotowicz E, Schachner M. Transgenic overexpression of the cell adhesion molecule L1 in neurons facilitates recovery after mouse spinal cord injury. Neuroscience 2013; http://dx.doi.org/10.1016/j.neuroscience.2013.07.067.

Jarrett JT, Berger EP, Lansbury PT. The carboxyl terminus of the beta amyloid protein is critical for the seeding of amyloid formation: Implication for the pathogenesis of Alzheimer's disease. Biochemistry 1993; 32:4693-7.

Jicha GA, Abner EL, Schmitt FA, Kryscio RJ, Riley KP, Cooper GE et al. Preclinical AD Workgroup staging: Pathological correlates and potential challenges. Neurobiol Aging 2012; 33:662.e1–662.e16.

Jones L, Holmans PA, Hamshere ML, Harold D, Moskvina V, Ivanov D et al. Genetic evidence implicates the immune system and cholesterol metabolism in the aetiology of Alzheimer's disease. PLoS One 2010; 5:e13950.

Jorissen E, Prox J, Bernreuther C, Weber S, Schwanbeck R, Serneels L et al. The disintegrin/metalloproteinase ADAM10 is essential for the establishment of the brain cortex. J Neurosci 2010; 30:4833-44.

Jouet M, Moncla A, Paterson J, McKeown C, Fryer A, Carpenter N et al. New domains of neural cell-adhesion molecule L1 implicated in X-linked hydrocephalus and MASA syndrome. Am J Hum Genet 1995; 56:1304–14.

Jucker M, D'Amato F, Mondadori C, Mohajeri H, Magyar J, Bartsch U et al. Expression of the neural adhesion molecule L1 in the deafferented dentate gyrus. Neuroscience 1996; 75:703-15.

Jucker M, Walker LC. Pathogenic protein seeding in Alzheimer disease and other neurodegenerative disorders. Ann Neurol 2011; 70:532-40.

Kadmon G, von Bohlen und Halbach F, Horstkorte R, Eckert M, Altevogt P, Schachner M. Evidence for cis interaction and cooperative signalling by the heat- stable antigen nectadrin (murine CD24) and the cell adhesion molecule L1 in neurons. Eur J Neurosci 1995; 7:993-1004.

Kadmon G, Kowitz A, Altevogt P, Schachner M. Functional cooperation between the neural adhesion molecules L1 and N- CAM is carbohydrate dependent. J Cell Biol 1990a; 110:209-18.

Kadmon G, Kowitz A, Altevogt P, Schachner. The neural cell adhesion molecule N-CAM enhances L1-dependent cell-cell interactions. J Cell Biol 1990b; 110:193-208.

Kamal A, Stokin GB, Yang Z, Xia CH, Goldstein LS. Axonal transport of amyloid precursor protein is mediated by direct binding to the kinesin light chain subunit of kinesin-I. Neuron 2000; 28:449-59.

Kamiguchi H, Long KE, Pendergast M, Schaefer AW, Rapoport I, Kirchhausen T et al. The neural cell adhesion molecule L1 interacts with the AP-2 adaptor and is endocytosed via the clathrin-mediated pathway. J Neurosci 1998; 18:5311–21.

Kang J, Lemaire HG, Unterbeck A, Salbaum JM, Masters CL, Grzeschik KH et al. The precursor of Alzheimer's disease amyloid A4 protein resembles a cell-surface receptor. Nature 1987; 325:733–6.

King GD, Cherian K, Turner RS. X11alpha impairs gamma- but not beta-cleavage of amyloid precursor protein. J Neurochem 2004; 88:971-82.

King GD, Scott Turner R. Adaptor protein interactions: modulators of amyloid precursor protein metabolism and Alzheimer's disease risk? Exp Neurol 2004; 185: 208–19.

Kiyota T, Gendelman HE, Weir RA, Higgins EE, Zhang G, Jain M. CCL2 affects β-amyloidosis and progressive neurocognitive dysfunction in a mouse model of Alzheimer's disease. Neurobiol Aging 2013; 34:1060-8.

Knauer MF, Orlando RA, Glabe CG. Cell surface APP751 forms complexes with protease nexin 2 ligands and is internalized via the low density lipoprotein receptor-related protein (LRP). Brain Res 1996; 740:6-14.

Koike H, Tomioka S, Sorimachi H, Saido TC, Maruyama K, Okuyama A et al., S. Membrane-anchored metalloprotease MDC9 has an alphasecretase activity responsible for processing the amyloid precursor protein. Biochem J 1999; 343:371-5.

Kong GK, Adams JJ, Harris HH, Boas JF, Curtain CC, Galatis D et al. Structural studies of the Alzheimer's amyloid precursor protein copper-binding domain reveal how it binds copper ions. J Mol Biol 2007; 367:148–61.

Konig G, Monning U, Czech C, Prior R, Banati B, Schreiter-Gassre U et al. Identification and differential expression of a novel alternative splice isoform of the A4 amyloid precursor protein (APP) mRNA in leukocytes and brain microglia cells. J Biol Chem 1992; 267:10804- 9.

Kotilinek LA, Bacskai B, Westerman M, Kawarabayashi T, Younkin L, Hyman BT et al. Reversible memory loss in a mouse transgenic model of Alzheimer's disease. J Neurosci 2002; 22:6331–5.

Kounnas MZ, Moir RD, Rebeck GW, Bush AI, Argraves WS, Tanzi RE et al. LDL receptor-related protein, a multifunctional ApoE receptor, binds secreted beta-amyloid precursor protein and mediates its degradation. Cell 1995; 82:331-40.

Krabbe G, Halle A, Matyash V, Rinnenthal JL, Eom GD, Bernhardt U et al. Functional impairment of microglia coincides with Beta-amyloid deposition in mice with Alzheimer-like pathology. PLoS One 2013; 8:e60921.

Kuan YH, Gruebl T, Soba P, Eggert S, Nesic I, Back S et al. PAT1a modulates intracellular transport and processing of amyloid precursor protein (APP), APLP1, and APLP2. J Biol Chem 2006; 281:40114-23.

Kuhn TB, Stoeckli ET, Condrau MA, Rathjen FG, Sonderegger P. Neurite outgrowth on immobilized axonin-1 is mediated by a heterophilic interaction with L1 (G4). J Cell Biol 1991; 115: 1113-26.

Kuhn PH, Wang H, Dislich B, Colombo A, Zeitschel U, Ellwart JW et al. ADAM10 is the physiologically relevant, constitutive alpha-secretase of the amyloid precursor protein in primary neurons. EMBO J 2010; 29:3020-32.

Kwok JBJ, Li Q-X, Hallupp M, Milward L, Whyte S, Schofield PR. Novel familial early-onset Alzheimer's disease mutation (Leu723Pro) in amyloid precursor protein (APP) gene increases production of 42(43) amino-acid isoform of amyloid beta peptide. Neurobiology of Aging 1998; 19 Supp4:S91.

Lagenaur C, Lemmon V. An L1-like molecule, the 8D9 antigen, is a potent substrate for neurite extension. Proc Natl Acad Sci USA 1987; 84:7753-7.

Lammich S, Kojro E, Postina R, Gilbert S, Pfeiffer R, Jasionowski M et al. Constitutive and regulated alphasecretase cleavage of Alzheimer's amyloid precursor protein by a disintegrin metalloprotease. Proc Nat Acad Sci USA 1999; 96:3922-7.

Lavdas AA, Chen J, Papastefanaki F, Chen S, Schachner M, Matsas R et al. Schwann cells engineered to express the cell adhesion molecule L1 accelerate myelination and motor recovery after spinal cord injury. Exp Neurol 2009; 221:206-16.

Lee HJ, Bian S, Jakovcevski I, Wu B, Irintchev A, Schachner M. Delayed applications of L1 and chondroitinase ABC promote recovery after spinal cord injury. J Neurotrauma 2012; 29:1850-63.

Leissring MA, Murphy MP, Mead TR, Akbari Y, Sugarman MC, Jannatipour M et al. A physiologic signaling role for the gamma-secretase-derived intracellular fragment of APP. Proc Natl Acad Sci USA 2002; 99:4697-702.

Lemere CA, Maier M, Jiang L, Peng Y, Seabrook TJ. Amyloid-beta immunotherapy for the prevention and treatment of Alzheimer disease: lessons from mice, monkeys, and humans. Rejuvenation Res 2006; 9:77–84.

Levy E, Carman MD, Fernandez-Madrid IJ, Power MD, Lieberburg I, van Duinen SG et al. Mutation of the Alzheimer's disease amyloid gene in hereditary cerebral hemorrhage, Dutch type. Science 1990; 248:1124-6.

Levy-Lahad E, Wasco W, Poorkaj P, Romano DM, Oshima J, Pettingell WH et al. Candidate gene for the chromosome 1 familial Alzheimer's disease locus. Science 1995; 269:973-7.

Li HL, Roch JM, Sundsmo M, Otero D, Sisodia S, Thomas R et l. Defective neurite extension is caused by a mutation in amyloid beta/A4 (A beta) protein precursor found in familial Alzheimer's disease. J Neurobiol 1997; 32:469–80.

Liao YF, Wang BJ, Cheng HT, Kuo LH, Wolfe MS. Tumor necrosis factor-{alpha}, interleukin-1{beta}, and interferon-{gamma} stimulate {gamma}-secretase-mediated cleavage of amyloid precursor protein through a JNK-dependent MAPK pathway. J Biol Chem 2004; 279:49523-32.

Lindner J, Rathjen FG, Schachner M. L1 mono- and polyclonal antibodies modify cell migration in early postnatal mouse cerebellum. Nature 1983; 305:427-30.

Loffler J, Huber G. Amyloid precursor protein isoforms in various rat brain regions and during brain development. J Neurochem 1992; 59:1316-24.

Lorent K, Overbergh L, Moechars D, De Strooper B, Van Leuven F, Van den Berghe H. Expression in mouse embryos and in adult mouse brain of three members of the amyloid precursor protein family, of the alpha-2-macroglobulin receptor/low density lipoprotein receptor-related protein and of its ligands apolipoprotein E, lipoprotein lipase, alpha-2-macroglobulin and the 40,000 molecular weight receptorassociated protein. Neuroscience 1995; 65:1009-25.

Luo Y, Bolon B, Kahn S, Bennett BD, Babu-Khan S, Denis P et al. Mice deficient in BACE1, the Alzheimer's beta-secretase, have normal phenotype and abolished beta-amyloid generation. Nat Neurosci 2001; 4:231–2.

Lutz D, Wolters-Eisfeld G, Joshi G, Djogo N, Jakovcevski I, Schachner M et al. Generation and nuclear translocation of a sumoylated transmembrane fragment of the cell adhesion molecule L1. J Biol Chem 2012; 287:17161-75.

Maness PF, Schachner M. Neural recognition molecules of the immunoglobulin superfamily: signaling transducers of axon guidance and neuronal migration. Nat Neurosci 2007; 10:19–26.

Martini R, Schachner M. Immunoelectron microscopic localization of neural cell adhesion molecules (L1, N-CAM, and MAG) and their shared carbohydrate epitope and myelin basic protein in developing sciatic nerve. J Cell Biol 1986; 103:2439-48.

Martini R, Schachner M. Immunoelectron microscopic localization of neural cell adhesion molecules (L1, N-CAM, and myelin-associated glycoprotein) in regenerating adult mouse sciatic nerve. J Cell Biol 1988;106:1735-46.

Mattson MP, Cheng B, Culwell AR, Esch FS, Lieberburg I, Rydel RE. Evidence for excitoprotective and intraneuronal calcium-regulating roles for secreted forms of the beta-amyloid precursor protein. Neuron 1993; 10:243-54.

Mattson MP. Pathways towards and away from Alzheimer's disease. Nature 2004; 430:631-9.

McPhie DL, Coopersmith R, Hines-Peralta A, Chen Y, Ivins KJ, Manly SP et al. DNA synthesis and neuronal apoptosis caused by familial Alzheimer disease mutants of the amyloid precursor protein re mediated by the p21 activated kinase PAK3. J Neurosci 2003; 23:6914-27.

Meade CA, Figueredo-Cardenas G, Fusco F, Nowak TS, Pulsinelli WA, Reiner A. Transient global ischemia in rats yields striatal projection neuron and interneuron loss resembling that in Huntington's disease. Exp Neurol 2000; 166:307-23.

Mehanna A, Mishra B, Kurschat N, Schulze C, Bian S, Loers G et al. Polysialic acid glycomimetics promote myelination and functional recovery after peripheral nerve injury in mice. Brain 2009; 132:1449-62.

Mehanna A, Jakovcevski I, Acar A, Xiao M, Loers G, Rougon G et al. Polysialic acid glycomimetic promotes functional recovery and plasticity after spinal cord injury in mice. Mol Ther 2010; 18:34-43.

Monning U, Konig G, Banati B, Mechler H, Czech KC, Gehrmann J. Alzheimer beta A4-amyloid protein precursor in immunocompetent cells. J Biol Chem 1992; 267: 2350-6.

Moos M, Tacke R, Scherer H, Teplow D, Früh K, Schachner M. Neural adhesion molecule L1 as a member of the immunoglobulin superfamily with binding domains similar to fibronectin. Nature 1988; 334:701-3.

Morellini F, Sivukhina E, Stoenica L, Oulianova E, Bukalo O, Jakovcevski I et al. Improved reversal learning and working memory and enhanced reactivity to novelty in mice with enhanced GABAergic innervation in the dentate gyrus. Cereb Cortex 2010; 20:2712-27.

Mullan M, Crawford F, Axelman K, Houlden H, Lilius L, Winblad B et al. A pathogenic mutation for probable Alzheimer's disease in the APP gene at the N-terminus of beta-amyloid. Nat Genet 1992; 5:345-7.

Muller T, Concannon CG, Ward MW, Walsh CM, Tirniceriu AL, Tribl F et al. Modulation of gene expression and cytoskeletal dynamics by the amyloid precursor protein intracellular domain (AICD). Mol Biol Cell 2007; 18:201-10.

Muller U, Cristina N, Li ZW, Wolfer DP, Lipp HP, Rulicke T et al. Behavioral and anatomical deficits in mice homozygous for a modified beta-amyloid precursor protein gene. Cell 1994; 79:755-65.

Multhaup G. Identification and regulation of the high affinity binding site of the Alzheimer's disease amyloid protein precursor (APP) to glycosaminoglycans. Biochimie 1994; 76:304-11.

Multhaup G, Schlicksupp A, Hesse L, Beher D, Ruppert T, Masters CL et al. The amyloid precursor protein of Alzheimer's disease in the reduction of copper(II) to copper(I). Science 1996; 271:1406-1409.

Muresan Z, Muresan V. Coordinated transport of phosphorylated amyloid-beta precursor protein and c-Jun NH2-terminal kinase-interacting protein-1. J Cell Biol 2005; 171:615-25.

Nagele RG, Wegiel J, Venkataraman V, Imaki H, Wang KC, Wegiel J. Contribution of glial cells to the development of amyloid plaques in Alzheimer's disease. Neurobiol Aging 2004; 25:663–74.

Naj AC, Jun G, Beecham GW, Wang LS, Vardarajan BN, Buros J et al. Common variants at MS4A4/MS4A6E, CD2AP, CD33 and EPHA1 are associated with late-onset Alzheimer's disease. Nat Genet 2011; 43:436-41.

Nakata A, Kamiguchi H. Serine phosphorylation by casein kinase II controls endocytic L1 trafficking and axon growth. J Neurosci Res 2007; 85:723–34.

Neve R, Finch E, Dawes L. Expression of the AIzheimer amyloid precursor gene transcripts in the human brain. Neuron 1988; 1:669-77.

Nikonenko AG, Sun M, Lepsveridze E, Apostolova I, Petrova I, Irintchev A et al. Enhanced perisomatic inhibition and impaired long-term potentiation in the CA1 region of juvenile CHL1-deficient mice. Eur J Neurosci 2006; 23:1839-52.

Ninomiya H, Roch JM, Sundsmo MP, Otero DA, Saitoh T. Amino acid sequence RERMS represents the active domain of amyloid beta/A4 protein precursor that promotes fibroblast growth. J Cell Biol 1993; 121:879–86.

Nishimune H, Bernreuther C, Carroll P, Chen S, Schachner M, Henderson CE. Neural adhesion molecules L1 and CHL1 are survival factors for motoneurons. J Neurosci Res 2005; 80:593-9.

Noviello C, Vito P, Lopez P, Abdallah M, D'Adamio L. Autosomal recessive hypercholesterolemia protein interacts with and regulates the cell surface level of Alzheimer's amyloid beta precursor protein. J Biol Chem 2003; 278:31843-7.

Ourednik V, Ourednik J, Xu Y, Zhang Y, Lynch WP, Snyder EY et al. Cross-talk between stem cells and the dysfunctional brain is facilitated by manipulating the niche: evidence from an adhesion molecule. Stem Cells 2009; 27:2846-56.

Paradisi S, Sacchetti B, Balduzzi M, Gaudi S, Malchiodi-Albedi F. Astrocyte modulation of *in vitro* beta-amyloid neurotoxicity. Glia 2004; 46:252–60.

Park JH, Gimbel DA, GrandPre T, Lee JK, Kim JE, Li W et al. Alzheimer precursor protein interaction with the Nogo-66 receptor reduces amyloid-beta plaque deposition. J Neurosci 2006; 26:1386-95.

Peng SP, Kügler S, Ma ZK, Shen YQ, Schachner M. Comparison of AAV2 and AAV5 in gene transfer in the injured spinal cord of mice. Neuroreport 2011; 22:565-9.

Perez RG, Zheng H, Van der Ploeg LH, Koo EH. The beta-amyloid precursor protein of Alzheimer's disease enhances neuron viability and modulates neuronal polarity. J Neurosci 1997; 17:9407-14.

Ponte P, Gonzalez-DeWhite P, Schilling J, Miller J, Hsu D, Greeburg B et al. A new A4 amyloid mRNA contains a domain homologous to serine proteinase inhibitors. Nature 1988; 331:525-32.

Radde R, Bolmont T, Kaeser SA, Coomaraswamy J, Lindau D, Stolze L et al. Aβ42-driven cerebral amyloidosis in transgenic mice reveals early and robust pathology. EMBO reports 2006; 7:940-6.

Ransohoff RM. The chemokine system in neuroinflammation: an update. J Infect Dis 2002; 186 Suppl 2:S152-6.

Rathjen FG, Schachner M. Immunocytological and biochemical characterization of a new neuronal cell surface component (L1 antigen) which is involved in cell adhesion. EMBO J 1984; 3:1-10.

Riedle S, Kiefel H, Gast D, Bondong S, Wolterink S, Gutwein P et al. Nuclear translocation and signalling of L1-CAM in human carcinoma cells requires ADAM10 and presenilin/gamma-secretase activity. Biochem J 2009; 420:391-402.

Ring S, Weyer SW, Kilian SB, Waldron E, Pietrzik CU, Filippov MA et al. The secreted beta-amyloid precursor protein ectodomain APPs alpha is sufficient to rescue the anatomical, behavioral, and electrophysiological abnormalities of APP-deficient mice. J Neurosci 2007; 27:7817-26.

Robakis NK, Wisniewski HM, Jenkins EC, Devine-Gage EA, Houck GE, Yao XL et al. Chromosome 21q21 sublocalisation of gene encoding beta-amyloid peptide in cerebral vessels and neuritic (senile) plaques of people with Alzheimer disease and Down syndrome. Lancet 1987; 1:384–5.

Robert R, Wark KL. Engineered antibody approaches for Alzheimer's disease immunotherapy. Arch Biochem Biophys 2012; 526:132–8.

Rogaev EI, Sherrington R, Rogaeva EA, Levesque G, Ikeda M, Liang Y et al. Familial Alzheimer's disease in kindreds with missense mutations in a gene on chromosome 1 related to the Alzheimer's disease type 3 gene. Nature 1995; 376:775-8.

Roncarati R, Sestan N, Scheinfeld MH, Berechid BE, Lopez PA, Meucci O et al. The gamma-secretase generated intracellular domain of beta-amyloid precursor protein binds Numb and inhibits Notch signaling. Proc Natl Acad Sci USA 2002; 99:7102-7.

Roonprapunt C, Huang W, Grill R, Friedlander D, Grumet M, Chen S et al. Soluble cell adhesion molecule L1-Fc promotes locomotor recovery in rats after spinal cord injury. J Neurotrauma 2003; 20:871-82.

Rose SP. Glycoproteins and memory formation. Behav Brain Res 1995; 66:73-8.

Rosen DR, Martin-Morris L, Luo L, White K. A Drosophila gene encoding a protein resembling the human beta-amyloid protein precursor. Proc Natl Acad Sci USA 1989; 86:2478–82.

Rosendorff C, Beeri MS, Silverman JM. Cardiovascular risk factors for Alzheimer's disease. Am J Geriatr Cardiol 2007; 16:143-9.

Rossjohn J, Cappai R, Feil SC, Henry A, McKinstry WJ, Galatis D et al. Crystal structure of the N-terminal, growth factor-like domain of Alzheimer amyloid precursor protein. Nat Struct Biol 1999; 6:327-31.

Rotshenker S. The role of galectin-3/MAC-2 in the activation of the innate-immune function of phagocytosis in microglia in injury and disease. J Mol Neurosci 2009; 39:99-103.

Russo C, Venezia V, Repetto E, Nizzari M, Violani E, Carlo P et al. The amyloid precursor protein and its network of interacting proteins: physiological and pathological implications. Brain Res Brain Res Rev 2005; 48:257-64.

Saghatelyan AK, Nikonenko AG, Sun M, Rolf B, Putthoff P, Kutsche M et al. Reduced GABAergic transmission and number of hippocampal perisomatic inhibitory synapses in juvenile mice deficient in the neural cell adhesion molecule L1. Mol Cell Neurosci 2004; 26:191-203.

Saiz-Sanchez D, Ubeda-Bañon I, De la Rosa-Prieto C, Martinez-Marcos A. Differential expression of interneuron populations and correlation with amyloid-β deposition in the olfactory cortex of an AβPP/PS1 transgenic mouse model of Alzheimer's disease. J Alzheimers Dis 2012; 31:113-29.

Samland H, Huitron-Resendiz S, Masliah E, Criado J, Henriksen SJ, Campbell IL. Profound increase in sensitivity to glutamatergic- but not cholinergic agonist-induced seizures in transgenic mice with astrocyte production of IL-6. J Neurosci Res 2003; 73:176-87.

Sandbrink R, Masters CL, Beyreuther K. A4-amyloid protein precursor mRNA isoforms without exon 15 are ubiquitously expressed in rat tissues including brain, but not in neurons. J Biol Chem 1994; 269: 1510-17.

Savage MJ, Kawooya JK, Pinsker LR, Emmons TL, Mistretta S, R. Siman et al. Elevated A-beta levels in Alzheimer's disease brain are associated with selective accumulation of A-beta42 in parenchymal amyloid plaques and both A-beta40 and Abeta42 in cerebrovascular deposits. Int J Exp Clin Invest 1995; 2:234-40.

Schaefer AW, Kamei Y, Kamiguchi H, Wong EV, Rapoport I, Kirchhausen T et al. L1 endocytosis is controlled by a phosphorylationdephosphorylation cycle stimulated by outside-in signaling by L1. J Cell Biol 2002; 157:1223–32.

Schaefer AW, Kamiguchi H, Wong EV, Beach CM, Landreth G, Lemmon V. Activation of the MAPK signal cascade by the neural cell adhesion molecule L1 requires L1 internalization. J Biol Chem 1999; 274:37965–73.

Schmid RS, Maness PF. L1 and NCAM adhesion molecules as signaling coreceptors in neuronal migration and process outgrowth. Curr Opin Neurobiol 2008; 18:245–50.

Schwaller B, Tetko IV, Tandon P, Silveira DC, Vreugdenhil M, Henzi T et al. Parvalbumin deficiency affects network properties resulting in increased susceptibility to epileptic seizures. Mol Cell Neurosci 2004; 25:650-63.

Selkoe D and Kopan R. Notch and Presenilin: regulated intramembrane proteolysis links development and degeneration. Annu Rev Neurosci 2003; 26:565-97.

Serneels L, Dejaegere T, Craessaerts K, Horré K, Jorissen E, Tousseyn T et al. Differential contribution of the three *Aph1* genes to γ-secretase activity *in vivo*. Proc Natl Acad Sci USA 2005; 102:1719–24.

Sherrington R, Rogaev EI, Liang Y, Rogaeva EA, Levesque G, Ikeda M et al. Cloning of a gene bearing missense mutations in early-onset familial Alzheimer's disease. Nature 1995; 375:754-60.

Simpson JE, Ince PG, Lace G, Forster G, Shaw PJ, Matthews F et al. MRC Cognitive Function and Ageing Neuropathology Study Group. Astrocyte phenotype in relation to Alzheimer-type pathology in the ageing brain. Neurobiol Aging 2010; 31:578–90.

Small DH, Nurcombe V, Reed G, Clarris H, Moir R, Beyreuther K et al. A heparin-binding domain in the amyloid protein precursor of Alzheimer's disease is involved in the regulation of neurite outgrowth. J Neurosci 1994; 14: 2117–27.

Soba P, Eggert S, Wagner K, Zentgraf H, Siehl K, Kreger S et al. Homo- and heterodimerization of APP family members promotes intercellular adhesion. EMBO J 2005; 24:3624-34.

Song W, Nadeau P, Yuan M, Yang X, Shen J, Yankner BA. Proteolytic release and nuclear translocation of Notch-1 are induced by presenilin-1 and impaired by pathogenic presenilin-1 mutations. Proc. Natl Acad. Sci. USA 1999; 96:6959–63.

Stine WB, Jungbauer L, Yu C, LaDu MJ. Preparing synthetic Aβ in different aggregation states. Methods Mol Biol 2011; 670:13-32.

Strekalova H, Buhmann C, Kleene R, Eggers C, Saffell J, Hemperly J et al. Elevated levels of neural recognition molecule L1 in the cerebrospinal fluid of patients with Alzheimer disease and other dementia syndromes. Neurobiol Aging 2006; 27:1-9.

Suzuki N, Cheung TT, Cai XD, Odaka A, Otvos L Jr, Eckman C et al. An increased percentage of long amyloid beta protein secreted by familial amyloid beta protein precursor (beta APP717) mutants. Science 1994; 264:1336-40.

Takami M, Nagashima Y, Sano Y, Ishihara S, Morishima-Kawashima M, Funamoto S et al. γ-Secretase: successive tripeptide and tetrapeptide release from the transmembrane domain of β-carboxyl terminal fragment. J Neurosci 2009; 29:13042–52.

Tanaka S, Nakamura S, Ueda K, Kameyama M, Shiojiri S, Takahashi Y et al. Three types of amyloid protein precursor mRNA in human brain: their differential expression in Alzheimer's disease. Biochem Biophys Res Commun 1988; 157:472-9.

Terry RD, Masliah E, Hansen LA. Structural basis of the cognitive alterations in Alzheimer disease. In: Terry RD, Katzman R, Bick KL, editors. Alzheimer Disease. New York: Raven Press; 1994. p. 179-96.

Terry RD, Masliah E, Salmon DP, Butters N, DeTeresa R, Hill R et al. Physical basis of cognitive alterations in Alzheimer's disease: synapse loss is the major correlate of cognitive impairment. Ann Neurol 1991; 30:572-80.

Thelen K, Kedar V, Panicker AK, Schmid RS, Midkiff BR, Maness PF. The neural cell adhesion molecule L1 potentiates integrin-dependent cell migration to extracellular matrix proteins. J Neurosci 2002; 22:4918–31.

Tomlinson BE, Blessed G, Roth M. Observations on the brains of non-demented old people. J Neurol Sci 1968; 7:331-56.

Tomlinson BE, Blessed G, Roth M. Observations on the brains of demented old people. J Neurol Sci 1970; 11:205–42.

Van Broeckhoven C, Kumar-Singh S. Genetics and pathology of α-secretase site AβPP mutations in the understanding of Alzheimer's disease. J Alzheimers Dis 2006; 9:389–98.

Varvel NH, Bhaskar K, Patil AR, Pimplikar SW, Herrup K, Lamb BT. Abeta oligomers induce neuronal cell cycle events in Alzheimer's disease. J Neurosci 2008; 28:10786-93.

Vassar R, Bennett BD, Babu-Khan S, Kahn S, Mendiaz EA, Denis P et al. Beta-secretase cleavage of Alzheimer's amyloid precursor protein by the transmembrane aspartic protease BACE. Science 1999; 286:735-41.

Verret L, Mann EO, Hang GB, Barth AM, Cobos I, Ho K et al. Inhibitory interneuron deficit links altered network activity and cognitive dysfunction in Alzheimer model. Cell 2012; 149:708-21.

Walsh DM, Minogue AM, Sala Frigerio C, Fadeeva JV, Wasco W, Selkoe DJ. The APP family of proteins: similarities and differences. Biochem Soc Trans 2007; 35:416-20.

Wang P, Yang G, Mosier DR, Chang P, Zaidi T, Gong YD et al. Defective neuromuscular synapses in mice lacking amyloid precursor protein (APP) and APP-Like protein 2. J Neurosci 2005; 25:1219-25.

Wang Y, Ha Y. The X-ray structure of an antiparallel dimer of the human amyloid precursor protein E2 domain. Mol Cell 2004; 15:343–353.

Wang YJ, Zhou HD, Zhou XF. Clearance of amyloid-beta in Alzheimer's disease: progress, problems and perspectives. Drug Discov Today 2006; 11:931-8.

Wasco W, Bupp K, Magendantz M, Gusella J, Tanzi RE, Solomon F. Identification of a mouse brain cDNA that encodes a protein related to the Alzheimer disease-associated amyloid beta protein precursor. Proc Natl Acad Sci USA 1992; 89:10758–62.

Wasco W, Gurubhagavatula S, Paradis MD, Romano DM, Sisodia SS, Hyman BT et al. Isolation and characterization of APLP2 encoding a homologue of the Alzheimer's associated amyloid beta protein precursor. Nat Genet 1993; 5:95–9.

Weiner HL, Frenkel D. Immunology and immunotherapy of Alzheimer's disease. Nat Rev Immunol 2006; 6:404–16.

Wei W, Nguyen LN, Kessels H, Hagiwara H, Sisodia S, Malinow R. Amyloid beta from axons and dendrites reduces local spine number and plasticity. Nat Neurosci 2010; 13:190-6.

Weller S, Gärtner J. Genetic and clinical aspects of X-linked hydrocephalus (L1 disease): mutations in the L1CAM gene. Hum Mutat 2001; 18:1–12.

White AR, Reyes R, Mercer JF, Camakaris J, Zheng H, Bush AI et al. Copper levels are increased in the cerebral cortex and liver of APP and APLP2 knockout mice. Brain Res 1999; 842:439–44.

Wisniewski HM, Vorbrodt AW, Moretz RC, Lossinsky AS, Grundke-Iqbal I. Pathogenesis of neuritic (senile) and amyloid plaque formation. Exp Brain Res 1982; (Suppl 5):3–9.

Wisniewski HM, Wegiel J, Wang KC, Kujawa M, Lach B. Ultrastructural studies of the cells forming amyloid fibers in classical plaques. Can J Neurol Sci 1989; 16:535-42.

Wolfe MS. When loss is gain: reduced presenilin proteolytic function leads to increased Aβ42/Aβ40. Talking point on the role of presenilin mutations in Alzheimer disease. EMBO Rep 2007; 8:136–40.

Wood PM, Schachner M, Bunge RP. Inhibition of Schwann cell myelination in vitro by antibody to the L1 adhesion molecule. J Neurosci 1990a; 10:3635-45.

Wood P, Moya F, Eldridge C, Owens G, Ranscht B, Schachner M, Bunge M, Bunge R. Studies of the initiation of myelination by Schwann cells. Ann N Y Acad Sci 1990b; 605:1-14.

Wu J, Stoica BA, Faden AI. Cell cycle activation and spinal cord injury. Neurotherapeutics 2011; 8:221-8.

Wyss-Coray T. Inflammation in Alzheimer disease: driving force, bystander or beneficial response? Nat Med 2006; 12:1005-15.

Xu J-C, Bernreuther C, Cui Y-F, Jakovcevski I, Hargus G, Xiao M-F et al. Transplanted L1 expressing radial glia and astrocytes enhance recovery after spinal cord injury. J Neurotrauma 2011; 28:1921-37.

Yagishita S, Morishima-Kawashima M, Tanimura Y, Ishiura S, Ihara Y. DAPT-induced intracellular accumulations of longer amyloid β-proteins: further implications for the mechanism of intramembrane cleavage by γ-secretase. Biochemistry 2006; 45:3952–60.

Young-Pearse TL, Bai J, Chang R, Zheng JB, LoTurco JJ, Selkoe D. A critical function for beta-amyloid precursor protein in neuronal migration revealed by in utero RNA interference. J Neurosci 2007; 27:14459-69.

Younkin SG. Evidence that A beta 42 is the real culprit in Alzheimer’s disease. Ann Neurol 1995; 37:287-8.

Zhang-Nunes SX, Maat-Schieman ML, van Duinen SG, Roos RA, Frosch MP, Greenberg SM. The cerebral β- amyloid angiopathies: hereditary and sporadic. Brain Pathol 2006; 16:30–9.

Zhang YW, Wang R, Liu Q, Zhang H, Liao FF, and Xu, H. Presenilin/gamma-secretase-dependent processing of beta-amyloid precursor protein regulates EGF receptor expression. Proc Natl Acad Sci USA 2007; 104:10613-8.

Zheng H, Jiang M, Trumbauer ME, Sirinathsinghji DJ, Hopkins R, Smith DW et al. Beta-amyloid precursor protein-deficient mice show reactive gliosis and decreased locomotor activity. Cell 1995; 81:525–31.

Zheng P, Eastman J, Vande Pol S, Pimplikar SW. PAT1, a microtubule-interacting protein, recognizes the basolateral sorting signal of amyloid precursor protein. Proc Natl Acad Sci USA 1998; 95:14745-50.

Zhou L, Barao S, Laga M, Bockstael K, Borgers M, Gijsen H et al. The neural cell adhesion molecules L1 and CHL1 are cleaved by BACE1 protease in vivo. J Biol Chem 2012; 287:25927-40.

9. ORIGINAL ARTICLES

Djogo N*, Jakovcevski I*, Müller C, Lee HJ, Xu JC, Jakovcevski M, Kügler S, Loers G, Schachner M. Adhesion molecule L1 binds to amyloid beta and reduces Alzheimer's disease pathology in mice. Neurobiol Dis 2013; 56:104-15.

Stemmer N*, Strekalova E*, **Djogo N***, Plöger F, Loers G, Lutz D, Buck F, Michalak M, Schachner M, Kleene R. Generation of amyloid-β is reduced by the interaction of calreticulin with amyloid precursor protein, presenilin and nicastrin. PLoS One 2013; 8:e61299.

Jakovcevski I, **Djogo N**, Hölters LS, Szpotowicz E, Schachner M, Transgenic overexpression of the cell adhesion molecule L1 in neurons facilitates recovery after mouse spinal cord injury. Neuroscience 2013; doi: http://dx.doi.org/10.1016/j.neuroscience.2013.07.067.

Wu B, Matic D, **Djogo N**, Szpotowicz E, Schachner M, Jakovcevski I. Improved regeneration after spinal cord injury in mice lacking functional T- and B-lymphocytes. Exp Neurol 2012; 237:274-85.

Lutz D*, Wolters-Eisfeld G*, Joshi G*, **Djogo N**, Jakovcevski I, Schachner M, Kleene R. Generation and nuclear translocation of sumoylated transmembrane fragment of cell adhesion molecule L1. J Biol Chem 2012; 287:17161-75.

Andjus PR, Bataveljić D, Vanhoutte G, Mitrecic D, Pizzolante F, **Djogo N**, Nicaise C, Gankam Kengne F, Gangitano C, Michetti F, van der Linden A, Pochet R, Bacić G. In vivo morphological changes in animal models of amyotrophic lateral sclerosis and Alzheimer's-like disease: MRI approach. Anat Rec (Hoboken) 2009; 292:1882-92.

Andric M, Dozic B, Popovic B, Stefanovic D, Basta-Jovanovic G, **Djogo N**, Andjus P, Milasin J. Survivin expression in odontogenic keratocysts and correlation with cytomegalovirus infection. Oral Dis 2010; 16:156-9.

Jakovcevski I*, Siering J*, Hargus G*, Karl N*, Hoelters L, **Djogo N**, Yin S, Zecevic N, Schachner M, Irintchev A. Close homologue of adhesion molecule L1 promotes survival of Purkinje and granule cells and granule cell migration during murine cerebellar development. J Comp Neurol 2009; 513:496-510.

Bataveljić D, **Djogo N**, Zupunski L, Bajić A, Nicaise C, Pochet R, Bacić G, Andjus PR. Live monitoring of brain damage in the rat model of amyotrophic lateral sclerosis. Gen Physiol Biophys 2009; 28 Spec No:212-8.

(* equal contribution)

10. ABBREVIATIONS

aa amino acid

Aβ amyloid-beta peptide

APP amyloid precursor protein

APS ammonium persulfate

BCA bicinchoninic acid

BSA bovine serum albumin

CAM cell adhesion molecule

CHL1 close homologue of L1

DNA deoxyribonucleic acid

DMEM Dulbeco’s minimum essential medium

DMSO dimethyl sulfoxide

DTT dithiothreitol or threo-1,4-dimercapto-2,3-butanediol

ECL enhanced chemiluminescence

EDTA ethylenediaminetetraacetic acid

ELISA enzyme-linked immunosorbent assay

FA formic acid

Fc fragment crystallizable

FCS foetal calb serum

g (RCF) standard gravity is used as a unit of acceleration (relative centrifugal force)

Fn fibronectin

GFP green fluorescent protein

h hour

HBSS Hanks' balanced salt solution

HFIP hexafluoroisopropanol

HRP horseradish peroxidase

Ig immunoglobulin

KO knockout

M concentration of solution in mol/L

min minute

NP40 nonyl phenoxypolyethoxylethanol 40

PAGE polyacrylamide gel electrophoresis

PBS phosphate buffered saline

RIPA radio immuno precipitation assay

SDS sodium dodecylsulfate

TMB Tetramethylbenzidine

TBS tris buffered saline

TEMED N,N,N',N'-Tetramethylethylenediamine

Triton X-100 polyethylene glycol p-(1,1,3,3-tetramethylbutyl)-phenyl ether

Tween 20 polyoxyethylene (20) sorbitan monolaurate

11. ACKNOWLEDGEMENTS

To many people I owe gratitude for the completion of this dissertation. First of all, I would like to thank Professor Melitta Schachner for this great opportunity to work at her Institute and for giving me such an interesting research project. Being able to discuss my research problems with such an accomplished scientist and one of the leading experts in the field was a great privilege.

I am grateful to Dr. Igor Jakovcevski, Dr. Gabriele Loers and Dr. Ralf Kleene for their supervision during the years of my PhD. I have to thank Igor for guidance through the entire work described in this thesis, for help with mouse surgery, as well as including me in other interesting projects and giving me the opportunity to learn so much. He has always been supportive and patient, and provided insightful discussions. Gaby is in many ways responsible for the success of this project. She helped me to learn different experimental techniques, especially binding studies, and has always been a person to go to for the practical solutions of any problems that emerged in everyday work in the laboratory. I am also very grateful to Ralf for always being there to answer my questions and help with the advice. I have to thank him for providing HEK cells for this project, but also for the experience I gained working with him on other interesting projects, which eventually helped me to complete this work.

I would like to thank Dr. Carsten Schmidt for many helpful suggestions.

I am thankful to our technical assistants, Emanuela Szpotowicz for the help with histology, and Ute Bork for teaching me how to do Western blot, and most of all I am grateful for their kindness.

Special thanks go to my lab mates Thomas, Kathrin, Dave, Michael, Jelena and others for their friendship and support during our years spent together in the lab.

Finally, I would like to thank my family and friends back home for believing in me, without their support this work would not be accomplished.